Department of Applied Geology

Coquina and related hypersaline facies evolution in Shark Bay: morphology, chronology, processes and relationships

Rodrigo Correia Baptista da Silva

This thesis is presented for the Degree of
Master of Philosophy
of
Curtin University

April 2014

Declaration

To the best of my knowledge and belief this thesis contains no material previously published by any other person except where due acknowledgment has been made.

This thesis contains no material which has been accepted for the award of any other degree or diploma in any university.

Signature: Rodrigo Correia B. da Silva

Date: 03/04/2014

ABSTRACT

Shark Bay World Heritage Area displays a unique Holocene coarse bioclastic (coquina) beach-ridge system in the supratidal environment of Hamelin Pool and L'Haridon Bight hypersaline basins. In Hamelin Pool, eastern and western shores have different degrees of vulnerability to the typically northwest approaching storms. Aerial imagery, GPR profiles, radiocarbon chronology and sedimentological data were used to delineate a depositional and evolutionary model for bioclastic beach-ridge deposits in Hamelin Pool eastern and western shores by assessing their internal and external architecture, facies and radiocarbon ages. Additionally, the potential for paleosalinity reconstructions using stable carbon and oxygen isotopic composition of *Fragum erugatum* shells was investigated. The onset of the bioclastic beach-ridge system took place about 5000 ^{14}C years BP facilitated by abundant shell supply and falling sea level conditions under episodes of high water levels induced by storms. Prograding seaward inclined GPR reflections are the prevailing architectural elements and result from swash-backwash processes in the beachface during elevated water level episodes caused by storms. Another important feature is a diachronous blanket of deposits generated by storm-surge events and eolian processes occasionally developing incipient soils that cap older beach-ridge deposits. During the latest Holocene, marked environmental changes within Hamelin Pool are suggested by a number of indications such as change in the depositional style of beach-ridge deposits (complex geometries of spit ridges start to prevail over the seaward inclined reflectors of prograding beachfaces); overall lower ridge elevations; the occurrence of an important erosive period after 1450 ^{14}C years BP in the western shore; and the indication by isotopic data of a period when salinities were more stable in the hypersaline field. Although the ages obtained for the ridge sets mapped in both eastern and western shores of Hamelin Pool are roughly similar, they exhibit differences in sedimentary architecture and coastal morphology as a result of different degrees of vulnerability to storms, and secondarily to variable reworking processes such as tidal currents, waves and longshore currents which may also be energetic enough during fair-weather conditions to transport sediment in the nearshore environment. A depositional model is proposed where washovers and storm-surge ridges are deposited by overwash episodes at the peak of major storms while berm construction occurs during the waning phase by swash, backwash, overtopping and minor overwashing processes. This model can be used as an analogue for other coquina deposits in the stratigraphic record providing an example of high-resolution depositional architecture that is useful for reservoir characterization and prediction.

ACKNOWLEDGEMENTS

I would like to thank my supervisor Professor Lindsay B. Collins for his support and guidance.

I am thankful for the sponsorship and support of Petroleo Brasileiro S.A. (PETROBRAS) and the approval of this MPhil research project by the Exploration and Production Director José Miranda Formigli Filho. I would also like to thank the endorsement of this project by the E&P managers Mario Carminatti, Jeferson Dias, Jobel Moreira, Jonilton Pessoa, Sylvia dos Anjos and Pierre Muzzi.

I am grateful to João Pinto Bravo Correia Guerreiro for his great help during field work and the exchange of ideas during this research.

I would like to thank Ricardo Jahnert for generously sharing his experience on conducting research at Curtin University, Western Australia and his knowledge on Shark Bay, coquinas and microbialites.

I am grateful to Roman Pevzner, Elmar Strobach and Dominic Howman from the Department of Exploration Geophysics at Curtin University for the acquisition and processing of Ground Penetrating Radar lines.

I would like to thank all the staff members of the Department of Applied Geology who assisted me during this project, especially Alexandra Stevens, Giada Bufarale, Ms. Annette Labrooy and Andrew Wieczorek.

I also would like to say thank you to professionals from different institutions who cooperated with this research: Dave Holley (Department of Parks and Wildlife – DPaW, Denham, WA), Ross Mack (Department of Parks and Wildlife – DPaW, Denham, WA), John Walker (Department of Spatial Sciences, Curtin University of Technology), Carl Lares (Department of Spatial Sciences, Curtin University of Technology), Grzegorz Skrzypek (The West Australian Biogeochemistry Centre - The University of Western Australia), Catherine Kealley and William Rickard (Centre for Materials Research – Curtin University), Elaine Miller and Nigel Chen-Tan (Department of Imaging & Applied Physics).

I am thankful for the field support of Brian and Mary Wake (Hamelin Station).

I would like to thank Alonso Lluesma Parellada for the cooperation and providing a friendly atmosphere during the course of this work.

I am grateful to Juarez Silva and Cristiane Suemasu for their support with human resources matters and Danielle Lima, Joilma Lima and Nadja Oliveira for their secretarial work from Petrobras headquarters in Brazil.

Special thanks to my wife Raquel whose support, patience, encouragement and care have been essential to complete this work.

I am profoundly grateful to my parents Celia and Gilson, and my sister Viviane who have encouraged and supported me from distant Brazil.

"No man is an island, entire of itself; every man is a piece of the continent, a part of the main."

John Donne

To Raquel,

Celia,

Gilson,

Viviane

and Livia

Statement of the Contribution of others:

This thesis was supported by Petroleo Brasileiro S.A. (PETROBRAS) and Curtin University. A collaborative work was produced with the Department of Applied Geology and the Department of Exploration Geophysics - Curtin University with the assistance of the Department of Parks and Wildlife (DPaW), who provided access to protected sites in the Shark Bay World Heritage Area. However, as the author of this thesis I am responsible for the interpretation, research and development of the scientific content and material inside this dissertation.

Mr. Rodrigo Correia Baptista da Silva

Signature: Rodrigo Correia B. da Silva

Date: 03/04/2014

Professor Lindsay B. Collins (Supervisor)

Signature:

Date: 3/4/2014

Table of Contents

List of Figures

Chapter 2

Chapter 3

Chapter 4

Chapter 5

Chapter 6

List of Tables

Chapter 3

Chapter 4

Chapter 5

Chapter 6

Chapter **1**

Introduction

Shark Bay is a large shallow marine area located at the southern edge of the Carnarvon Basin, western coast of Australia. In a semi-arid to arid climatic zone, the bay is subject to insignificant runoff influx and evaporation by far exceeds precipitation. These factors allied to shoaling and hydrodynamic effects allow the development of a negative gradient where normal marine salinities are observed at the bay entrance and hypersaline conditions occur in the bay heads (Logan and Cebulski, 1970).

Hypersaline conditions in Hamelin Pool and L'Haridon Bight basins within Shark Bay set up a special ecosystem where a limited number of organisms can thrive. Microbial benthic communities and *Fragum erugatum* bivalve shells flourish in these hypersaline basins where ideal conditions for the occurrence of Shark Bay's renowned microbialites and coquinas developed during the Holocene in the last 6000 years.

High skeletal productivity of *Fragum erugatum* bivalves and the occurrence of frequent storms, able to transport shells from the subtidal to the supratidal environment are the major factors leading to the deposition of Shark Bay's coquina beach ridge system that borders Hamelin Pool and L'Haridon Bight coasts. Coquinas are of particular interest for the oil industry as they can be prolific hydrocarbon reservoirs. Modern examples of coquina deposits such as Shark Bay supratidal ridges can be useful as analogues for ancient systems and a better understanding of their origin and depositional architecture can be useful for the prediction of reservoir occurrence and distribution.

1.1. Objective

The objective of this master's thesis is to contribute to the understanding of coquina deposits by documenting architectural and sedimentary characteristics of Shark Bay coquina beach ridges outlining their depositional architecture and evolutionary framework using GPR, radiocarbon chronology, outcrop, trench and core data.

Chapter 2

Literature Review

2.1. Study Area

2.1.1. Geomorphology

Shark Bay is a large shallow embayment of approximately 8000 km^2 area, separated from the Indian Ocean by Edel Land, Dirk Hartog Island and the Bernier-Dorre island chain. Within the embayment, average water depth is around 10 m, although most of the area is occupied by shoals approximately 1 m deep (Butcher et al., 1984). The embayment is broken into gulfs, inlets and basins by peninsulas and islands composed of Pleistocene dunes and by seagrass banks which have formed during the Holocene (Logan, Read and Davies, 1970). The north-trending orientation of the peninsulas and islands is thought to follow subsurface Tertiary anticlines (Playford and Cockbain, 1976 as cited in Butcher et al., 1984). Logan, Read and Davies (1970) recognize four major geomorphologic subdivisions: (1) Edel Province, a site of calcareous dunes (Tamala Limestone); (2) Peron Province an area of red sand dunes over Peron Peninsula, Nanga Peninsula and Faure Island; (3) Wooramel Province, an alluvial coastal plain with river floodplain deposits; and (4) Yaringa Province, a terrain of dissected Cretaceous and Tertiary limestone units, which comprises essentially the Toolonga Plateau, later renamed Carbla Plateau by van de Graaf et al. (1980).

Hamelin Pool is a closed marine basin (Figure 2.1) that lies between the Yaringa and Peron Provinces. To the east and southeast, basin waters reach the Carbla Plateau of the Yaringa Province which is underlain by the Cretaceous Toolonga Calcilutite. The western basin margin is the Nanga Peninsula, part of the north-trending dune complex of the Peron Province (Figure 2.2) (Hagan and Logan, 1974).

Evaporite pans, locally known as “birridas” (Figure 2.3), are geomorphic features, usually isolated from the sea, that commonly occur in Edel and Peron Provinces. Their shape ranges from small, circular or oval to elongate or irregular interdune depressions and their dimensions vary from approximately 100 meters in diameter to several kilometers in length (Butcher et al., 1984).

The Gascoyne and Wooramel rivers drain into Shark Bay, but their flow is intermittent and their runoff is negligible (Logan & Cebulski, 1970), only transporting sediments after heavy rains caused either by tropical cyclones or winter storms (Logan, Read and Davies, 1970).

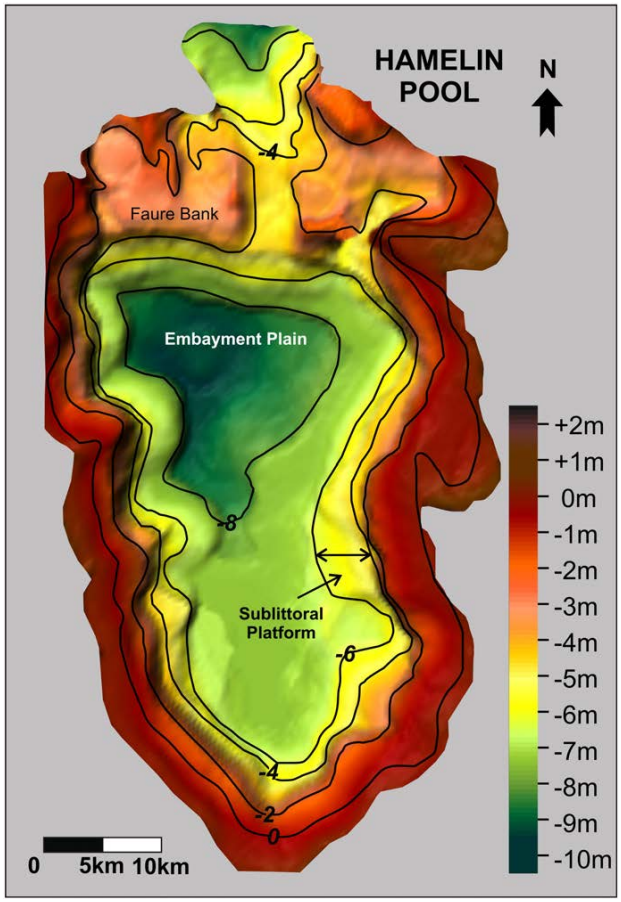

Figure 2.1 – Hamelin Pool bathymetric map (From: Jahnert and Collins, 2012).

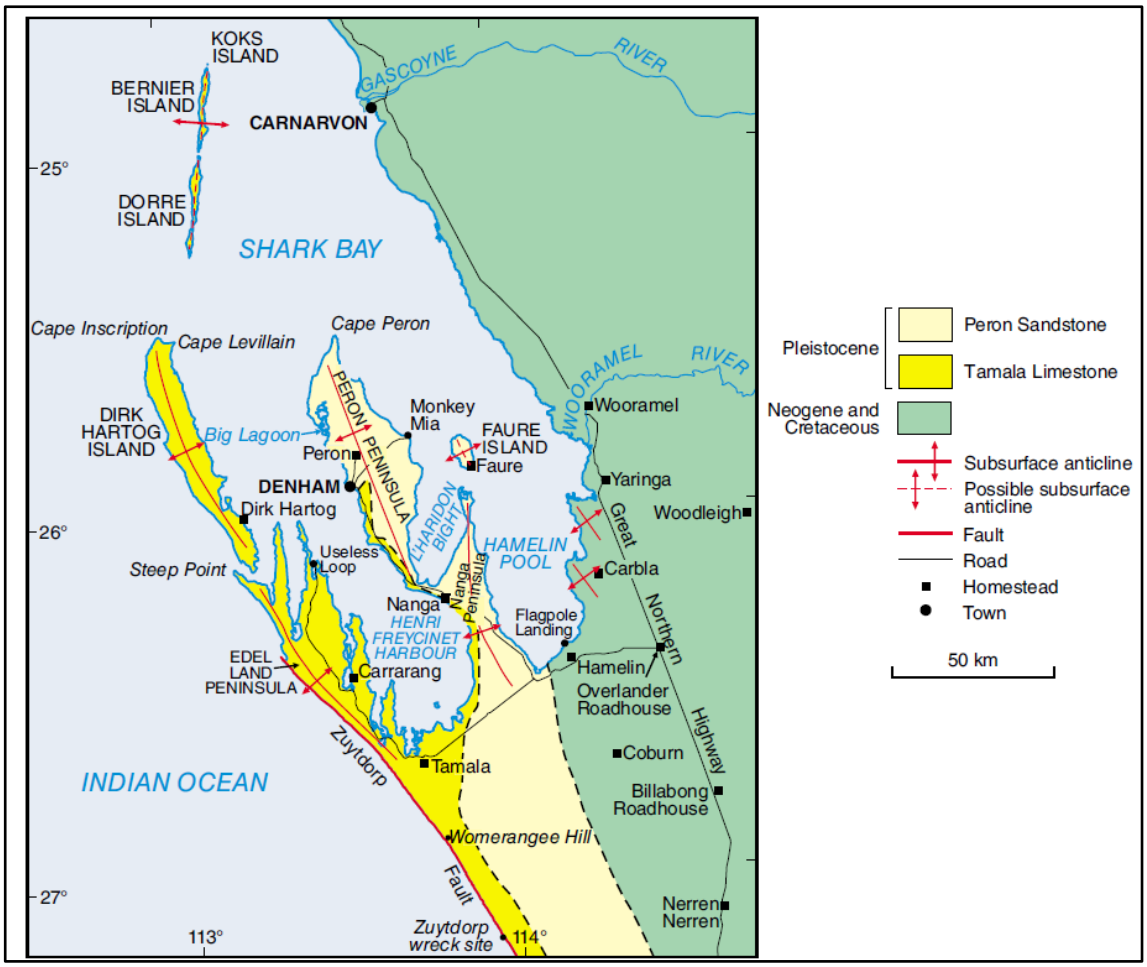

Figure 2.2 – Generalized geological map of Shark Bay vicinity (From: Playford et al., 2013).

Figure 2.3 – Evaporite pans ('birridas') in Peron Peninsula, Shark Bay.

2.1.2. Geology

2.1.2.1 Overview

Shark Bay is located in the Southern Carnarvon Basin at the central portion of the Gascoyne Platform, an elongate trough that shallows abruptly east and southward and gradually west and northward (Iasky et al., 2003). Seismic and gravity data indicate a northerly trending structural framework for the Gascoyne Platform (Iasky et al., 2003), also observed on the general orientation of the geomorphic features of Shark Bay area, such as peninsulas, islands, gulfs and inlets.

Apatite fission-track analysis and vitrinite reflectance data from wells on the Gascoyne Platform indicated major cooling episodes in the Early Permian, Late Jurassic, and Tertiary (Gibson et al., 1998 as cited in Iasky et al., 2003). These episodes may be related to the three main periods of tectonism known in the region: Late Carboniferous – Early Permian rifting, Late Jurassic rifting, and Miocene compression (Iasky and Mory, 1999; Iasky et al., 2003; Mory et al. 2003).

The infill of the Gascoyne Sub-basin is predominantly Silurian, with Devonian, Lower Carboniferous and minor Permian remnants in its northern part, and a westward-thickening Cretaceous and Cenozoic wedge (Hocking et al., 1987).

The Cretaceous sedimentary record in the Gascoyne Platform consists of the Winning Group, Haycock Marl, Toolonga Calcilutite, Korojon Calcarenite and Miria Formation. The oldest unit to outcrop in the Shark Bay area is the Toolonga Calcilutite, exposed over Carbla Plateau of the Yaringa Province. It consists of Santonian to Campanian age (Belford, 1958 as cited in Denman et al., 1985) fossiliferous mudstones deposited in low energy pelagic environments and is typically calcretized at the surface.

Quilty (1977) recognized four main Cenozoic sedimentation cycles in the Carnarvon Basin: (1) Late Paleocene to Early Eocene ; (2) Middle to Late Eocene; (3) Late Oligocene to Middle Miocene (4) Late Miocene to Holocene; suggesting that these cycles reflect major eustatic sea-level changes. The Tertiary sedimentary succession in the Gascoyne Platform consists of shallow-marine carbonate rocks (Cardabia and Giralia Calcarenites and Trealla Limestone; Hocking et al., 1987).

2.1.2.2. Quaternary Geology

2.1.2.2.1. Pleistocene

The Pleistocene climate was marked by repeated glacial events alternating with warmer interglacials. Throughout Australia, the interglacial periods were more humid and glacial times drier.

Glacial aridity is controlled by increased continentality, reduced precipitation and greatly intensified strength of atmospheric circulation (Bowler et al., 1976). The establishment of an arid climate led to the widespread formation of calcrete duricrust and development of prominent Pleistocene coastal dunes (Iasky and Mory, 1999) favored by accompanying reduced vegetation cover (Martin, 2006).

The Peron Sandstone consists of the oldest dune deposits in the Shark Bay area. The unit is composed of poorly consolidated quartz sandstones that are remarkably red in outcrop and forms the country rock of the Peron Province (Logan, Read and Davies, 1970). It overlies Cretaceous and Tertiary sediments unconformably and is overlain or onlapped by the Tamala Limestone (Logan, Read and Davies, 1970). A calcrete zone at the top of the Peron Sandstone has partially preserved the original morphology: a series of large interlinked transverse and longitudinal dunes (Hocking et al., 1987). The lack of marine fossils and the presence of soil profiles, containing insect pupal cases and rare land snails, confirm an eolian origin (Hocking et al., 1987).

The Tamala Limestone is present in most of the Edel Province and consists of a succession of limestone eolian dunes composed of consolidated to unconsolidated, coarse- to medium-grained, skeletal-fragment grainstone which commonly shows large-scale cross-bedding (Logan, Read and Davies, 1970). After the deposition of Tamala Limestone there were three separate marine sedimentation phases in the Shark Bay Region: Dampier, Bibra and the Holocene Transgression (Logan, Read and Davies, 1970).

The Dampier Limestone is the oldest marine Pleistocene unit in Shark Bay and outcrops in areas of the Edel and Peron Provinces. The unit, which is 30 to 120 cm in thickness, is composed mainly of pelecypod limestone (coquina), foraminiferal limestone, and lithoclast grainstone (Logan, Read and Davies, 1970). The Carbla Oolite Member occurs on the south-eastern parts of Shark Bay and is recognized as pertaining to the Dampier marine phase. It is a well-sorted largely unfossiliferous ooid grainstone, with a discontinuous basal fossiliferous conglomerate (Hocking et al., 1987). During Dampier Marine Phase normal oceanic salinities (35 - 40)

prevailed, increasing to metahaline (40 - 56) in restricted southern embayments and inlets (Logan, Read and Davies, 1970).

The Bibra Limestone (Figure 2.4) is a thin unit of coral biostrome, pelecypod coquina, and skeletal grainstone that crops out in the intertidal zone at several localities throughout the Shark Bay region (Logan, Read and Davies, 1970). The Bibra Formation appears to be absent from the Quaternary section in offshore, embayment-plain areas of Shark Bay (Logan, Read and Davies, 1970) and is believed to have formed during the last Pleistocene interglacial high sea-level stand, ca. 120,000 to 130,000 years ago (van de Graaff et al., 1983). The fossil content in Bibra Limestone is open-marine (Logan, Read and Davies, 1970) indicating that hypersaline conditions were not present in Hamelin Pool at that time.

Figure 2.4 – Open marine fossil content of a Bibra Limestone outcrop containing coral fragments and bivalve mollusk shells.

HOLOCENE-RECENT INTERVAL	Postglacial marine sequence, 0–30 ft thick, mainly marine carbonates. Skeletal-fragment sands, coquinas, ooid sands, stromatolitic sediments and structures, quartz sands, evaporites; minor deltaic sediments, Gascoyne and Wooramel Rivers. Transgressive, overlies all older units with erosional unconformity.	Postglacial beach-ridge and dune deposits; 2–35 ft thick; coquinas, ooid sands, skeletal-fragment and quartz sands, evaporites.
	Erosion surface with calcrete layers, weathering profiles, and incipient soil formation.	
"LATE" PLEISTOCENE	*Bibra Formation:* 2–3 ft thick. Marine carbonate sediments, skeletal-fragment sands, coquinas, and coral biostromes. Minor deltaic sediments, Gascoyne and Wooramel Rivers abandoned (?) subdeltas. Transgressive, overlies all older units with erosional unconformity.	Minor beach-ridge and dune deposits, as above.
	Erosion surface with calcrete layers, weathering profiles, and incipient soil formation. *Depuch Formation* in Edel Province.	
"MIDDLE" PLEISTOCENE	*Dampier Formation* and equivalent *Carbla Oolite:* 2–30 ft thick. Marine carbonate sediments, ooid grainstones, coquinas, skeletal-fragment sands. Transgressive, overlies all older units with erosional unconformity.	Minor beach-ridge and dune deposits, as above.
	Erosion surface	
"EARLY" PLEISTOCENE	*Tamala Eolianite:* max. thickness 500 ft. Skeletal-fragment calcarenites, material derived from adjacent shelf. Possible age, early Pleistocene. Overlies Peron Sandstone. *Peron Sandstone:* max. thickness 400 ft. Red, ferruginous quartz sandstones; probably laid down in dunes. Overlies older Tertiary and Cretaceous rocks with erosional unconformity. Possible age, Pliocene-early Pleistocene.	
	Unconformity	
	Tertiary and Cretaceous formations: *Toolonga Calcilutite, Giralia Calcarenite* (?), *Trealla Limestone.*	

Table 2.1 – Summary of Quaternary Stratigraphy, Shark Bay (From: Logan, Read and Davies, 1970).

2.1.2.2.2. Holocene

After the last glacial maximum a rapid transgression took place as a response to warming of the Earth and consequent glacial retreat during the Holocene. Collins et al. (2006) indicate a Holocene high-stand of about +2m at approximately 6800 U/Th years BP using coral pavement data from Houtman Abrolhos Islands, Western Australia. Other authors have also recognized evidence for falling sea-level conditions in Shark Bay during the last 6000 years BP (Logan et al., 1970; Logan et al., 1974; Jahnert and Collins, 2011; Jahnert and Collins, 2013).

Following the late Holocene maximum flooding, sea level falling conditions along with the growth of the Faure barrier bank and a highly evaporative semi-arid climate were responsible for the onset of hypersaline conditions in Hamelin Pool and L'Haridon bight basins within Shark Bay (Logan, Read and Davies, 1970; Hagan and Logan, 1974). Highly specialized species such as the mollusk *Fragum erugatum* and microbial benthic communities, which were able to bear hypersalinity, flourish in this environment where competition and predation are limited. Jahnert and Collins (2013) proposed an idealized sedimentary cycle pattern that reflects regression and salinity increase in Shark Bay during the Late Holocene (Figure 2.5).

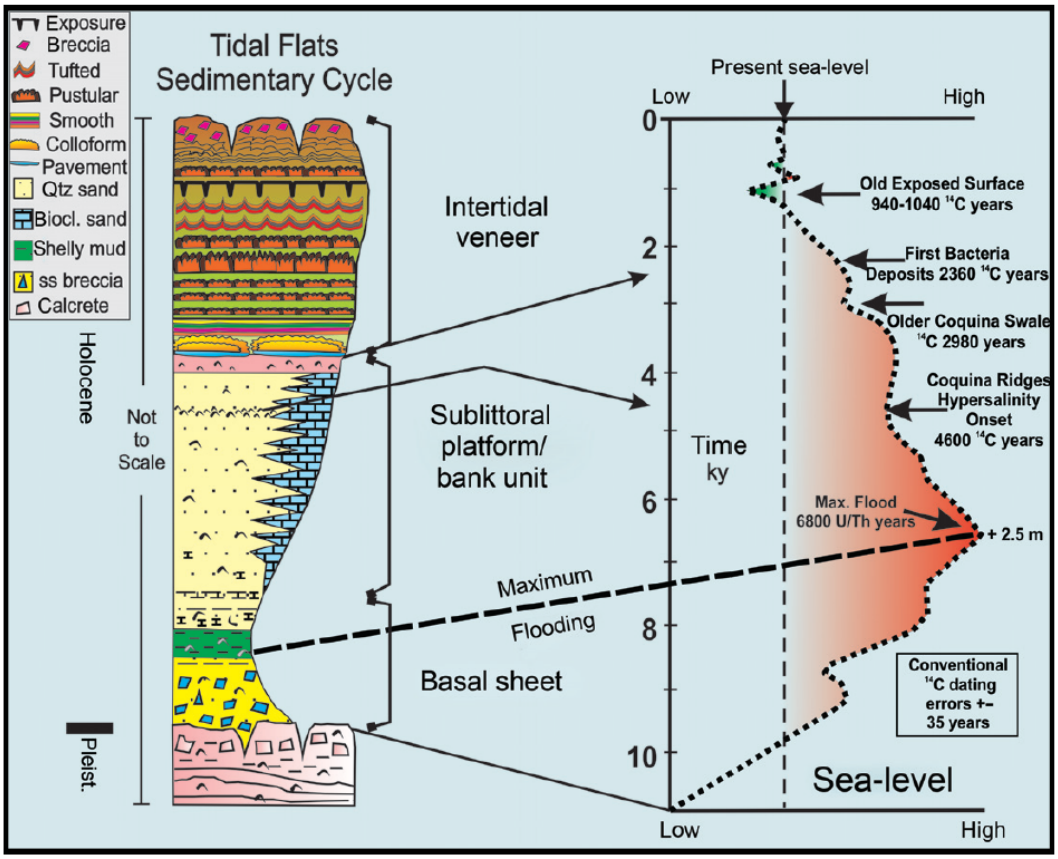

Figure 2.5 - Idealized sedimentary cycle pattern for the Late Holocene correlated with sea-level variations proposed by Jahnert and Collins (2013).

Modern and Late Holocene marine sedimentation in Shark Bay is composed mainly of biogenic carbonate sediments although ooids, intraclasts and other carbonate particles are also important (Logan, Read and Davies, 1970).

In the hypersaline environment of Shark Bay (Figure 2.6) the sediments consist mainly of microbial mats, stromatolites, thrombolites, cryptomicrobial deposits and coquinas (Logan et al., 1970; Logan et al., 1974; Jahnert and Collins, 2012). In the supratidal zone of Hamelin Pool and L'Haridon Bight occurs the Hamelin Coquina, a beach ridge system composed essentially of *Fragum* shell coquinas and secondarily grainstones whose constituents are, in variable proportions, ooids, bioclasts, intraclasts and quartz (Hagan and Logan, 1974). The intertidal zone has a dominance of microbial mats and heads, particularly pustular and tufted microbial deposits. Jahnert and Collins (2012) show that microbial deposits are extensive in the subtidal zone of Hamelin Pool Marine Reserve consisting mainly of smooth and colloform stromatolites and cryptomicrobial cerebroid structures and pavements. These authors also report a dominance

of seagrass and related bioclastic and quartz sand in areas lacking microbial carbonates and that in the "Embayment Plain" sedimentation consists of bivalve coquina, serpulids and algae.

Figure 2.6 – Shark Bay hypersaline environment. Coquina beach and microbialites in Hamelin Pool.

2.1.3. Environment

2.1.3.1. Climate and Winds

The climate is semi-arid presenting an average rainfall between 200 and 300 mm which is surpassed by the annual evaporation of 2400-2800 mm (Logan and Cebulski, 1970; Bureau of Meteorology, n.d.-b). Most precipitation occurs in winter months except for sporadic heavy rains associated with tropical cyclones. Annual average maximum temperatures are between 27 and 30^{o}C and minimum between 15 and 18^{o}C (Bureau of Meteorology, n.d.-a).

Prevailing winds are from the south (Figure 2.7) and are particularly strong during October to March, when velocities are 18-28 km/hour. During winter, winds tend to be more easterly and southeasterly, occasionally northerly (Bureau of Meteorology, n.d.-d). Tropical cyclones (Figure 2.8) occur periodically and are accompanied by gales (average 70-110 km/hour, gusting up to 180 km/hour) directed from east and northeast quadrants and heavy rainfall (Logan and Cebulski, 1970; Hagan and Logan, 1974).

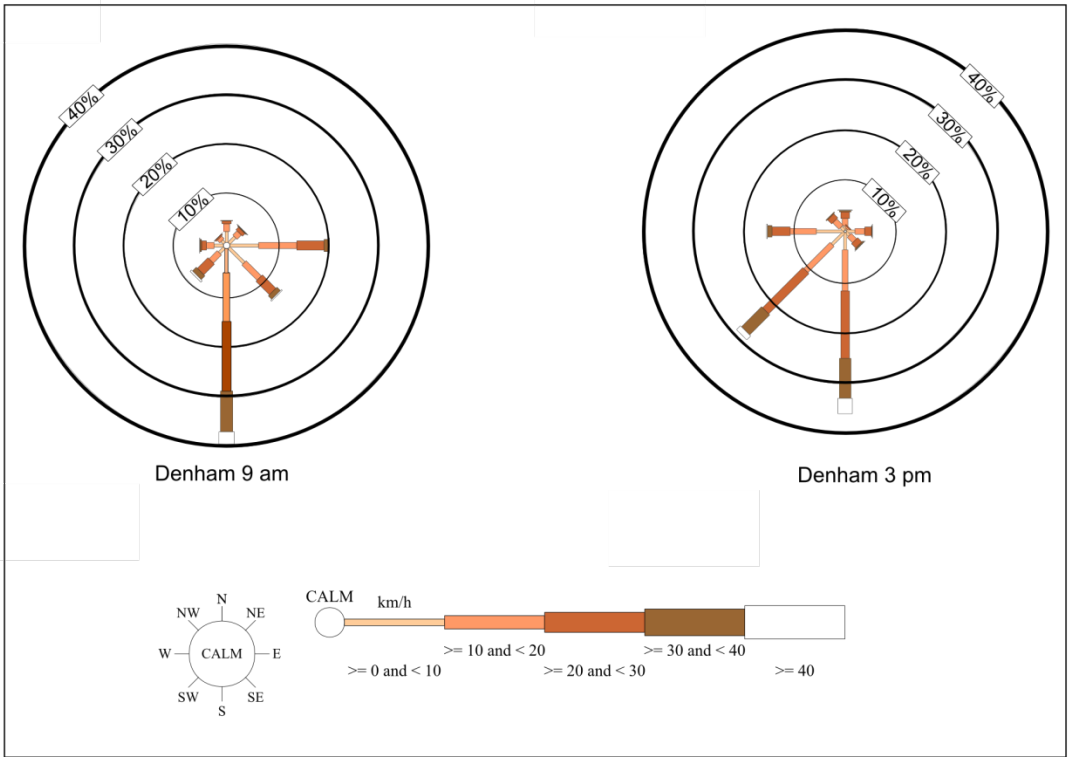

Figure 2.7 - Wind direction versus Wind speed in km/h at Denham location (Bureau of Meteorology, n.d.-d).

2.1.3.2. Waves, Wave Currents, Tides and Tidal Currents

The prevailing southerly winds can subject coasts with southeast or southwest aspect to wave action. Prevailing waves overpassing shallower areas of the bay generate longshore currents that tend to transport sediment particles along the shores in a net south-to-north direction. This longshore drift is particularly strong on eastern shores (Hagan and Logan, 1974). Although coasts with north and northwest aspect are infrequently subject to wave attack, they show several indications of substantial sediment transport as observed in the beach ridges, barrier islands and spits. In these areas sediment movement is probably driven by periodic storms which cause waves larger than normal to propagate from the north and affect north facing shores (Logan and Cebulski, 1970; Hagan and Logan, 1974).

The tidal regime in Shark Bay is mixed diurnal and the tidal range is approximately 1 meter (microtidal). In the eastern Gulf the tides are mainly semi-diurnal whilst in the western Gulf the tides are mainly diurnal (Burling et al., 2005). Logan and Cebulski (1970) suggest the tide is the major factor causing water circulation in the bay.

Tidal currents are of great importance on sills and sub-littoral platforms. Hagan and Logan (1974) report velocities as high as 90 cm/s in channels and up to 45 cm/s in sub-littoral

platforms and point out the importance of currents generated by tidal run-off in scouring microbial mats at the intertidal zone of certain areas.

Logan and Cebulski (1970) evoke ebb dominance on west-facing coasts when the prevailing south to north wind drift interacts with tides, while on east-facing coasts the lowering of levels by wind set-up produces flood dominance.

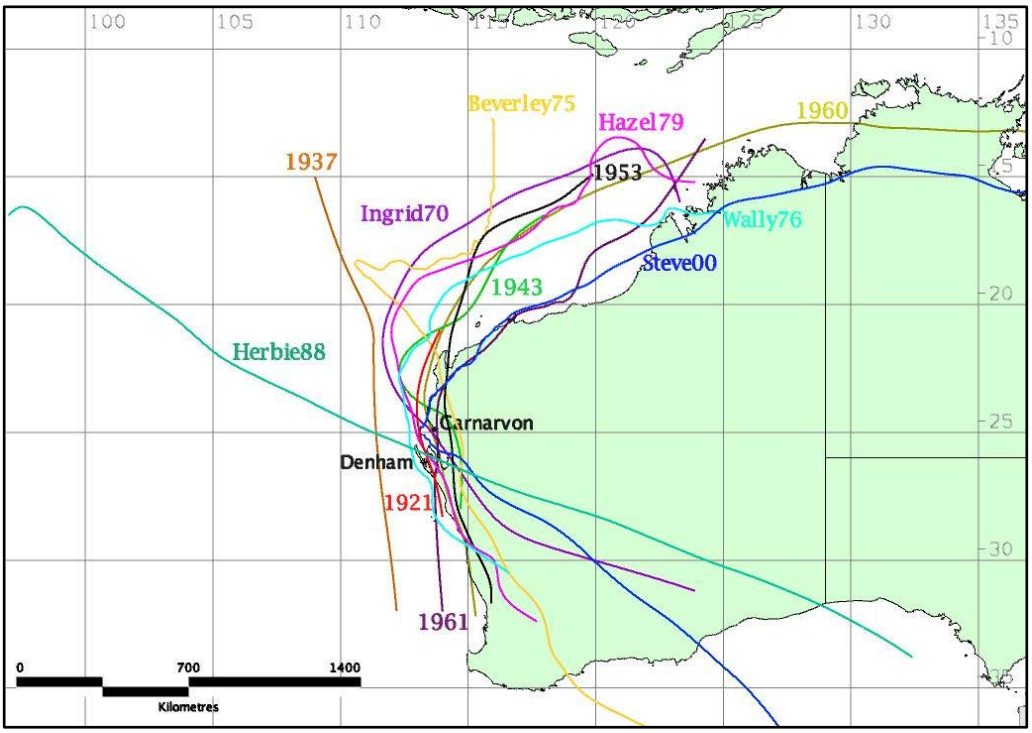

Figure 2.8 – Tracks of remarkable cyclones affecting Shark Bay (Bureau of Meteorology, n.d.-c)

2.1.3.3. Salinity and Hydrologic Structure

Logan and Cebulski (1970) subdivided Shark Bay waters into three separate categories: (1) oceanic, with salinities ranging from 30 to 40; (2) metahaline, where salinities range from 40 to 56; (3) hypersaline, with salinities from 56 to 70 (Figure 2.9). Shark Bay salinity distribution complies with the pattern of an inverse estuary exhibiting a general increase in salinity (and density) to the south, starting from oceanic salinity at the seaward opening to metahaline and hypersaline waters in the bay heads. Faure sill provides the circulation restriction, which in addition to high evaporation, causes the hypersaline conditions in Hamelin Pool and L'Haridon Bight basins. Water columns are isohaline surface to bottom and stratification occurs only in tidal channels with temporary overflow events (Hagan and Logan, 1974).

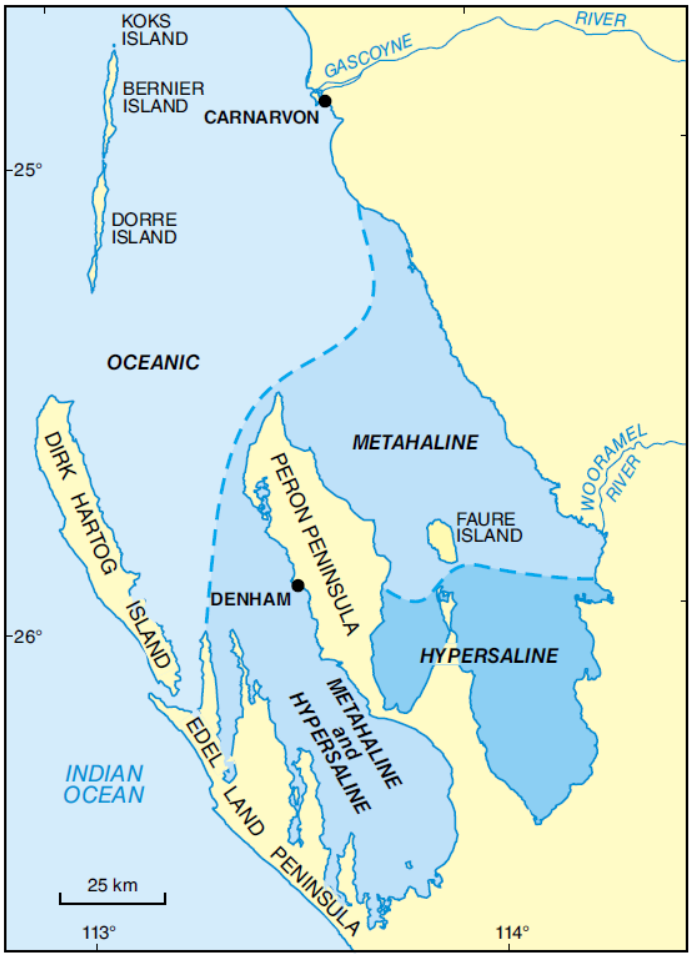

Figure 2.9 – Hydrologic structure of Shark Bay displaying 3 major categories separated by major salinoclines: oceanic, metahaline and hypersaline (Playford et al. (2013); after Logan and Cebulski (1970)).

2.1.3.4 Biota

Shark Bay has abundant and diverse organisms, many of which play an important role in carbonate sedimentation. Logan and Cebulski (1970) recognized three biotic groups (oceanic, metahaline and hypersaline) that are fairly coincident with the water salinity distribution within the bay. The suppliers of carbonate particles in order of abundance are coralline algae, mollusks, foraminifers, echinoids, serpulids and bryozoans (Logan and Cebulski, 1970). Seagrass communities play an important role by stabilizing the floor, trapping and baffling sediment and offering a substrate for habitation by several organisms (Logan and Cebulski, 1970). Microbial communities play a major role in trapping and binding sediments and also bio-inducing carbonate precipitation in intertidal and subtidal environments especially in hypersaline settings (Jahnert and Collins, 2011; 2012).

2.1.3.5. Biology of Fragum erugatum

In the hypersaline environment, the small cockle (< ≈ 15 mm long) *Fragum erugatum* is the major shell-secreting organism to provide particles for carbonate sedimentation. Despite living *Fragum erugatum* occurring in the subtidal zone, between 1.2 m and 6.5 m depth (Berry and Playford, 1997), a vast amount of shells are washed ashore by extreme events and accumulateas supratidal coquina ridges. The hypersaline, oligotrophic waters of Hamelin Pool and L'Haridon Bight lack a substantial food source for suspension feeders. Berry and Playford (1997) suggested that the unicellular photosymbiont zooxanthellae within F. *erugatum*, contribute with a significant portion of nutrients to the bivalve mollusk pointing out that the maximum depth distribution of *F. erugatum* would be limited by light penetration required for photosynthesis by its zooxanthellae. This small bivalve occurs in large numbers ($4000/m^2$) and probably completes its life cycle in 1 year (Morton, 2000). Berry and Playford (1997) determined through histological examination of the F. *erugatum* gonads that the species is reproductively active within Hamelin Pool and L'Haridon Bight; however the origin of larval recruitment to these restricted basins is not known.

2.2. Beach Ridges

2.2.1. Introduction

Beach ridges are coastal progradational landforms, approximately parallel to the coast which develop as a product of multiple nearshore processes. This diversity of formative (and interactive) processes led to confusion about the descriptive terminology of beach ridges (Taylor and Stone, 1996; Otvos, 2000; Hesp, 2006; Tamura, 2012).

Some authors proposed formal definitions for the term 'beach ridge' in an attempt to constrain its use, even though consensus is yet to be achieved. Otvos (2000) proposed a broad definition which designates beach-ridges as relict eolian and wave-built shore ridges whose clast dimensions can vary from fine sand to gravel. Hesp (2006) proposed a genetically restrictive re-definition of the term 'beach ridge' stating that they are entirely wave built and should be clearly set apart from 'berm' and 'foredune'. Taylor and Stone (1996) accepts beach ridges as being deposited by wind and wave processes occurring at the limit of the wave run-up but emphasizes that they should be clearly distinguished from cheniers.

Beach ridges are sensitive to changes in climate, coastal hydrodynamics, sediment supply and sea level, being useful indicators of environmental changes. Nevertheless, extra caution is required when using beach ridges for palaeoenvironmental interpretations as they originate by a number of coastal processes that may superimpose each other. Ground-penetrating radar (GPR)

in conjunction with radiocarbon and optical dating are advances that have been increasingly adopted in recent beach ridge studies.

2.2.2. Origin

Some mechanisms responsible for beach ridge formation and evolution have been documented in the literature and can be summarized in three main categories (Taylor and Stone, 1996; Otvos, 2000; Hesp, 2006; Tamura, 2012): (1) High-energy waves inundating the coast; (2) Beachface progradation under fair-weather waves; (3) Welding of longshore bars (Figure 2.10).

High-energy storm waves have been considered as agents for constructing coarse clast ridges which may be composed of gravel, coral rubble and shells (e.g. McKee, 1959; Nott, 2006; Nott, 2011; Jahnert et al., 2012; Tamura, 2012 and references therein). Although it is debatable whether storm waves can originate sandy beach ridges, Psuty (1967) attributed the construction of the ridges in Tabasco to overwash processes during storms. He observed that the ridges internal structure was largely composed of landward-dipping stratification. Moreover, Bendixen et al. (2013) proposed a model for sandy berm and beach-ridge formation where shallow bars migrate onshore during fair-weather conditions forming an incipient berm during somewhat high-water levels. In higher water and energy conditions (storms) the incipient berm is eroded to be deposited further up on the beachface expanding an already existing mature berm or originating a new one (Bendixen et al., 2013).

The formation of beach ridges under fair-weather waves is also stated in the literature. Tanner (1995) described sandy beach ridges and swales that are swash built and formed by decadal-scale sea level oscillations of 5-30cm amplitude. Several authors considered sand berms as the nucleus for beach ridges (Otvos, 2000 and references therein). Notably, it is still under debate whether berms can form under the dominance of fair-weather processes, or high-water levels coupled with high-energy conditions are fundamental to berm formation. Furthermore, Davies (1957) considered that vegetation growing on top of these berms would favor trapping of aeolian sand and develop a ridge having the backshore landward of the berm crest to form the swale.

Welding of longshore bars is a third important mode from which beach ridges can originate. Bars migrating onshore are welded to the beachface feeding the beach ridge system with new sediment. The newly accumulated sediment can be later reworked by swash processes. Carter (1986) reported a gradual accretion of longshore bars to form the berms and ridges of the beach-ridge plain at Magilligan, Ireland. Hine (1979) emphasized the role of swash-bar welding in berm development along a barrier spit complex in Cape Cod, Massachusetts and showed that occasionally the berm structure would preserve the swash bar morphology originating what he

called 'berm-ridge'. Lindhorst et al. (2008) showed that the welding of swash bars is the dominant processes responsible for ridge growth in a Holocene barrier spit in Sylt, Germany.

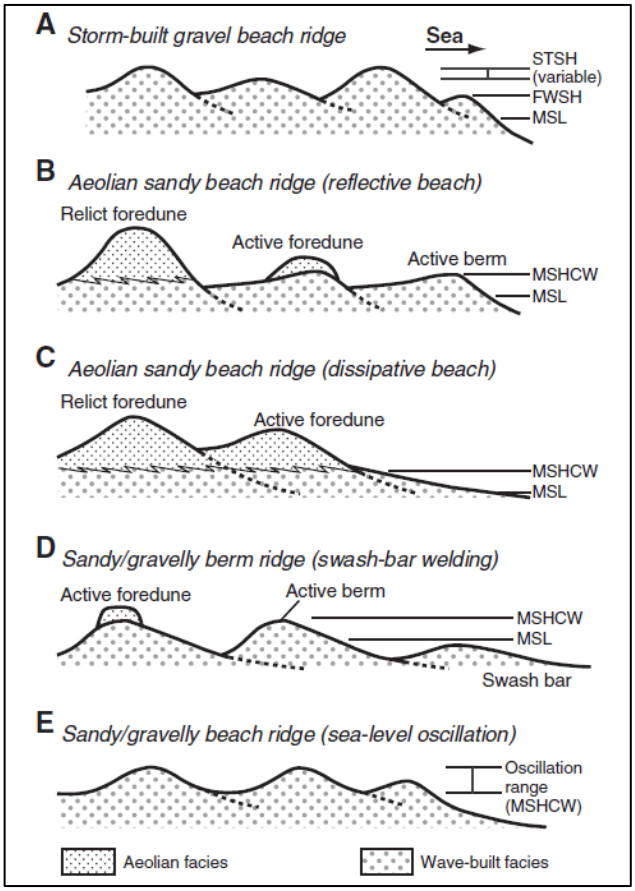

Figure 2.10 - Schematic illustration showing processes of beach-ridge formation from Tamura (2012). MSL, mean sea level; FWSH, fair-weather wave swash height; STSH, storm wave swash height; MSHCW, maximum swash height of constructive wave.

2.2.3. Internal Structure

Although the most common structure in beach environments is low-angle seaward dipping planar bedding related to swash processes in the beachface, beach ridges and berms often exhibit landward dipping structures. Overwash, overtopping and welding of swash bars are processes that generate gentle to moderately inclined landward dipping planar bed geometries within the ridges. Furthermore, reworking by aeolian processes and longshore currents generate bedding in the prevailing wind and longshore current directions. In isolated storm-surge ridges, Tanner (1995) commented on roughly concentric convex-up bedding. Keen and Stone (2000) also observed a concentrically bedded sand bar deposited by hurricanes in the subaerial beach and another sand bar with contrasting ridge internal geometry containing horizontal, cross bedding and erosion surfaces.

Tamura (2012) summarized the internal structures of beach ridges as reported in the literature (Figure 2.11).

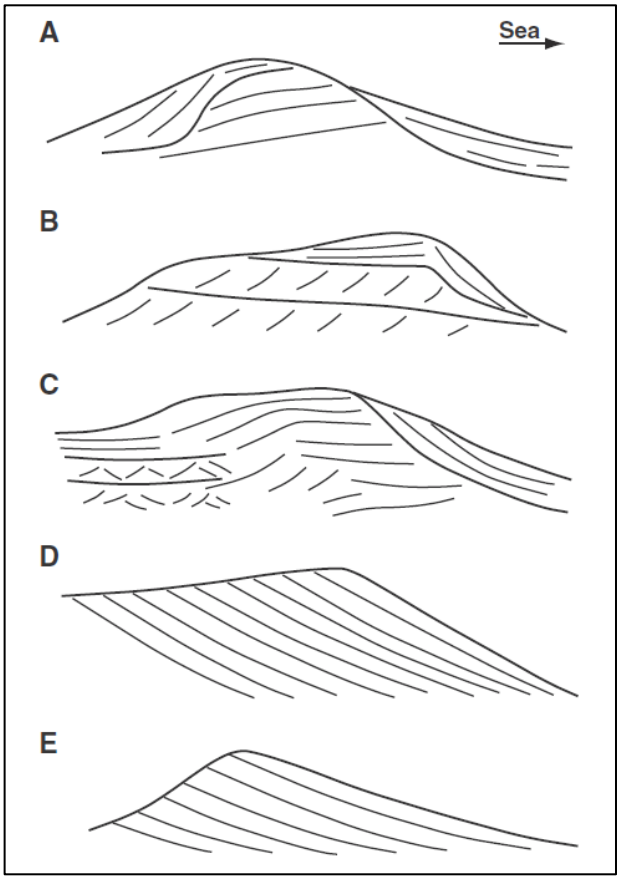

Figure 2.11 - Internal geometries of beach ridges reported by (A) Psuty (1965), (B) Hine (1979, (C, D) Carter (1986), and (E) Tanner and Stapor (1971). From Tamura (2012).

Chapters 3 and 4 deal with the internal geometry and evolution of a unique coarse clastic beach-ridge system generated by storm events transporting ashore shells from a hypersaline environment which facilitates high skeletal production of specialized bivalve mollusk *Fragum erugatum*.

2.3. Shell Concentrations

Shell concentrations are accumulations of ≥2mm biomineralized remnants of invertebrate animals preserved in their original mineralogies or as molds, casts or replaced by other minerals (Kidwell, 1991). These bioclastic gravels may have siliciclastic, carbonate or virtually no matrix. The term ‘coquina’ is normally used for allochthonous shell deposits, however it is not uncommon to use ‘coquina’ as a synonym for shell concentrations in general.

The processes that originate shell concentrations are either primarily biogenic, when the dense shell concentration is due to biologic processes, or physical, when erosion, transport and redeposition of skeletons generate the concentration. Kidwell et al. (1986) also referred to diagenetic processes as a third end-member capable of generating dense shell concentrations. Diagenetic concentrations occur when physical and chemical processes act after burial increasing the fossil density in a given deposit. Often the interplay of the end-member processes or the overprint of a concentration of one type by later processes of different nature originates mixed origin shell concentrations. Kidwell et al. (1986) proposed a broad genetic classification for skeletal concentrations based on these three end-members (Figure 2.12).

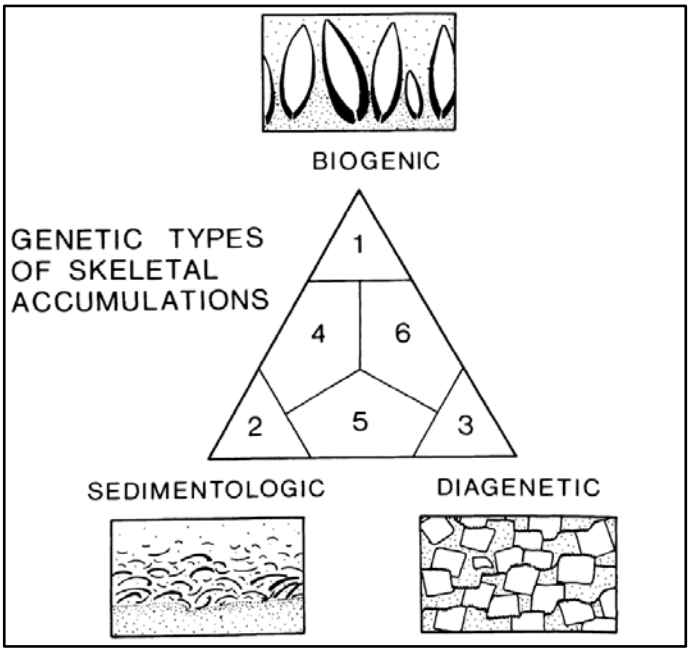

Figure 2.12 – Conceptual framework for the origin of shell concentrations based on three end-member groups of concentrating processes (Kidwell et al., 1986).

A broader process-related classification by Fürsich and Oschmann (1993) described nine types of skeletal concentrations in Jurassic shell beds of Kachchh basin, western India. These range along the onshore-offshore gradient from nearshore wave concentrations to offshore condensed concentrations (Figure 2.13).

The following sections present examples of ancient and Holocene shell concentrations aiming to exemplify the broad spectrum of environments, ages and formative processes they encompass.

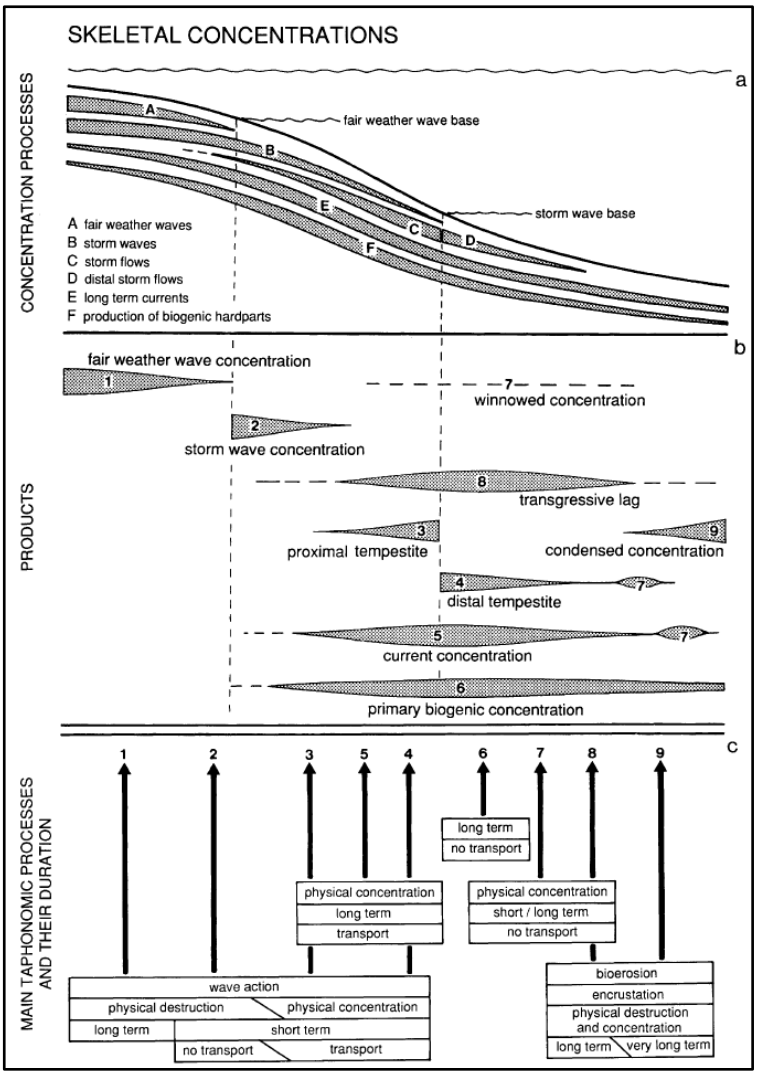

Figure 2.13 - Process-related classification of shell concentrations along an onshore-offshore transect based on data from the Jurassic of western India (From Fürsich and Oschmann (1993)).

2.3.1. Ancient Examples of Shell Concentrations

2.3.1.1. Lower Cretaceous lacustrine shell concentrations from Campos Basin, SE Brazil

Campos Basin is a prolific sedimentary basin in the Brazilian continental margin, located offshore of the State of Rio de Janeiro. The Lagoa Feia Group is an important stratigraphic unit in Campos Basin as it encompasses important petroleum reservoirs and prolific source rocks. The Itabapoana and Coqueiros Formations from the Lagoa Feia Group comprise alluvial-lacustrine sediments that were deposited during the Early Cretaceous (Eobarremian to Eoaptian) in a saline rift lake system (Carvalho et al., 2000; Winter et al., 2007).

The coquinoid facies consisting of bivalve calcirudites and secondary bioclastic, gastropod or ostracod calcirudites/calcarenites occur in the Coqueiros Formation and are intercalated with organic-rich shales (Carvalho et al., 2000; Winter et al., 2007).

The Eobarremian to Eoaptian thick bivalve coquina deposits (predominantly calcirudites and calcarenites) result from high-energy conditions generated by storm events, transporting and reworking shells as layers with and without matrix (Carvalho et al., 2000).

Carvalho et al. (2000) defined seven facies associations within the Eobarremian to Eoaptian interval of Lagoa Feia Group and interpreted them as related to the following depositional environments: (1) bioclastic sandy beaches, (2) bioclastic calcarenite beaches, (3) marginal, (4) bioclastic bars (Figure 2.14), (5) bioclastic sheets/bar fringes, (6) bioaccumulation banks, and (7) deep lacustrine. An extremely wave-influenced paleolake favored the deposition of bivalve calcirudites under high-energy conditions along syndepositional highs, whereas low-energy carbonate facies occur in more protected zones (Carvalho et al., 2000).

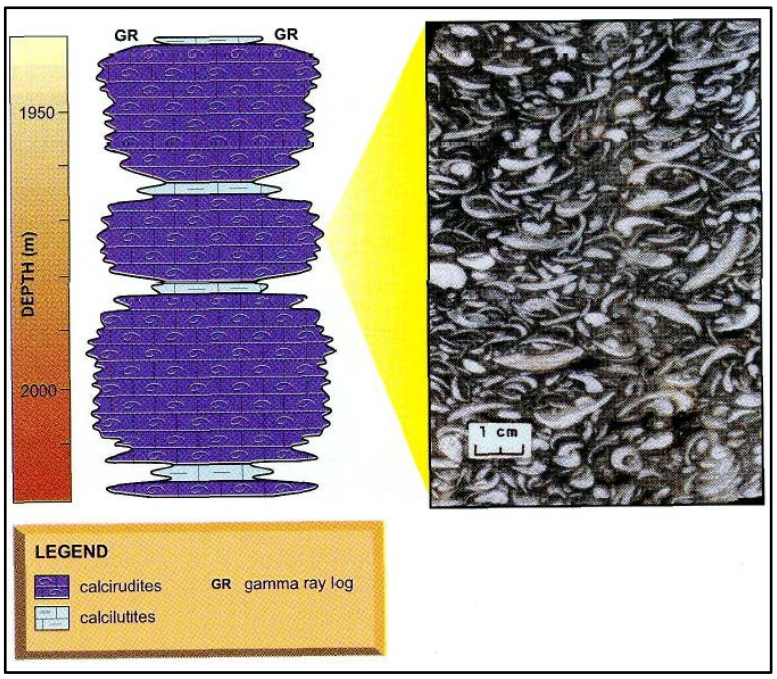

Figure 2.14 – Gamma ray log response and facies interpreted as pertaining to bioclastic bar deposits (Carvalho et al., 2000)

2.3.1.2. Upper Cretaceous shell concentrations from Cauvery Basin, southern India

Theupper Campanian-Maastrichtian Kallankurichchi Formation is approximately 40 m thick consisting of bioclastic limestones that may contain minor amounts of quartz sand (Guha and Mukhopadhyay, 1996 as cited in Fürsich and Pandley, 1999). These limestones encompass extensive shell concentrations dominated by large bivalves with minor amounts of larger

foraminifera, brachiopods and bryozoans. These skeletal components and biogenic sediments are abundant suggesting high biogenic productivity of hardparts. Moreover, high species abundance and large size of some specimens evidence optimal conditions for growth. In this context, Fürsich and Pandley (1999) reasoned that the benthic fauna of the Kallankurichchi Formation is characteristic of a low stress shallow water environment. Furthermore, these authors classified the late Cretaceous shell concentrations of Cauvery Basin according to the taxon or taxa that predominate in the skeletal material and traced their genetic histories based on the biofabric and taphonomic signature of their components. This approach made it possible for Fürsich and Pandley (1999) to deduce four principal formative agents of shell concentrations in the Kallankurichchi Formation: storm induced waves and currents, reduced sediment input, settling behaviour of taxa and productivity. In addition, these authors attempted to classify the shell concentrations studied according to the types proposed by Fürsich and Oschmann (1993) (Figure 2.13) and concluded that the shell beds pertain to the following genetic types: storm wave, proximal tempestite and primary biogenic. These types are in accordance with the inference of a shallow water depositional environment, clearly below fair weather wave base, although partially affected by storms.

2.3.1.3. Miocene brachiopod concentrations from Guadix Basin, southern Spain

Densely packed brachiopod shell concentrations outcrop in the northern margin of the Guadix Basin, one of the Neogene-Quaternary intramountain basins located in the Betic cordillera, southern Spain. Reolid et al. (2012) showed that the brachiopod *Terebratula terebratula* formed tens of centimeter- to meter-scale concentrations in a shallow siliciclastic, high-energy environment related to a seaway that connected the Atlantic Ocean to the Mediterranean Sea during the middle Miocene. These concentrations were parautochthonous in a prodelta setting and thin, predominantly allochthonous, tide and storm-reworked concentrations in offshore settings. Reolid et al. (2012) also showed differences in taphonomic features between prodelta and more offshore shell beds associated with differences in energy levels and rates of sedimentation leading to higher fragmentation and disarticulation, better sorting and a high proportion of convex-up oriented shells in more distal 3D-dunes and 3D-megaripples, indicating long-term activity of high-energy bottom currents. These currents, amplified by the geomorphic configuration of the seaway, reworked the brachiopods from shoreface-prodelta settings to more distal areas in an inner ramp setting (Figure 2.15).

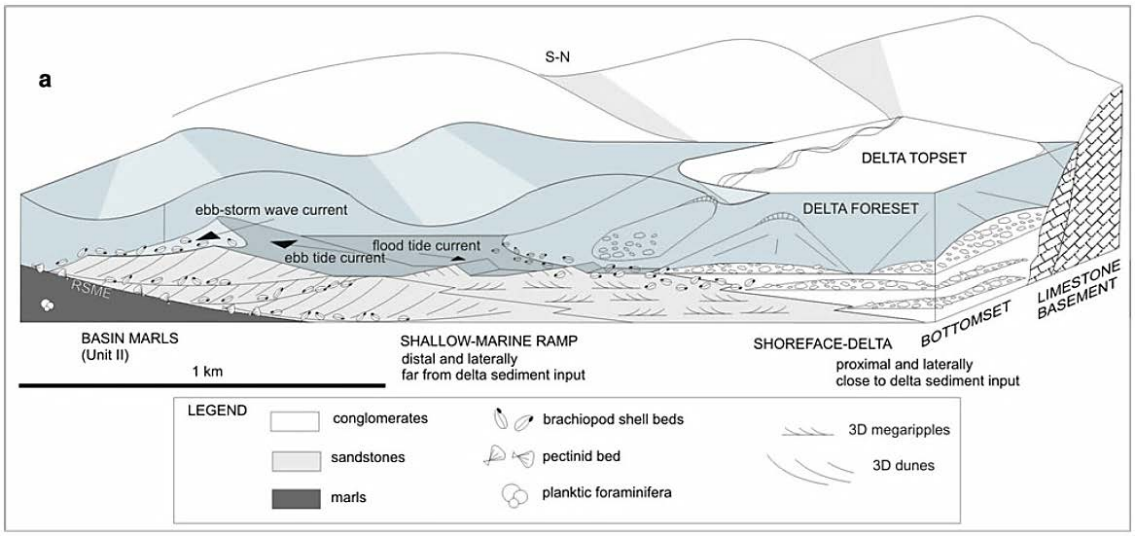

Figure 2.15 – Scheme illustrating distribution of depositional systems where the brachiopod shell concentrations occur (Reolid et al., 2012).

2.3.1.4. Miocene chemoherms of the northern Apennines, Italy

Hydrothermal and hydrocarbon venting sites are extreme environments of uncommon and variable fluid chemistry which have been discovered to be populated by thriving benthic fauna benefiting from chemosymbiosis to feed (Aharon, 1994; Hickman, 2003).

The Miocene sedimentary record of the Apennines in Italy display limestone blocks (locally known as 'calcari a lucina') densely packed with large bivalves interpreted as cold vent deposits (Conti and Fontana, 1999). These chemoherms generally display a monotonous and poorly diversified macrofauna composed mainly by lucinids and exhibit very negative $\delta^{13}C$ values (Taviani, 1994).

The Miocene appenninic chemoherms (Figure 2.16B) occur in diverse marine environments, from outer shelf to deep basins, and are not diagnostic of a specific paleogeographic or paleotectonic setting (Conti and Fontana, 1999).

Conti and Fontana (1999) described 2 types of primary chemoherms. The first consists of calcilutitic to calcarenitic carbonate bodies (pinnacles and lenses) with a close distribution, disconnected by marly and arenitic mudstones. Their dimensions range from 10 m to 200–300 m; the thicknesses are very uneven (5–30 m). The second type of primary chemoherm comprises several marly-calcareous lenses or irregular column-like bodies with dimensions from 20 cm to 5 m and thicknesses from 20–30 cm to 3 m. These carbonate bodies are dispersed and unrelated to a particular stratigraphic level and surrounding sediments consist of marls and mudstones. Furthermore, Conti and Fontana (1999) also reported brecciated structures and

interpret them as a result from fluid expulsion processes, not discarding extra reworking by gravity processes as fluidization intensified the instability of mudstones in which chemoherms are enclosed, favouring slumping processes.

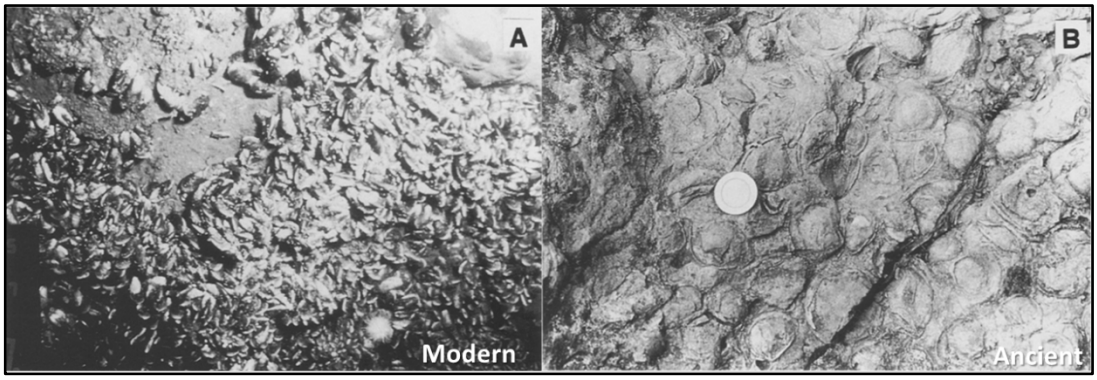

Figure 2.16 – Bivalve-rich chemoherms (Aharon, 1994). (A) Northern Gulf of Mexico (modern); (B) northern Apennines, Italy (Miocene), limestone with abundant lucinids.

2.3.1.5. Pliocene composite shell concentration of Salento, Italy

The Salento Peninsula is bordered by the Adriatic and the Ionian seas, located in the vicinity of seismically active coastal areas. Several thin shallow-water units constitute the local Plio-Pleistocene succession in the area, being composed mainly of bioclastic packstone and grainstone to rudstone (Massari et al., 2009). A Pliocene composite shell concentration, exhibiting species that live in very different shallow-marine environments, was interpreted by Massari et al. (2009) as a tsunami deposit they denominated 'T-layer' (Figure 2.17), a bioclastic packstone to floatstone with very high moldic porosity, containing debris of bivalves, gastropods, serpulids, bryozoans, fragments of echinoids, miliolids and rare planktonic foraminifers.

Massari et al. (2009) interpret the shell concentration ('T-layer') probably formed in a protected bay and is related to a tsunami event, providing several evidence to support this coquinoid tsunamite interpretation: (1) substantial erosion before deposition; (2) infilling of the scoured surface; (3) draping of previous substrate; (4) shells are well preserved with indications of erosion and transport of living bivalves and rapid burial; (5) different sources of sediment evidenced by grain bimodality; (6) Unusual shell assemblage across a large range of environments; and (7) occurrence of up to six sub-layers that are usually graded, indicating deposition took place during up to six surges (train of tsunami waves).

Figure 2.17 – Aspect of the Pliocene shell concentration interpreted as a coquinoid tsunamite (Massari et al., 2009).

2.3.1.6. Plio-Pleistocene Shell Concentrations in the Gulf of California

The Gulf of California is more than 1000km long and ranges from 90 to 210km in width. It is a trans-tensional rift basin linking the East Pacific Rise with the San Andreas Fault System. Meldahl (1993) reported on a total of 40 shell beds in Plio-Pleistocene sediments deposited at depths up to 10-15m on littoral or sub-littoral environments. He showed that these shell beds have considerably diverse distributions between the northern and southern Gulf being represented by five types of beds: community beds; storm beds; beach berm beds (Figure 2.18); tidal channel bed; and current/wave-winnowed beds. In the north, all five types of beds are present whereas the beach berm beds are the most common. In the south, current/wave-winnowed beds are most common and beach berm beds and tidal channel beds are absent (Meldahl, 1993).

The differences in distribution and abundance of the five types of shell beds, degree of autochthony and packing density between north and south Gulf are controlled by topographic relief and shelf width which influences the variability in the relative amount of terrigenous sediment and shells. Tidal current reworking variability also accounts for these differences (Meldahl, 1993).

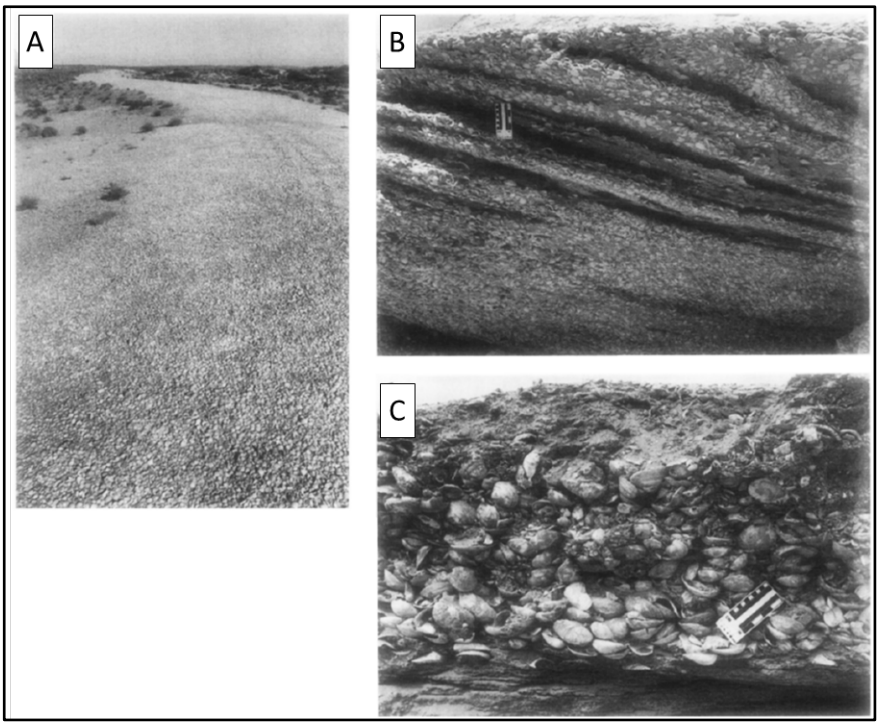

Figure 2.18 – 'Beach berm beds' in the Gulf of California. (A) Chenier at Marley Ridge formed nearly entirely of abraded valves. (B) Cross-section through beach berm bed at Cruz Point exhibiting landward-dipping crossbeds. (C) Beach berm bed exhibiting heavily abraded valves that occur preferentially concave-up and nested. From Meldahl (1993).

2.3.2. Holocene Examples of Shell Concentrations

2.3.2.2. Bivalve shell concentration in Atlantic City, United States

A particular shell concentration of infaunal bivalves was deposited near Atlantic City after a 1992 winter storm (Figure 2.19). This shell deposit occupied about 20 km of the beach varying from 10 to 50m in width (Boyajian and Thayer, 1995).

Two main facies were documented by Boyajian and Thayer (1995), one deposited on the beach and another behind the dunes. They described the beach deposit as fairly continuous laterally and able to reach up to 2 meters in thickness. The backdune deposits formed by storm-surge flooding transported shell fragments behind the dunes. Boyajian and Thayer (1995) also reported shell deposit densities ranging from $1/m^2$ to as high as $300/m^2$ observing that clams were transported alive and at the base of the deposit small clams were able to reburrow while larger clams and small ones above the base could not.

Moreover, Boyajian and Thayer (1995) enumerated particular characteristics that could be used to recognize analogous deposits in the fossil record: (1) inverse grading with small individuals below larger ones; (2) all shells are articulated; (3) individuals in life position are comparatively small and found at the base of the deposit; (4) chips on the edges of larger shells suggesting

collision with other shells during high-energy transport event; (5) deposit made of more than 90% of a single species; (6) elongate, shore-parallel bed geometry; (7) surge channels in the dune field containing a layer of shell fragments.

Boyajian and Thayer (1995) also comment that this shell deposit doesn't match published descriptions (e.g. Kidwell, 1991; Kidwell and Bosence, 1991) but has several similarities with the storm bed described by Meldahl (1993) (section 2.3.2.6).

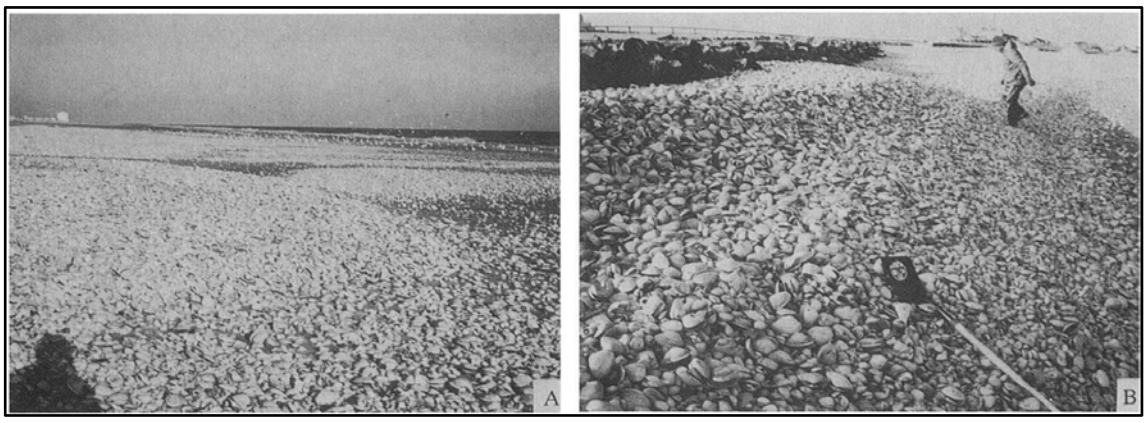

Figure 2.19 – Shell concentration near Atlantic City, New Jersey deposited after a winter storm (Boyajian and Thayer, 1995).

2.3.2.3. Shell ridges along the southwest coast of Bohai Bay, China

Shell ridges of the south-western coast of Bohai Bay occur in Wudi County, Shandong Province, on the Yellow River delta plain. These ridges display high shell content as compared to other cheniers and can possess up to 70%-95% of shells and shell fragments (Liu et al., 2005). ^{14}C dating in shells indicate ages for these cheniers between 1100-2000 years BP (Liu et al., 2005 and references therein).

Two main facies were described by Liu et al. (2005): (1) layers of shells and shell fragments forming plane-parallel and high-angle cross bedding; and (2) layers of shell fragments forming landward dipping bedding (Figure 2.20). Liu et al. (2005) discussed the conditions that favoured Bohai Bay chenier deposition, highlighting that high shell supply, storm waves winnowing and accumulating shell material near high-water, aeolian reworking and a period of low river discharge into the bay were preponderant for the configuration of these shell ridges.

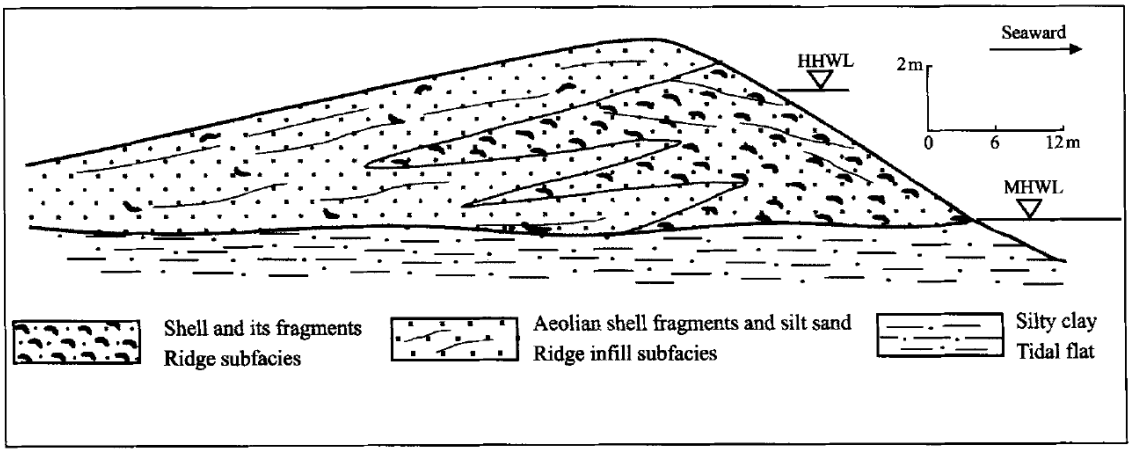

Figure 2.20 - Cross section of a chenier on Wangzi Island, Bohai Bay (Liu et al., 2005).

2.3.2.1. Shark Bay Coquinas

Hamelin Coquina is a supratidal beach-ridge system composed of coquina, microcoquina and sand (Figure 2.21) that occurs around the shores of Hamelin Pool and L'Haridon Bight (Hagan and Logan, 1974). Highly specialized bivalve mollusk *Fragum erugatum* thrives in the hypersaline basins of Shark Bay and the coquinas are composed almost entirely of their shells. High skeletal production in this special hypersaline ecosystem, together with powerful periodic storms that wash ashore shells from the subtidal environment are the main factors contributing to the coquina beach-ridge system formation. The onset of the coquina beach-ridge system is considered to be around 5000 years BP (Jahnert et al., 2012; Jahnert and Collins, 2013; Playford et al., 2013) and the system has been prograding ever since.

Nott (2011) investigated the coquina ridges in Nilemah embayment aiming to model past cyclone intensities and outline their chronology. His modelling suggests that ridges between 3 and 6 meters in height were a product of category 2-4 tropical cyclones. Nott (2011) also advocates that these cyclones have a ciclicity between 190 and 270 years.

Jahnert et al. (2012) distinguished three depositional categories in the system: (1) a tabular layer complex, displaying several prograded tabular beds consisting of layers containing whole disarticulated shells interbedded with layers of oriented shells and shell fragments, interpreted as a product of ridge-face progradation during storms and storm-surge events; (2) convex-up ridges, comprised of mounded features with rounded crests parallel to the coast, composed of beds with convex-up oriented shells, interpreted as storm-surge ridges; and (3) washover deposits, occurring as lobate forms with landward dipping or sub horizontal layers, product of barrier overwash during storms. The recurrence proposed by Jahnert et al. (2012) for the cyclones causing significant inundations at Hamelin Pool is of 10-30 years.

Playford et al. (2013) described Hamelin Coquina elements similar to those which Jahnert et al. (2012) called 'tabular layer complex' and 'convex-up ridges' although presenting a somewhat different interpretation. Playford et al. (2013) described the seaward dipping tabular beds as cycles of dense *Fragum erugatum* coquina layers, locally exhibiting nesting of shells; and layers of sandy or shelly calcarenite having disoriented valves of *Fragum erugatum* in a sandy matrix sometimes marked by a layer of oriented convex-up shells. They interpret the dense coquina layers with nested shells as being deposited *en masse* by high-energy waves associated with tropical cyclones, while the upper sandy part is attributed to be deposited at the peak of the cyclone. Additionally, strong winds after the water level had fallen would originate thin layers of convex-up shells. Playford et al. (2013) also describe linear and isolated mounds and interpret those as dunes deposits associated with strong tropical cyclone winds in contrast with Jahnert et al. (2012) interpretation which characterized their 'convex-up ridges' as storm-surge ridges (cf. Tanner, 1995). Playford et al. (2013) suggest a periodicity of once in every 100 years for tropical cyclones capable of affecting Hamelin Pool.

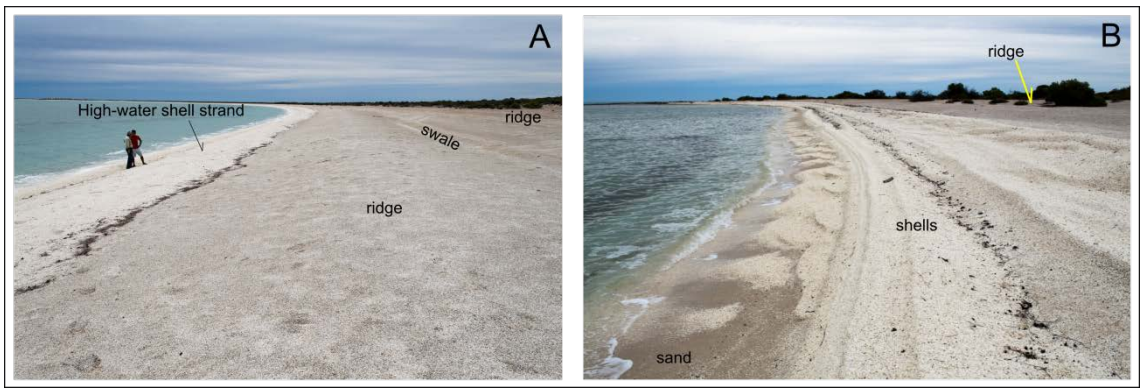

Figure 2.21 – Coquina ridges in the western shore of Hamelin Pool, Shark Bay. (A) High-water shell strand associated to a relatively recent storm. (B) Detail in the shell strand. Note sand is abundant seaward of the small shell ridge.

This section presented a brief overview of shell concentrations and their wide range of occurrence in geologic time, from the Cambrian (Li and Droser, 1997) to Recent; and depositional context (Figure 2.22), from the supralittoral environment to relatively deep waters in either open marine, marine restricted and lacustrine settings. Shell concentrations also originate from a wide variety of processes from entirely biogenic to entirely hydrodynamic or even diagenetic processes (Kidwell et al., 1986; Kidwell, 1991).

Recent studies in Shark Bay coquina beach-ridges show remarkable similarities but also important differences. Chapters 3, 4 and 5 will add to the debate presenting investigations conducted on the coquinas occurring in the eastern and western shores of Hamelin Pool.

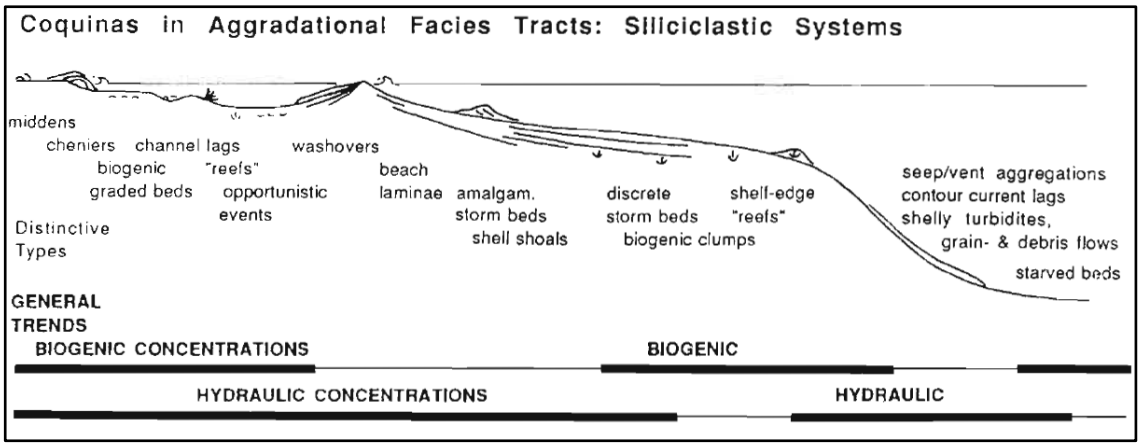

Figure 2.22 – Idealized onshore-offshore trends in the occurrence of shell concentrations (from Kidwell, 1991).

Chapter 3

Coquina Beach-Ridge System Sedimentary Architecture and Evolution in the Eastern Shore of Hamelin Pool, Shark Bay, Western Australia

3.1. Introduction

Beach ridges are coastal progradational landforms, approximately parallel to the coast. They develop in various settings around the world as a result of multiple coastal and nearshore processes where sediment supply is sufficiently high.

In Shark Bay (Figure 3.1), *Fragum erugatum* coquina beaches and beach ridges are a typical coastal feature. They form when large quantities of shells are transported to the supratidal environment by storm events. The high productivity and availability of *Fragum* shells is characteristic of Shark Bay hypersaline environments where this bivalve mollusk thrives by benefiting from an endosymbiotic relationship with zooxanthellae algae (Berry and Playford, 1997).

Storms and tsunamis are extreme events that cause temporary marine inundations of coastal areas. Such inundations combine with waves and transport marine coarse sediment onto the shore and deposit it on the supratidal zone. Worldwide, a number of shell-rich deposits have been interpreted as products of extreme events (Aigner, 1985; Boyajian and Thayer, 1995; Carvalho et al., 2000; Morales et al., 2008; Massari et al., 2009; Nott, 2011; Varela et al., 2011; Jahnert et al., 2012). Scheffers et al. (2008) demonstrate a number of coastal areas in Western Australia that provide evidence of tsunami effects but reject any direct tsunami impact to the inner parts of Shark Bay since they are relatively protected from the open sea. On the other hand, tropical cyclones are common hazards in the area, with a historical average (since 1906) of about one cyclone impact in the vicinity of Shark Bay per five years, potentially causing storm surges as high as 4.3 m (Bureau of Meteorology, n.d.-c).

After the regional work of Logan et al. (1970) and Logan et al. (1974), only recently Shark Bay coquinas have attracted scientific interest with respect to their evolution and sedimentary architecture. Nott (2011) used numerical modelling of palaeo-cyclone intensities and radiocarbon chronology to appraise palaeotempestological aspects of the Holocene climate in the Shark Bay area. Jahnert et al. (2012) focused on the depositional evolution of coquina beach ridges in Shark Bay describing their sedimentary architecture and assessing their chronology.

The aim of this chapter is to document the architectural and sedimentary characteristics of coquina beach ridges using GPR, radiocarbon chronology, outcrop, trench and core data proposing a depositional model that outlines an evolutionary framework for coquinas and associated facies deposited NE of Hamelin Pool's bay head in Shark Bay, Western Australia.

3.2. General Setting

Shark Bay is a large shallow embayment of approximately 8000 km^2 area, where overall water depths are less than 30 m. It is separated from the Indian Ocean by Edel Land, Dirk Hartog Island and the Bernier-Dorre island chain (Figure 3.1B). The peninsulas and islands within Shark Bay display an overall north-trending orientation, which is linked to controlling subsurface Tertiary anticlines (Playford and Cockbain, 1976 as cited in Butcher et al., 1984).

The climate is semi-arid with an average rainfall between 200 and 300 mm which is surpassed by the annual evaporation of 2400-2800 mm (Logan and Cebulski, 1970; Bureau of Meteorology, n.d.-b). The Gascoyne and Wooramel rivers drain into Shark Bay, but their flow is spasmodic and their runoff is negligible, only transporting sediments after heavy rains caused by storms and cyclones (Logan & Cebulski, 1970; Logan, Read and Davies, 1970).

The dominant wind direction in Shark Bay is from the south, nonetheless winds tend to be more easterly and southeasterly, occasionally northerly during winter (Bureau of Meteorology, n.d.-d). Intense barometric depressions originate in the Timor Sea and progress south-west along the coast before weakening. These tropical cyclones and storms occur periodically and are accompanied by heavy rainfall and gales that can gust up to 180 km/hour (Logan and Cebulski, 1970; Hagan and Logan, 1974; Bureau of Meteorology, n.d.-c).

Shark Bay salinity distribution is affected by the restriction of water exchange with the ocean provided by a number of islands, flats, and sills. Furthermore, Shark Bay salinities increase to the south, from normal marine at the seaward opening to hypersaline in the bay heads. Logan and Cebulski (1970) subdivided Shark Bay waters into three separate categories: oceanic, with salinities ranging from 30 to 40; metahaline, where salinities range from 40 to 56 and; hypersaline, with salinities from 56 to 70.

The onset of an hypersaline environment took place in Hamelin Pool and L'Haridon Bight (Figure 3.1C) as a result of (1) restriction to oceanic water circulation within the bay provided by Faure seagrass bank growth; (2) High evaporation under semi-arid climatic setting; and (3) Falling sea-level conditions after a Holocene post glacial transgressive period (Logan and Cebulski, 1970; Logan et al., 1974). Collins et al. (2006) indicate a Holocene high-stand of about +2m at approximately 6800 U/Th years BP using coral pavement data from Houtman Abrolhos Islands, Western Australia. Other authors have also recognized evidence for falling

sea-level conditions in Shark Bay during the last 6000 years BP (e.g. Logan et al., 1974; Jahnert and Collins, 2011; Jahnert and Collins, 2013).

The small bivalve mollusk (< 15 mm long) *Fragum erugatum* has a high skeletal productivity within Shark Bay hypersaline environments where competition and predation are limited. Despite living *Fragum* occurring in the subtidal zone between 1.2 and 6.5m depth (Berry and Playford, 1997), a vast amount of shells are washed ashore by storms and accumulated as supratidal coquina ridges.

In the hypersaline basins of Shark Bay the sediments consist mainly of microbial mats, stromatolites, thrombolites, cryptomicrobial deposits and coquinas (Logan et al., 1970; Logan et al., 1974; Jahnert and Collins, 2012). Ooid, bioclast and quartz sands are also important lithologies observed in the Hamelin Pool nearshore environment.

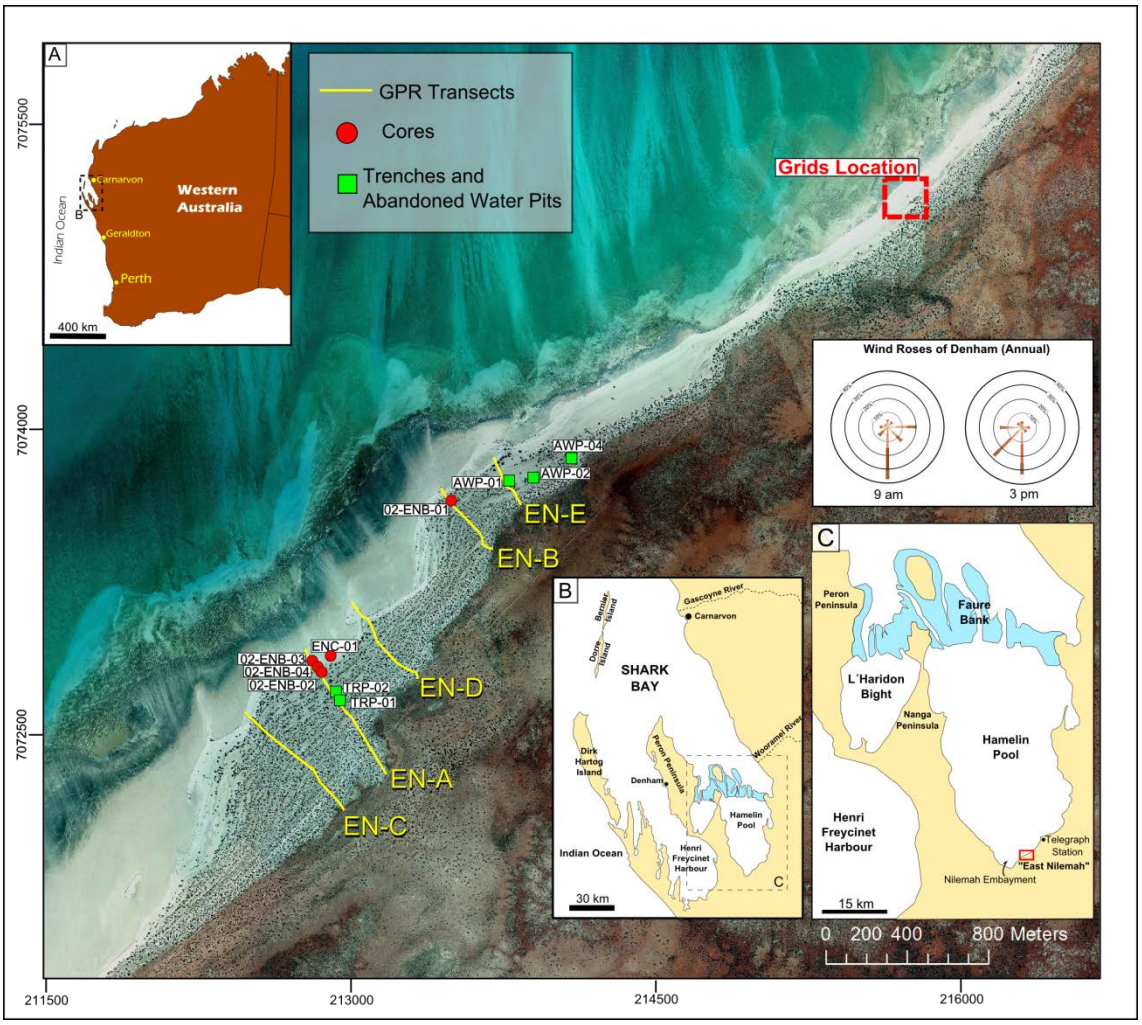

Figure 3.1 - Location map of Shark Bay outlining the study area informally named "East Nilemah". Aerial imagery displays the coquina beach-ridge system and location of GPR transects, cores, trenches and abandoned water pits. Wind roses are from Bureau of Meteorology (n.d.-d).

3.3. Materials and Methods

Georeferenced maps were constructed using high resolution (50 cm/pixel) Shark Bay orthophotos from Department of Parks and Wildlife and from Landgate (Perth, Western Australia) on ArcGIS software.

Ground Penetrating Radar (GPR) equipment from Mala Professional Explorer coupled with a high precision real time kinematic (RTK) GPS system was employed to obtain subsurface images. GPR data was acquired using a 500 MHz antenna. The trace increment was 5 cm, and the time sampling interval 0.2 ns. The Thales ZMAX RTK GPS system consists of a base station with radio transmitter continuously correcting positions measured by the mobile Rover unit to obtain centimeter accurate elevations. Coordinates were directly linked to the recorded GPR traces by the acquisition software Groundvision 2, while GPR measurements were triggered in the distance domain with a wheel. Radar penetration depth was limited by the saline water table. Thirteen different radar facies were identified in the GPR lines (Fig. 3.2). A standard terminology which is summarized by Neal (2004) was used with minor adaptations for the description of radar reflection geometries.

Sediment sampling consisted of push cores and hand samples. The cores have a maximum depth of 2m, using 50mm PVC tubes. Sedimentary structures were generally not preserved in the push cores as coring was performed by percussion in mostly dry loose sediment. Only the last few centimeters of the core bottoms intercepted the water table where sand or finer sediments tend to be more compact. Hand samples were collected at the surface or in pits with a maximum depth of 1.9m.

^{14}C ages were determined using analytical procedures of Beta Analytic Radiocarbon Dating Laboratory, Florida, USA. All samples were counted using AMS techniques on *Fragum erugatum* shells.

Thin-sections were produced by Minerex Services, Esperance, Australia and analyzed using a Nikon ECLIPSE LV100POL microscope (Nikon Corporation, Tokyo, Japan) and imaged with Nikon NIS Elements software at Curtin University, Australia.

Mineralogical analyses using X-ray diffraction were performed by the Centre for Materials Research X-ray laboratory at Curtin University.

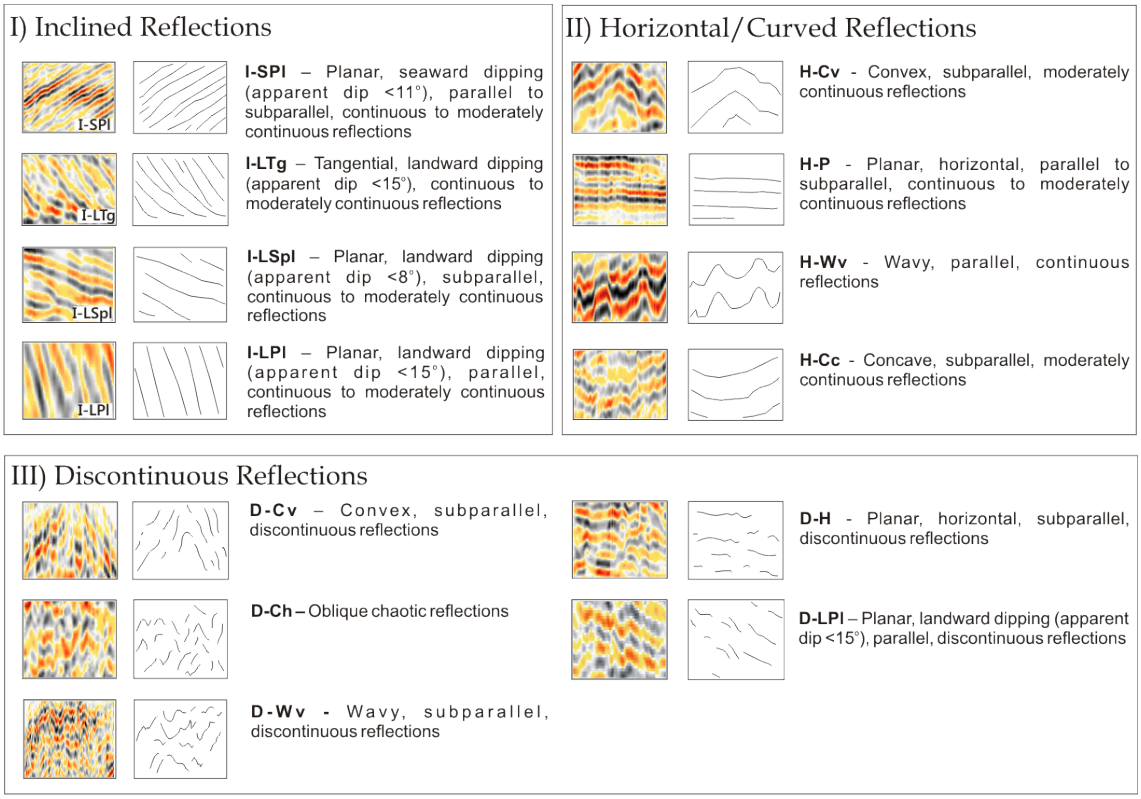

Figure 3.2 – The main radar facies identified in GPR lines can be divided into three major groups: inclined, horizontal/curved and discontinuous reflections.

3.4. Results

Shark Bay region is subject to sporadic storm events, especially tropical cyclones that exert an important control on coastal geomorphology inducing complex cut-and-fill structures and extensive sediment remobilization in the nearshore environment. To address the depositional complexity of coquinas and related deposits in the beach-ridge system, multiple approaches were used emphasizing the geomorphology, geometric and textural characteristics of deposits and their temporal relationships. Three elementary categories were used to guide the interpretation of the processes that governed the formation, shaping and evolution of the beach-ridge system in the study area. These categories are geomorphic elements, depositional elements and depositional domains.

3.4.1. Geomorphic elements

Geomorphic elements are the surficial expression of beach ridge system building processes. Seven main geomorphic elements of different hierarchies were recognized based on aerial imagery of the study site (Figure 3.3): beach ridges, spit ridges, longshore bars, washover fans, beach-ridge sets, tidal flats and beach-ridge system. Their size ranges from a few meters (longshore bars) to several kilometers (beach ridge system).

3.4.2. Depositional Elements, Depositional Element Sets and Depositional Domains

The term 'depositional element' is here used to distinguish genetically linked sedimentary bodies with particular geometries and associated textures. Thus, depositional elements reflect specific sedimentary processes that generate geometries which can be interpreted in GPR lines, outcrops and trenches complemented by push-cores that provided textural information in selected locations. In view of that, six depositional elements were recognized based on GPR profiles, cores, orthophoto images and field observations (Table 3.1): beach, washover, welded longshore bar, spit and storm-surge ridge.

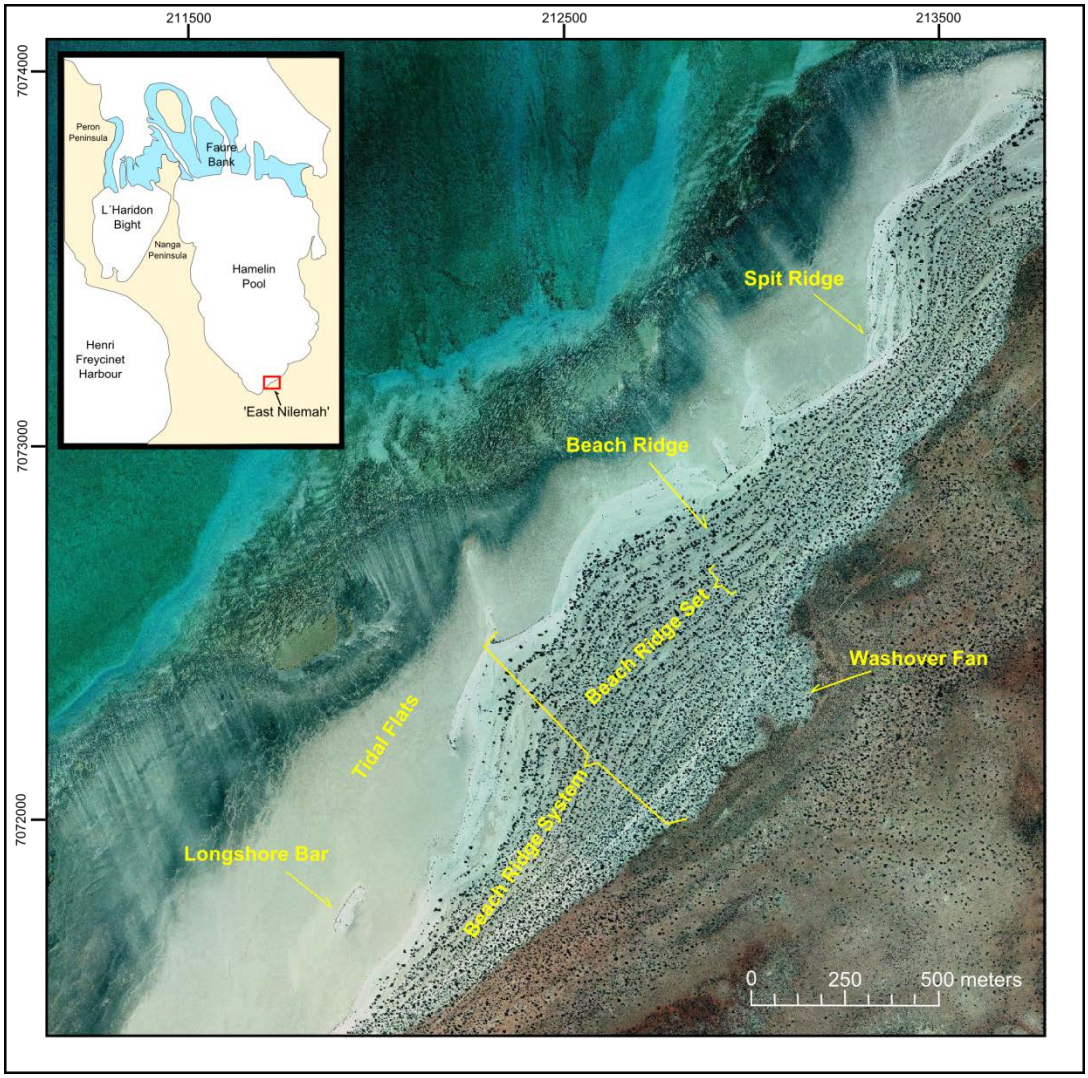

Figure 3.3 – Orthophoto providing a plan view of geomorphic elements in the study area.

The beach depositional element results from sedimentation on the sloping face of the beach (beachface) and on the berm crest resulting from swash, backwash, overtopping and minor overwashing processes. Figure 3.4(A) illustrates an active berm in Hamelin Pool during low water level. In GPR profiles, this element exhibits seaward dipping reflectors with gentle slope. Occasionally, high-water shell strands and berm crests are preserved from erosion. They display a mounded external geometry and internally possess horizontally parallel, convex-up or reflection-free radar facies.

The washover depositional element refers to sedimentary deposits that result from the overwashing of a barrier under high-energy conditions. Figure 3.4(D) illustrates a washover fan on the western shore of Hamelin Pool. In GPR profiles washovers were identified by horizontal to landward dipping reflectors occurring in the landward side of a ridge. Figures 3.3 illustrates an example of a washover fan at "East Nilemah" site as seen in aerial imagery.

The welded longshore bar (or swash bar) is a depositional element that consists of sandy or shelly bars with landward dipping stratification downlapping on the beachface. This kind of welded bar is usually not preserved being incorporated into the beachface deposits by swash and backwash processes.

The Spit depositional element comprises a sedimentary body initially built by longshore currents. Figures 3.4(B) and 3.4(C) show modern spit ridges occurring on the eastern shore of Hamelin Pool and illustrate their internal and external geometry. This element commonly exhibits bedding that dips in the direction of the prevailing longshore current, although horizontal and landward bedding are also observed when the ridge has been reworked by overwash and overtopping processes.

Storm-surge ridges are depositional elements that occur isolated and display horizontal, moderately wavy or convex-up bedding. These deposits are interpreted to be a result of sediment settling from suspension in the supratidal zone during a storm (Tanner, 1995; Keen and Stone, 2000). The facies and internal geometry of this element were accessed by trenching and the use of ground penetrating radar (Figure 3.5).

The study area presents depositional elements that ideally assemble in two distinct groups reflecting different sedimentary processes that predominate during their deposition (Figure 3.6). Firstly, depositional set type 1 reflects deposition predominantly under swash and backwash processes in the beachface and occasional overtopping and minor overwashing leading to berm crest growth by aggradation. On the other hand, depositional set type 2 reflects deposition under the dominance of longshore currents. In addition, storm-surge ridges occur as isolated depositional elements (Figure 3.5) not being characteristic of either depositional set.

Depositional domains are discrete areas of the beach-ridge system where a given depositional element predominates as a result of prevailing sedimentary processes and environmental conditions for a certain period of time.

Four depositional domains identified in 'East Nilemah' were named according to the dominant depositional element occurring within each of them: Washover Domain, Beach Domain, Spit-Ridge Domain and Storm-surge Domain (Figure 3.7). Their architectural characteristics follow the predominant depositional element except for the spit ridge depositional domain which may locally display a mix of spit, swash bar, beach and washover element geometries.

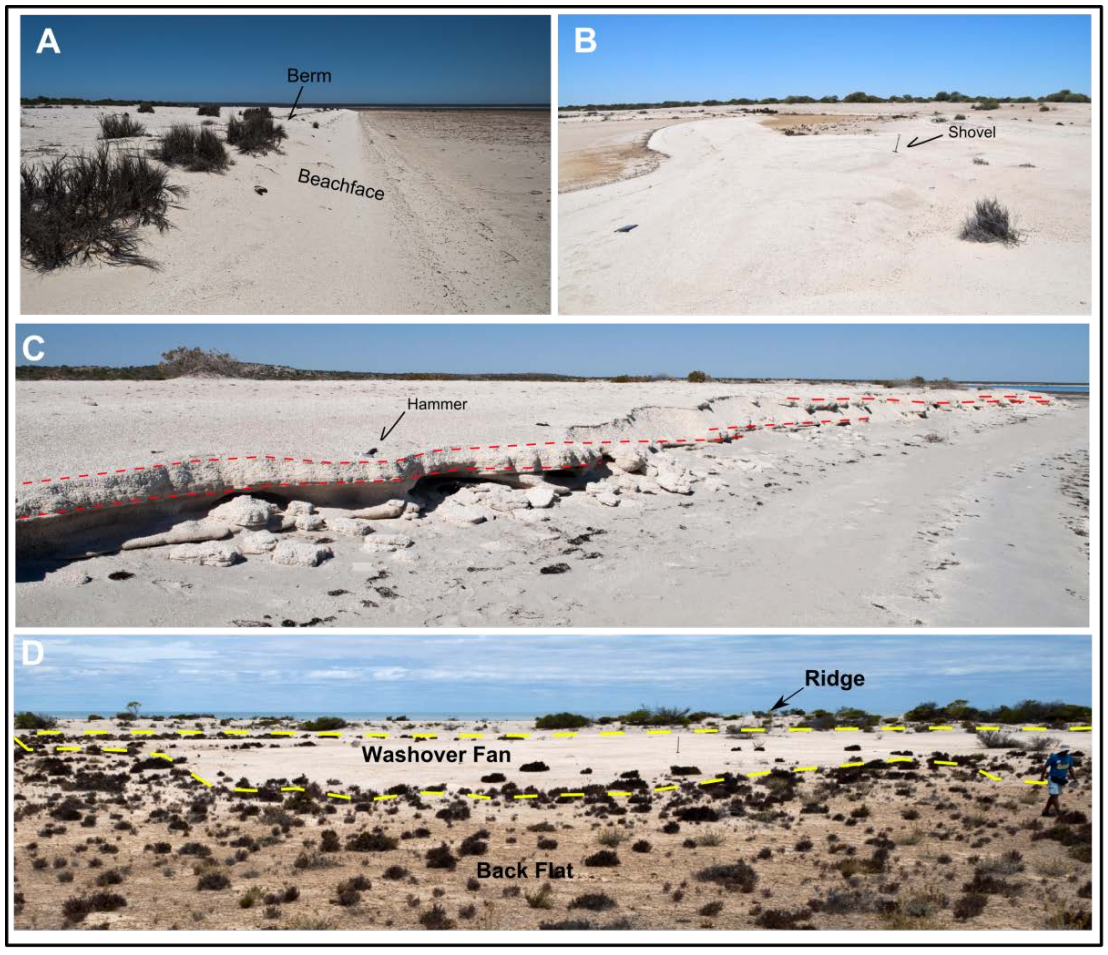

Figure 3.4 – Field expression of depositional elements. (A) Active berm in 'East Nilemah'. (B) Spit in 'East Nilemah' (C) Internal structure of a spit ridge at Sweeney Mia, eastern shore of Hamelin Pool. Bedding dips southeast, parallel to the shore. (D) Washover fan at Fishermen's Point, western shore of Hamelin Pool.

Depositional Element	Lithology and Sedimentary Structures	Shape	Internal Geometry	Geometric Relationships
Beach	Bioclastic sand; shell gravel with or without coarse bioclastic sand matrix and ooid sands. Plane-parallel lamination and oriented shells are common	Wedge or Lens	Seaward dipping parallel to moderately oblique bedding. Updip may display gently landward dipping, horizontal or curved convex bedding.	Progradational feature. Radar Facies: I-Spl; (H-P; H-Cv)
Washover	Bioclastic sand; shell gravel with or without coarse bioclastic sand matrix and ooid sands	Wedge or mound (fan)	Horizontal bedding or Low to moderate angle landward dipping stratification	Occurs landward of a pre-existing adjacent ridge. Radar Facies: I-LTg; H-P; D-H; D-Wv; D-Cv; (D-Ch)
Welded Longshore/swash bar	Bioclastic sand; shell gravel; ooid sands.	Mound (bar)	Low to moderate angle landward dipping stratification	Welds to the beachface. Radar Facies: I-LTg
Spit	Coarse bioclastic sand; shell gravel with coarse bioclastic sand matrix; shell gravel; ooid sands	Elongate Mound (ridge)	Bedding dips low angle shore parallel. Locally may exhibit shore normal foreset stratification	Occur either grouped or as isolated features. Radar Facies: H-P; I-LSpl; H-Cv; I-Lpl
Storm-surge ridge	Shell gravel	Mound (ridge)	Horizontal, moderately wavy or curved convex bedding	Commonly on top of an erosive surface over the beachface element. Radar Facies: D-Cv; D-Wv; H-Cv; I-Lspl; D-Lpl; D-Ch

Table 3.1 – Depositional elements and their textural and geometric characteristics. For radar facies description see Fig. 3.2.

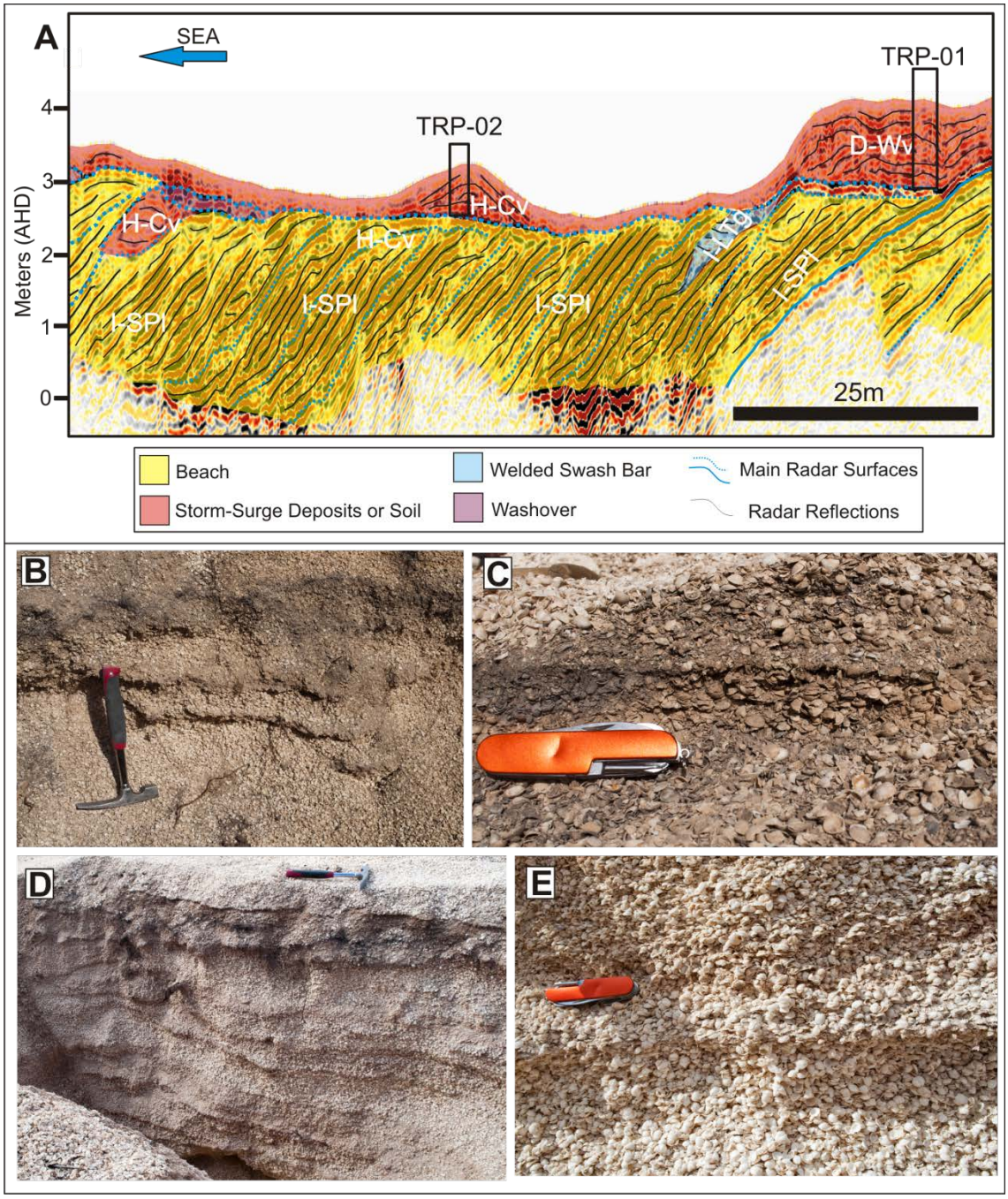

Figure 3.5 – Architectural characteristics of storm-surge ridges in 'East Nilemah'. (A) Segment of GPR line EN-A (Figures 3.8 and 3.9) showing the internal geometry of two trenched storm-surge ridges and their relationship with beach deposits underneath. (B) Trench TRP-02 showing sand-free shell gravels and centimetric irregular layers of shell gravels containing organic matter, plant roots and fine grained particles (clay and silt). (C) Detail of irregular layer of shell gravel containing windblown fine grained sediment indicating incipient soil formation (exposure surface). Note the predominance of bedding concordant oriented shells. (D) Trench TRP-01 exhibiting sand-free shell gravels and irregular layers of shell gravel with fine grained infiltrated sediment, roots and organic matter. (E) Detail of sand-free shell gravel in trench TRP-01 showing roughly bed-concordant oriented shells.

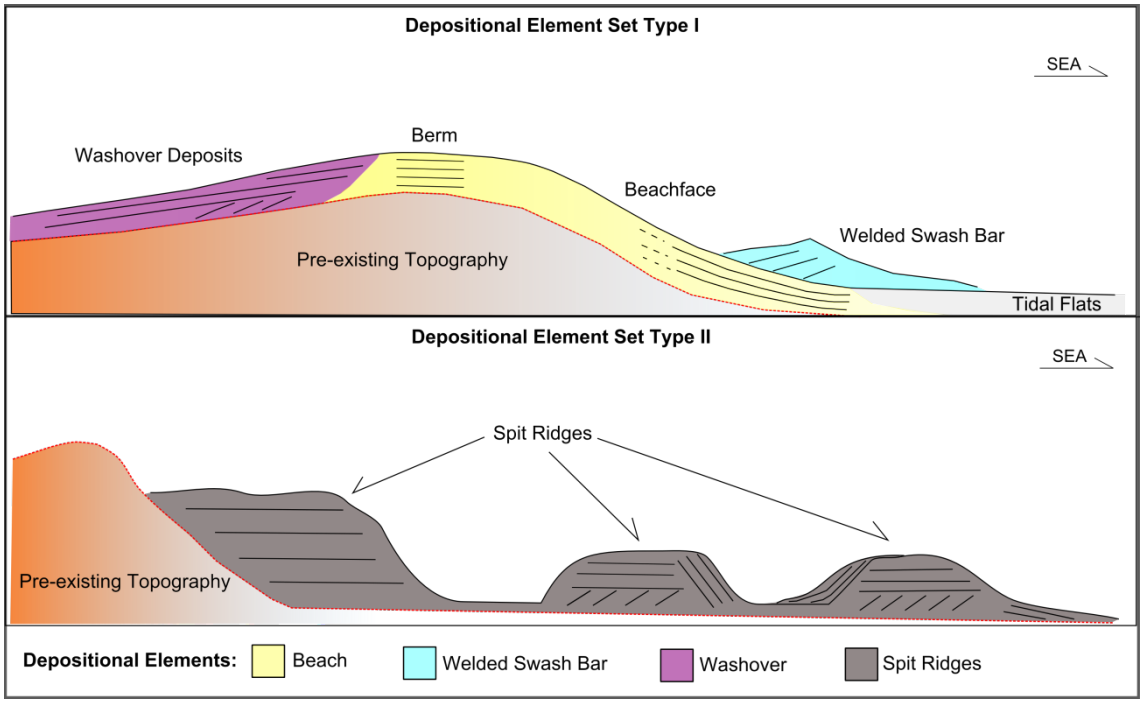

Figure 3.6 – Depositional element sets. Type I (top) occurs when swash and backwash processes predominate in the beach depositional environment. Type II (bottom) is a result of the prevalence of longshore currents in beach sedimentation.

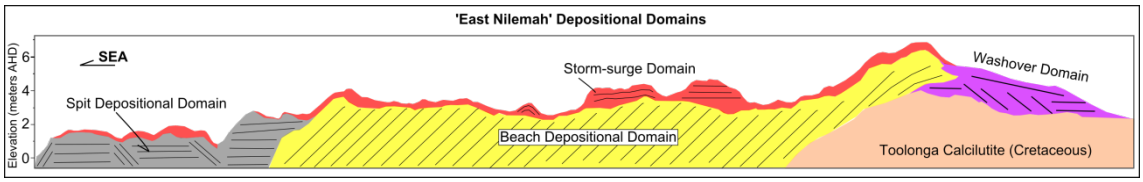

Figure 3.7 – Cross-section sketch illustrating depositional domains and prevailing internal geometries.

3.4.3. GPR profile interpretation

The radar profiles provide 2-D images of the coquina beach-ridge system internal architecture and together with facies information from cores, trenches and outcrops allow the interpretation of the depositional elements and the sedimentary evolution of the system.

Long radar lines (EN-A, EN-B, EN-C, EN-D and EN-E) were run perpendicular to the beach ridges (Figure 3.1) revealing their geometry along the depositional dip. Additionally, two irregular grids (Figures 3.1 upper right and 3.16) were acquired in the northernmost sector of 'East Nilemah' in order to obtain detailed architectural information of beach ridges adjacent to outcropping coquina deposits. The radar reflections were grouped into radar facies according to their shape, dip and continuity (Figure 3.2).

3.4.3.1. GPR Profile EN-A

Radar line EN-A is 650m long and offers a clear image of 3 distinct domains (Figures 3.8 and 3.9). The first and most landward domain has a predominance of washover deposits, while seaward of it follows a domain where seaward inclined reflectors of the beach depositional element prevail being capped by storm-surge deposits and soil. The spit ridge domain shows a complex reflector configuration and lower ridge elevations.

Occasionally, landward dipping reflectors rest on top of the beach element sloping face (beachface) and are interpreted as welded longshore (or swash) bars indicating that welding of intertidal and subtidal bars plays an important role in supplying the beach ridge system with new sediment during storms (Houser et al., 2006; Houser and Greenwood, 2007; Lindhorst et al., 2008).

Mounded bodies resting on top of marked erosive surfaces are additional noteworthy features which display an internal geometry composed of curved convex and wavy reflectors. These sedimentary bodies cap older beach-ridge deposits and are interpreted as storm-surge ridges following observations of Keen and Stone (2000) and Tanner (1995) in Florida, United States and Jahnert *et al.* (2012) in Shark Bay, Western Australia. In order to investigate these storm-surge deposits, 2 trenches were made along line EN-A (Figure 3.5) and their sedimentary characteristics are described in Section 3.4.4.1.2.

The transition from the beach depositional domain to the spit ridge domain display an overall decrease in ridge elevation and change in reflector configuration implying that hydrodynamic conditions have changed from swash and backwash dominated to more longshore current dominated processes.

3.4.3.2. GPR Line EN-B

Radar Line EN-B is 410m long in the depositional dip direction (Figure 3.10). The overall configuration of this line is characterized by the beach element progradational style capped by storm-surge and soil deposits. Welded swash bars are relatively common elements interpreted in this line.

An important feature in line EN-B observed around 300m shows a complete beach depositional element radar image. This portion of EN-B displays the horizontally parallel radar facies of berm crests transitioning to seaward inclined reflectors of the beachface. Given that the berm crest is frequently eroded by succeeding storm events, the record of an entire berm, and not only the beachface, is uncommon in the study area.

3.4.3.3. GPR Line EN-C

Radar line EN-C is the longest at 'East Nilemah' covering 729 meters and crossing all five ridge sets and the older washover deposits in the study site (Figures 3.11 and 3.12). It displays an overall configuration similar to EN-A with three domains identifiable in the profile (washover, prograding beach element capped by storm-surge deposits and spit ridges).

Noteworthy in this line are the well-developed storm-surge ridges that can reach up to 7.4m in elevation above AHD. It is also important to note a general decrease in ridge elevation and change in overall reflector configuration at approximately 525m, similarly to what is observed on EN-A GPR profile.

3.4.3.4. GPR Line EN-D

Line EN-D encompasses 520m and covers 4 ridge sets (Figures 3.13, 3.14 and 3.28). Overall configuration is similar to EN-A and EN-C although welded swash bars are scarcer. Furthermore, between 300 and 400m, the step observed in other lines also occurs. This step was observed in the three lines (EN-A, EN-C and EN-D) located southwest of EN-B.

3.4.3.5. GPR Line EN-E

GPR line EN-E is the shortest line in 'East Nilemah' covering 309 m (Figure 3.15). The prograding beach element capped by storm-surge deposits and soil are the predominant depositional elements in this area. Both elements were accessed in an abandoned water pit intercepted by this line. In Figure 3.24, the detail in GPR line EN-E displays two distinct reflector configurations separated by a roughly horizontal radar surface (*rs.E1*). The top package, interpreted as storm-surge deposits, displays reflectors in conformable convex-up pattern blanketing a seaward inclined series of reflectors interpreted as prograding beachface deposits.

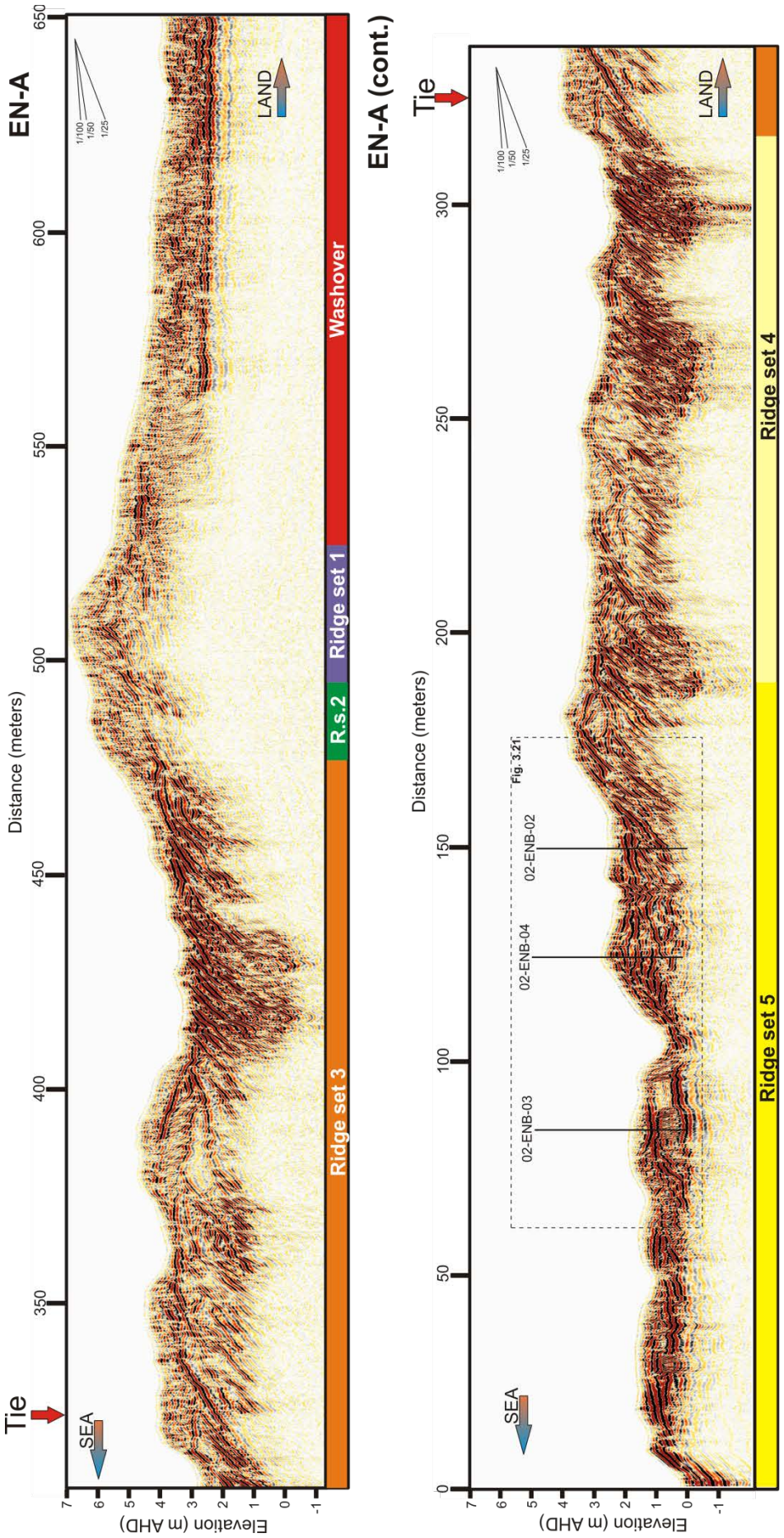

Figure 3.8 - EN-A uninterpreted GPR line. Top and bottom figures are from a continuous transect and tie as indicated by the red arrow in the upper ruler.

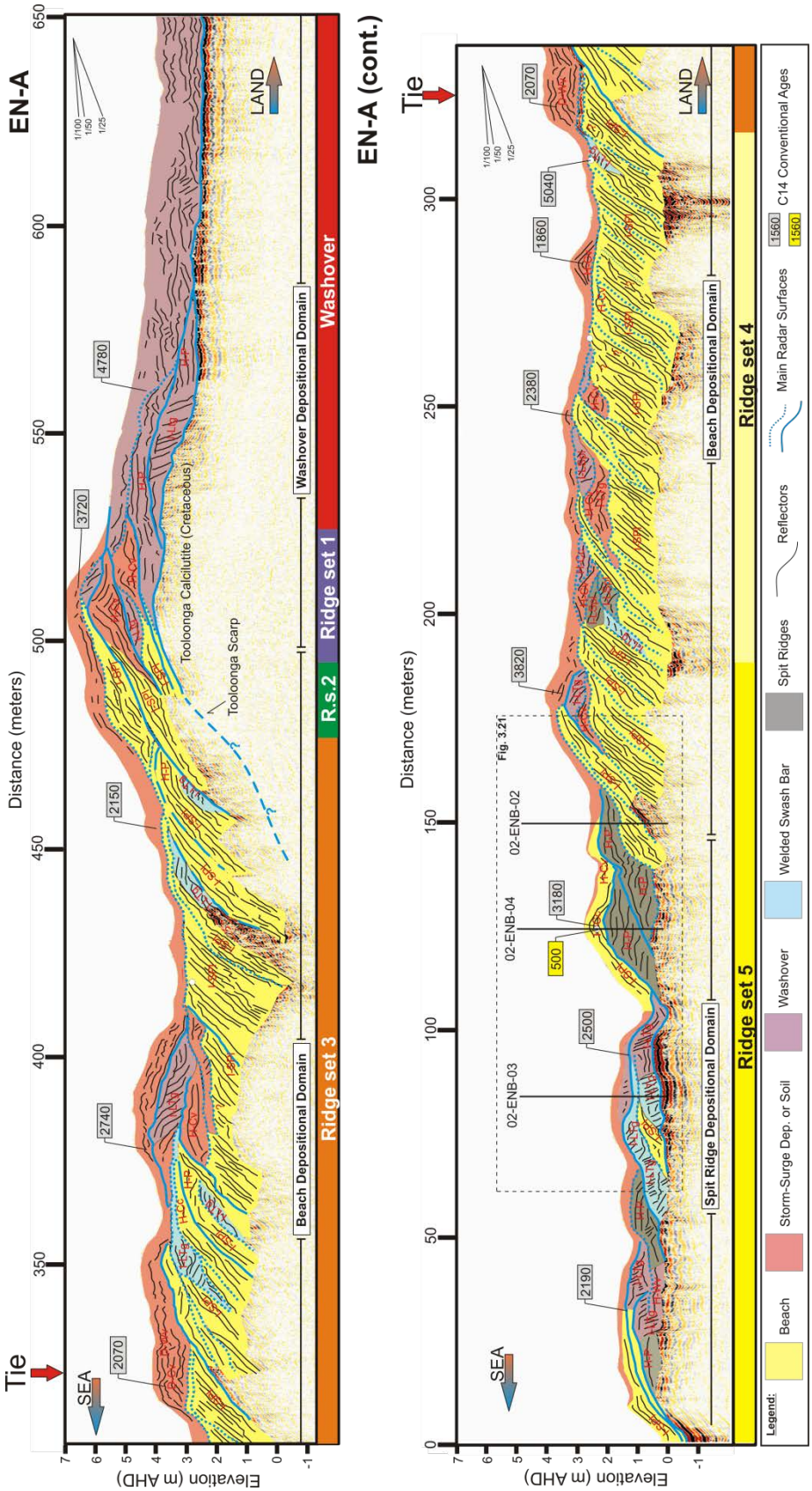

Figure 3.9 - EN-A interpreted GPR line (see Fig. 3.1 for location). Top and bottom figures are from a continuous transect and tie as indicated by the red arrow in the upper ruler. Depositional domains and ridge sets are indicated in the bottom of profiles. Note the complex internal architecture of the spit ridge domain in contrast with the beach domain which exhibits simpler geometries dominated by seaward dipping reflections. The transition from beach to spit ridge domain is marked by a pronounced elevation step. Storm-surge deposits and soil cap the beach and spit-ridge domains. The landward-most domain comprises washover deposits that date to the onset of the system exhibiting ages as old as 4760 ^{14}C years BP. Figure 3.21 is an inset that shows details on the cores ENB-02, ENB-03 and ENB-04.

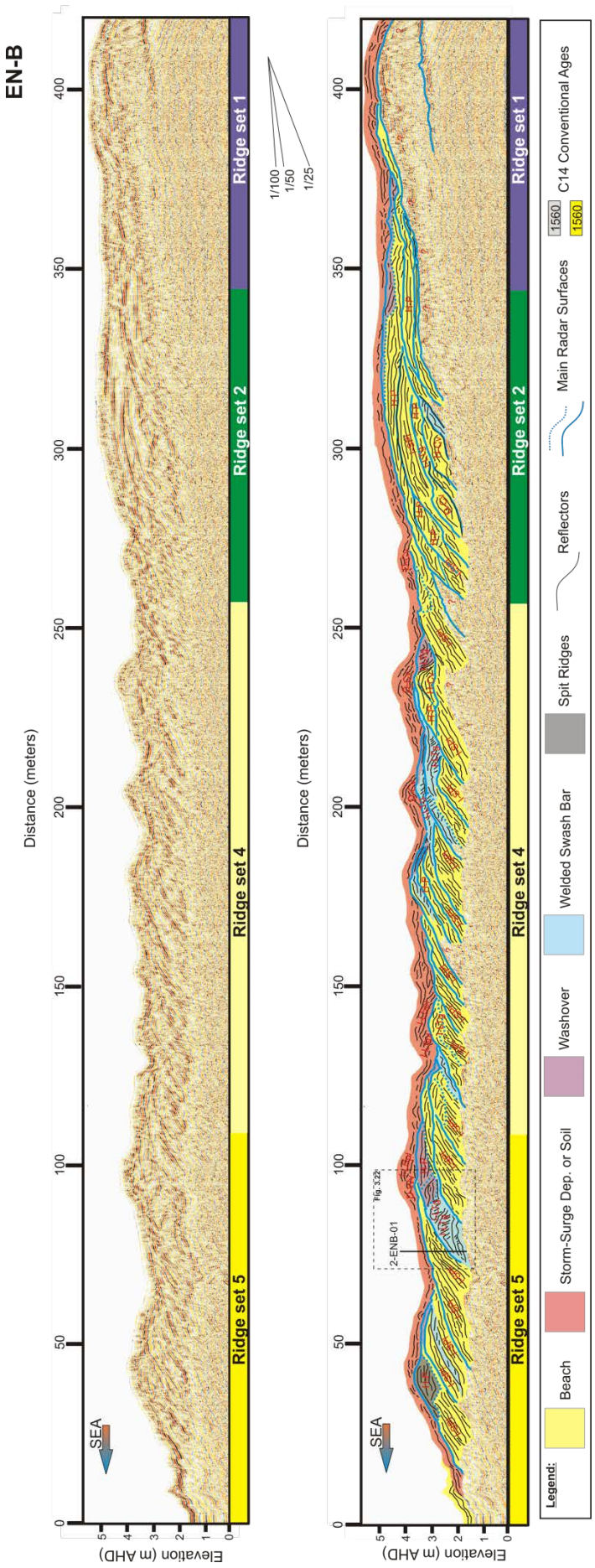

Figure 3.10 – Uninterpreted (top) and interpreted (bottom) GPR line EN-B (see Figure 3.1 for location). Ridge sets are indicated in the bottom of profiles. Seaward dipping reflections of the beach depositional domain predominate and are capped by storm-surge deposits and soil. Note that in the area of ridge set 2 the beach depositional element displays its complete morphology as described in Fig. 3.6A, showing mounded or wedge-shaped features, interpreted as berm crests, updip of seaward inclined reflections.

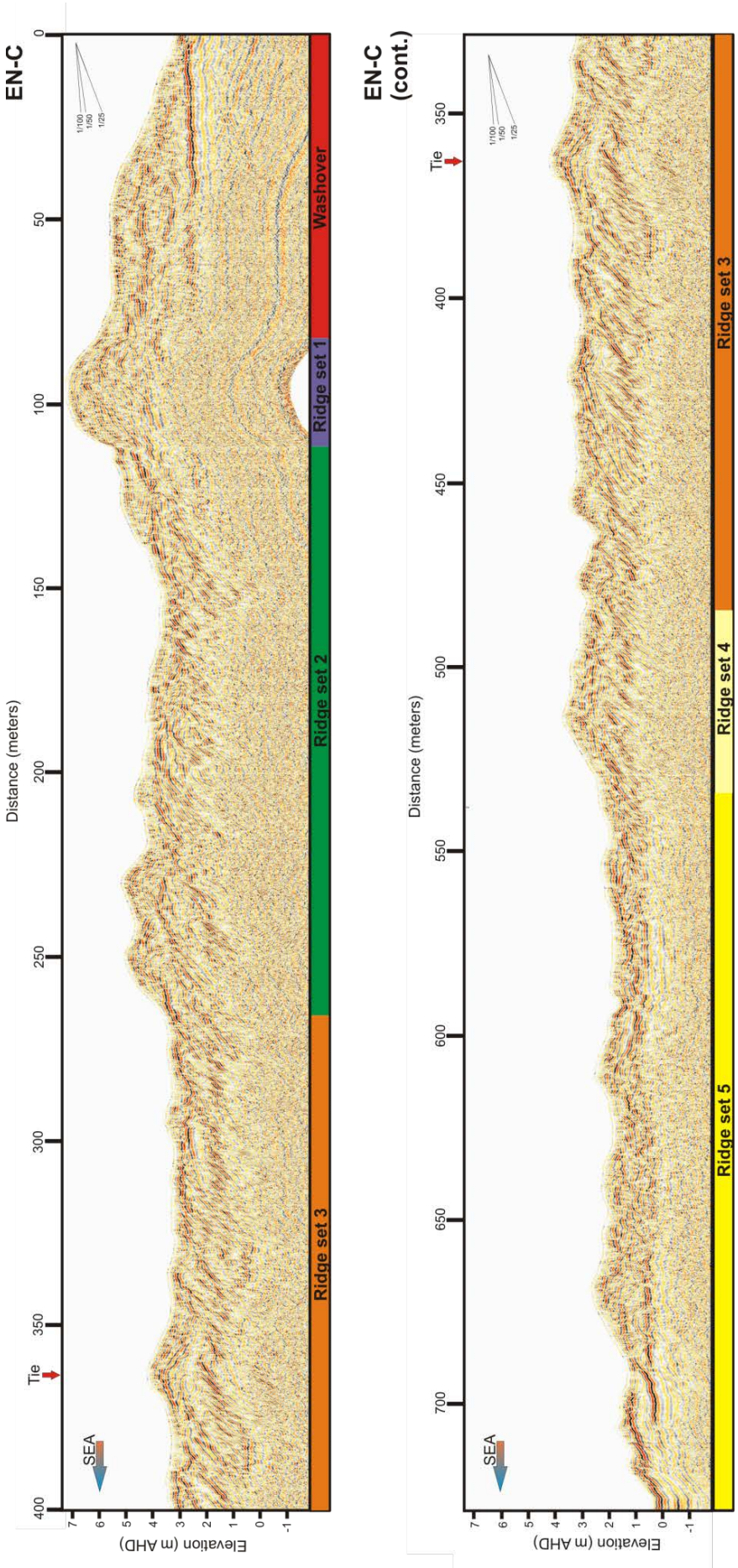

Figure 3.11 - EN-C uninterpreted GPR line. Top and bottom figures are from a continuous transect and tie as indicated by the red arrow in the upper ruler.

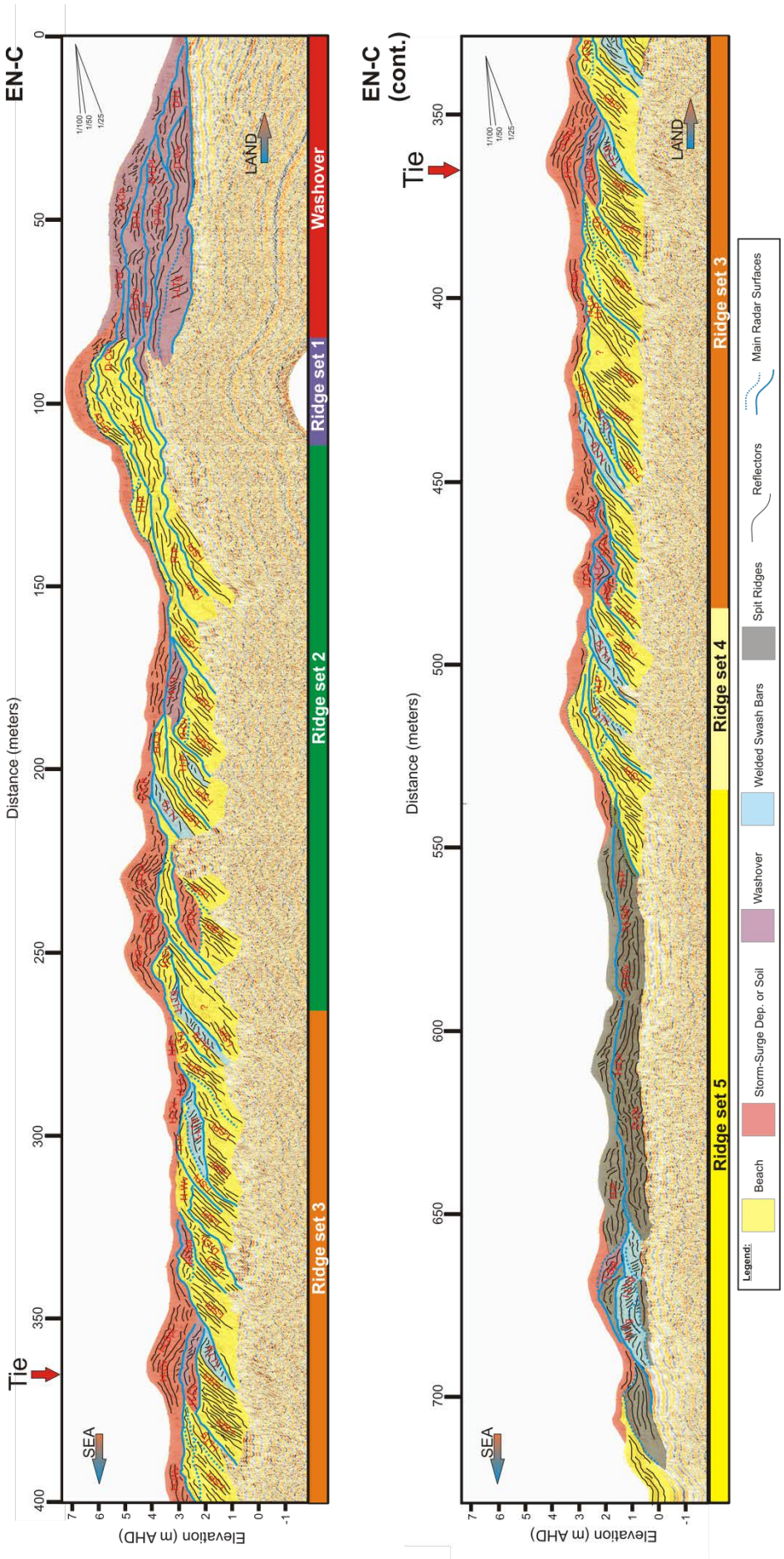

Figure 3.12 - EN-C interpreted GPR line (see Figure 3.1 for location). Top and bottom figures are from a continuous transect and tie as indicated by the red arrow in the upper ruler. The transition from seaward inclined reflections of the beach domain to the spit ridge domain is marked by an elevation step. Storm-surge deposits and soil cap beach and spit-ridge domains. The landward-most domain comprises washover deposits.

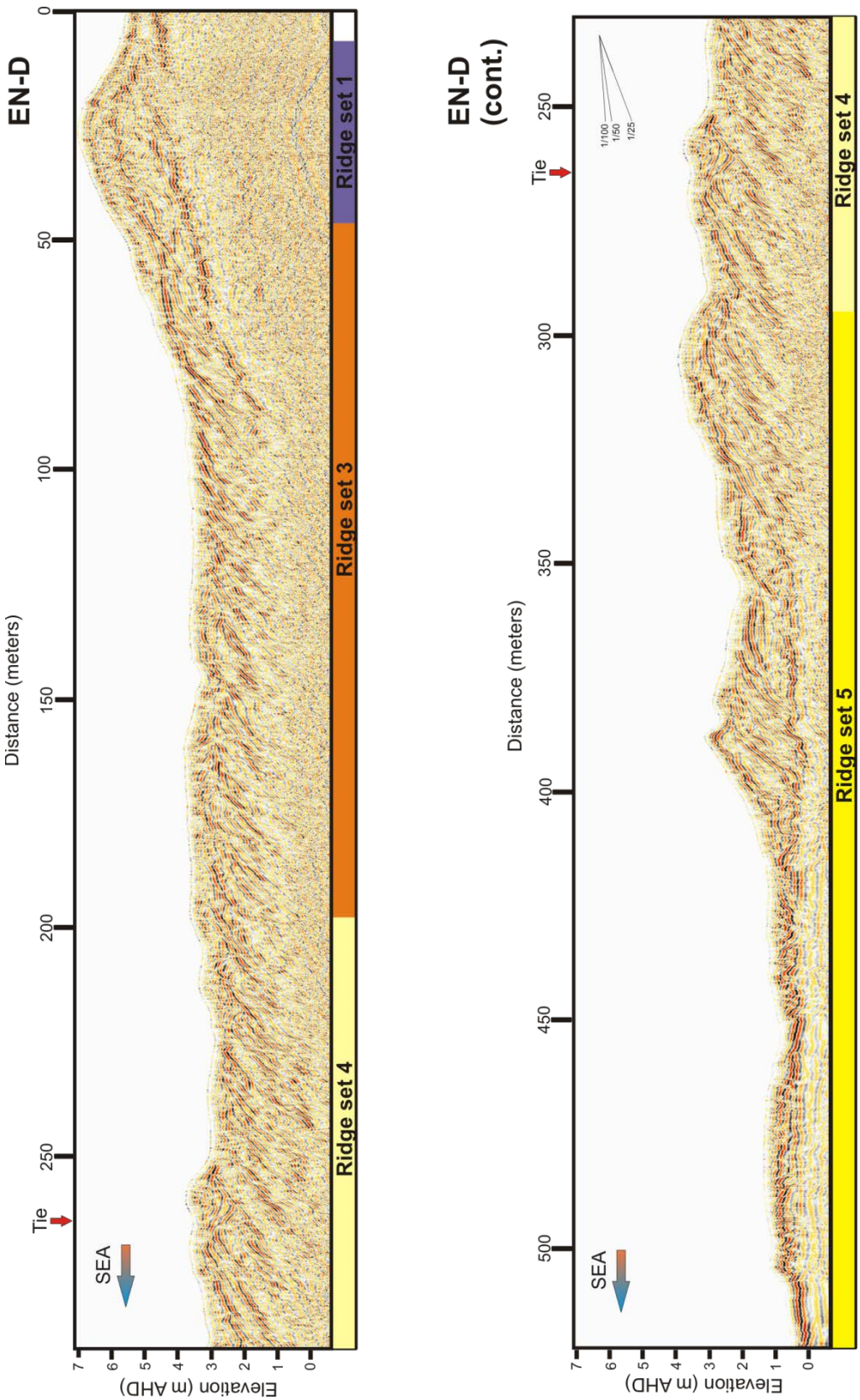

Figure 3.13 - EN-D uninterpreted GPR line. Top and bottom figures are from a continuous transect and tie as indicated by the red arrow in the upper ruler.

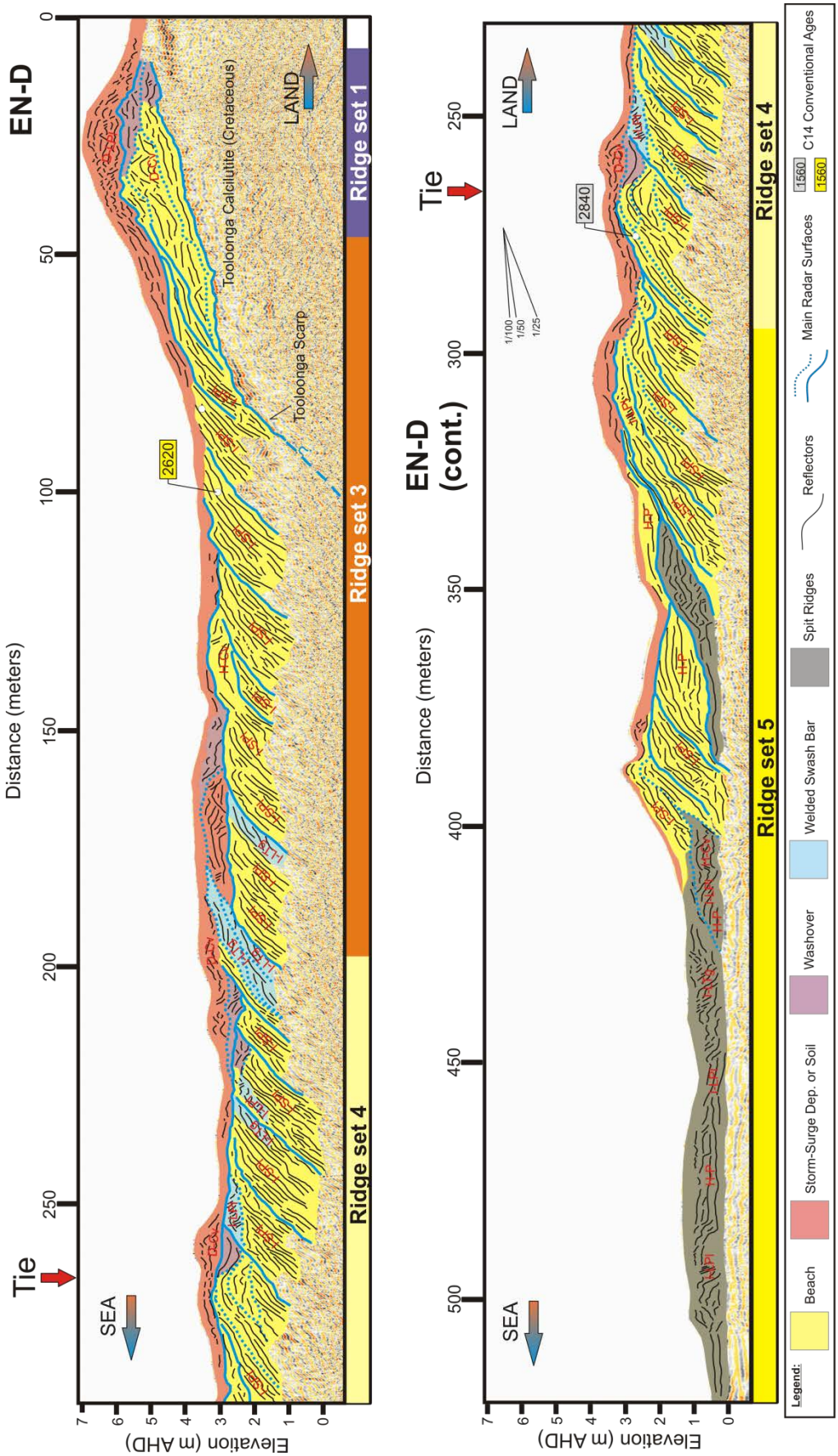

Figure 3.14 - EN-D interpreted GPR line (see Fig. 3.1 for location). Top and bottom figures are from a continuous transect and tie as indicated by the red arrow in the upper ruler. The transition from seaward inclined reflections of the beach domain to the spit ridge domain is marked by an elevation step. Storm-surge deposits and soil cap beach and spit-ridge domains.

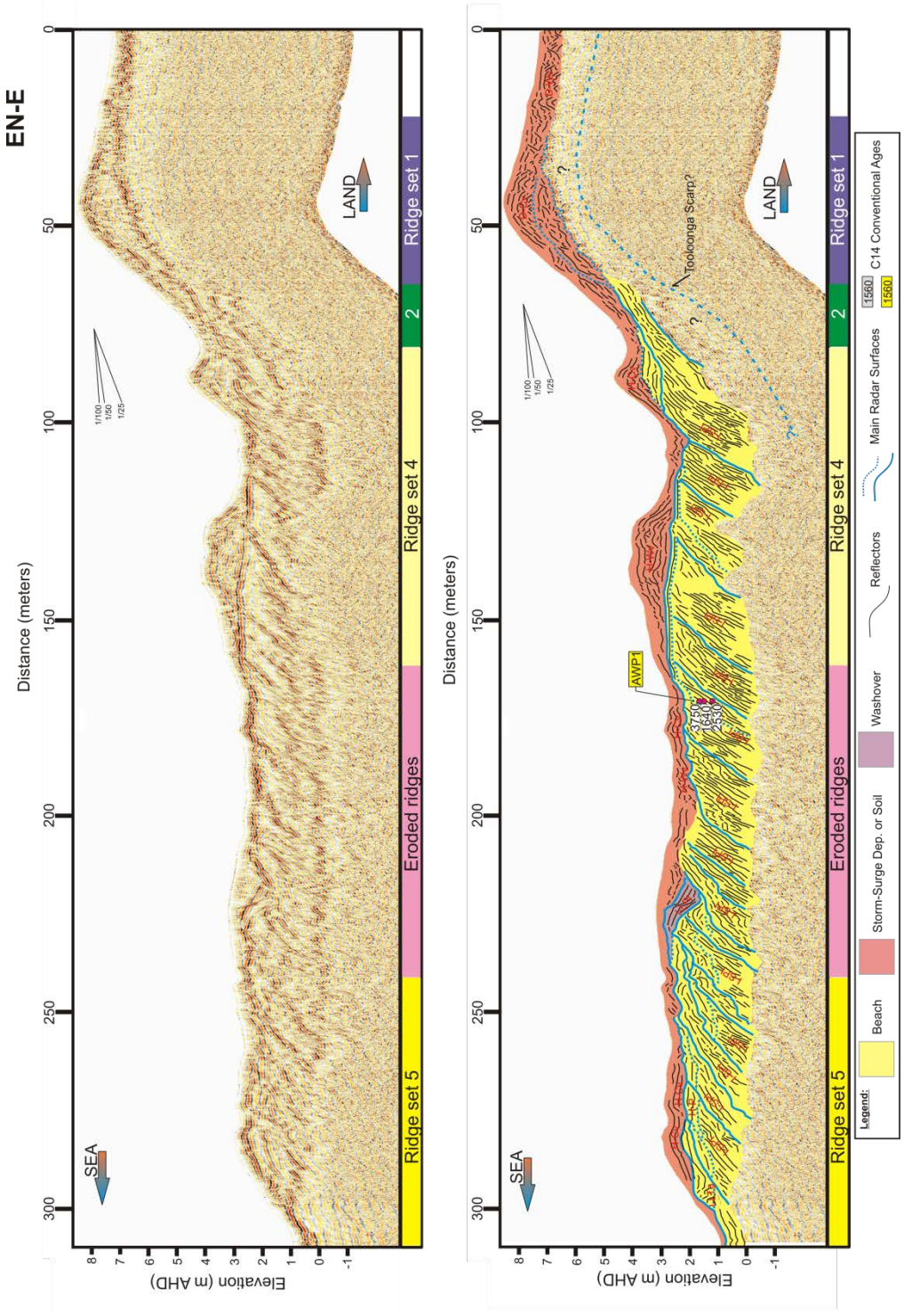

Figure 3.15 - Uninterpreted (top) and interpreted (bottom) GPR line EN-E (see Figure 3.1 for location). Seaward dipping reflections of the beach depositional domain predominate and are capped by storm-surge deposits and soil. Abandoned water pit AWP-01 is located in this line and three ^{14}C dates were obtained in the pit as indicated.

3.4.3.6. GPR to Outcrop Correlation

In addition to the longer GPR lines made parallel to the depositional dip, two irregular grids (Figure 3.16) were acquired in the northernmost sector of 'East Nilemah' where the beach ridges are partially eroded and coquina outcrops in the margins of a drainage channel present an opportunity for comparing and integrating GPR lines with outcrop data (Figure 3.26). Moreover, these GPR grids were used to investigate geometries of depositional elements in both depositional dip and strike directions adding further detail to observations in the long GPR lines.

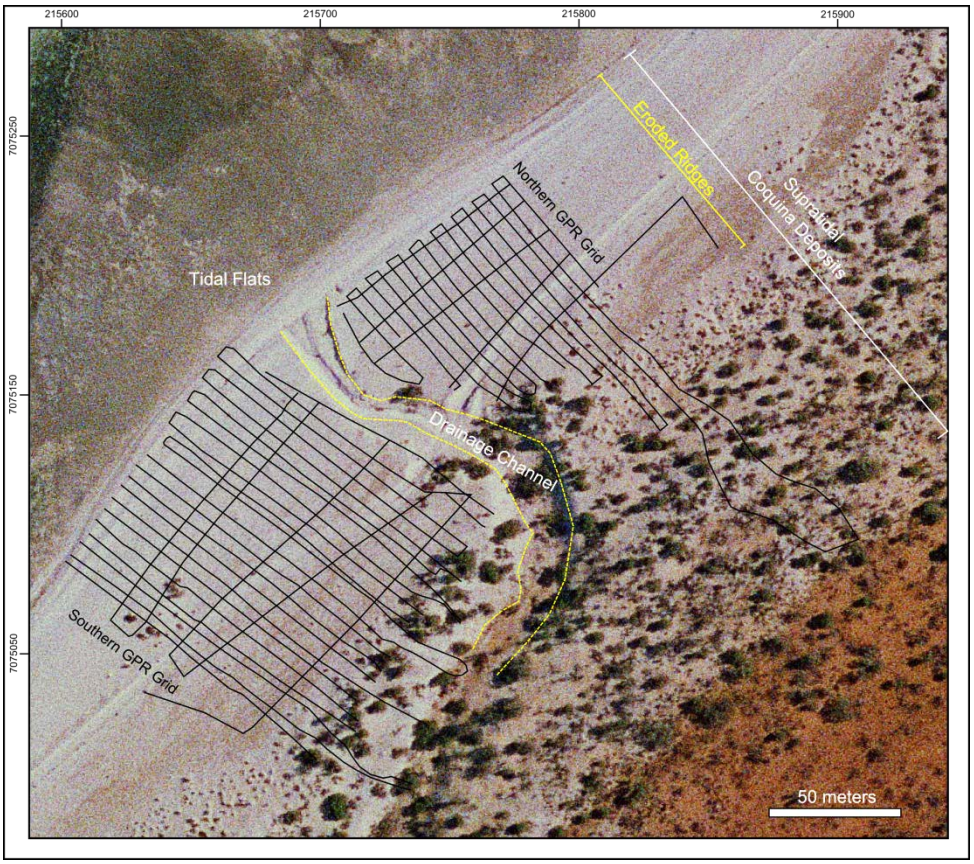

Figure 3.16 - Aerial image of the partially eroded coquina beach-ridge system and location of the irregular GPR grids SW and NE of a drainage channel exposing coquina deposits. For location see Figure 3.1.

Although tracking radar surfaces and radar packages is made difficult by cut and fill processes that occur on the beach environment, Figure 3.17 is an attempt to show lateral variations within radar packages taking place in both depositional dip and strike directions in the southern grid. In spite of some packages showing a limited lateral extent or significant thickness variations in short distances, the overall prograded depositional style observed in the long lines is also evident in the grid area. Additionally, landward dipping reflectors on top of a distinctive erosion surface are interpreted as washover deposits and interrupt the otherwise prograding configuration (Figures 3.18 and 3.19).

The seaward-most ridge in the grid area corresponds to a mature berm whose facies and depositional architecture are illustrated in Figure 3.26. Berm progradation is an important mechanism for beach growth in this area, although the berm top is a feature commonly eroded during storms.

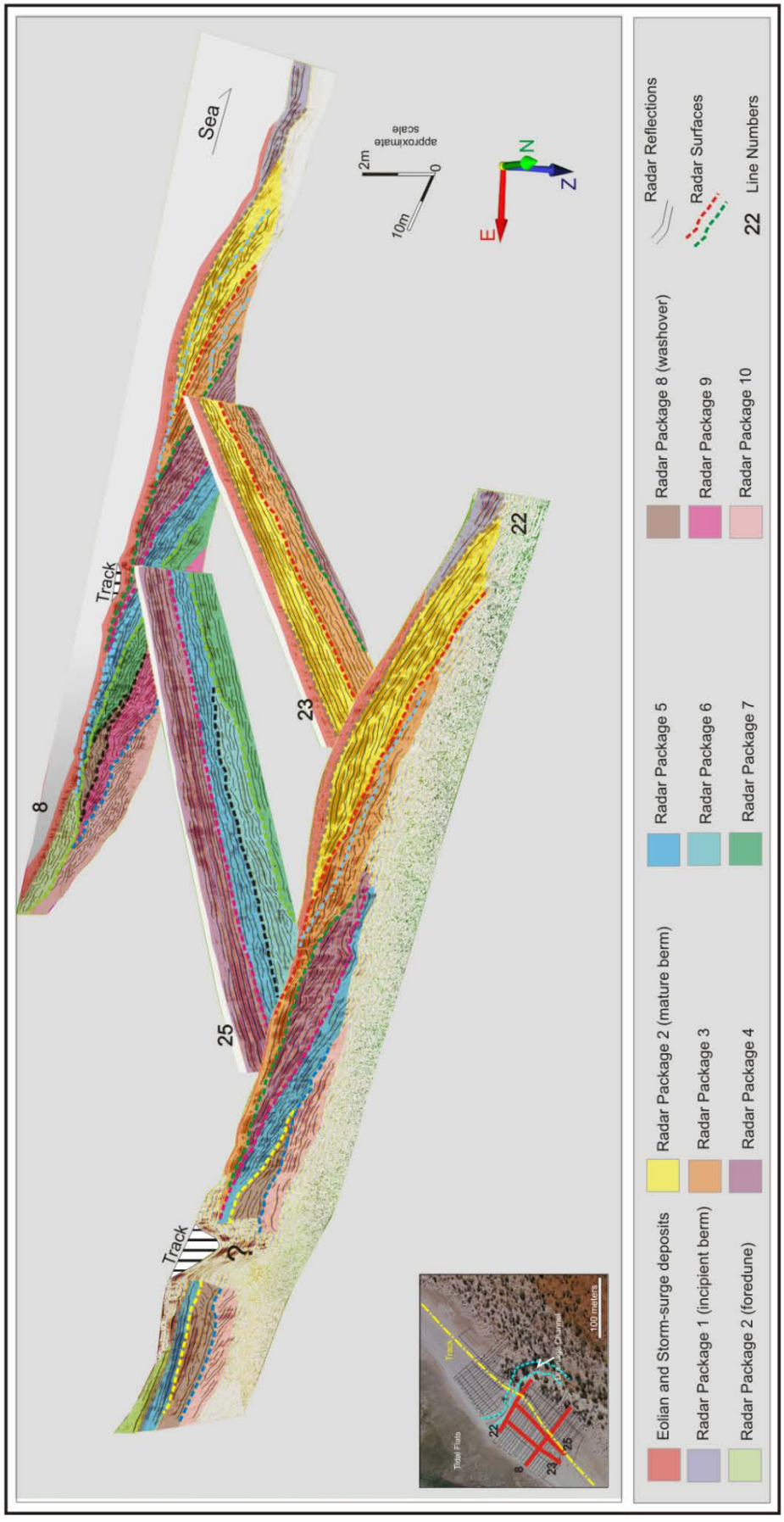

Figure 3.17 – Interpretation for selected GPR lines in grid SW of the drainage channel. Depositional architecture results from berm (and beachface) progradation truncated by erosion surfaces and washover deposits (radar package 8). Eolian and storm-surge deposits cap the prograding succession.

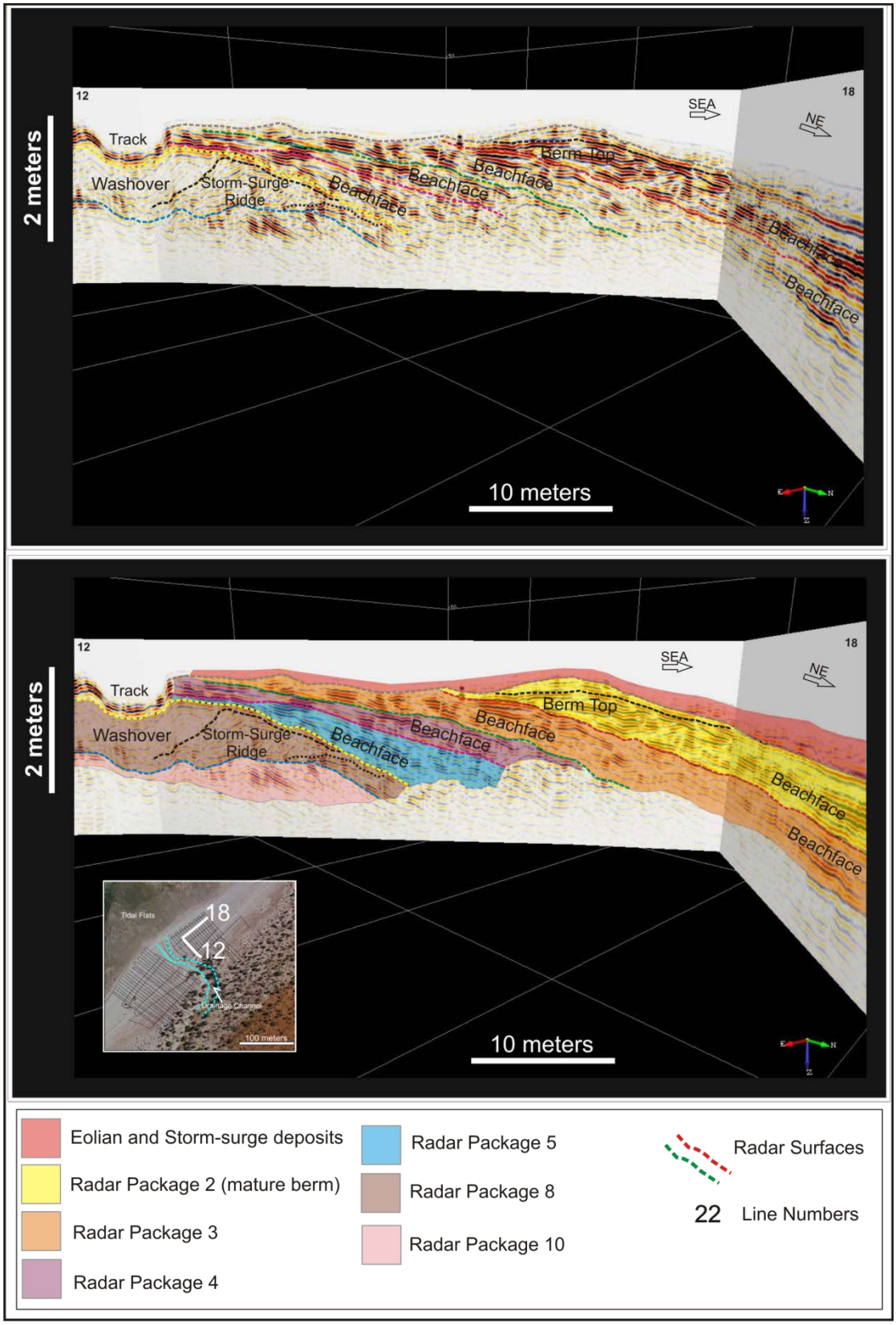

Figure 3.18 - Interpretation for selected GPR lines in grid NE of the drainage channel. Radar packages are correlative to those in Figure 3.17. The geometries observed result from washover and storm-surge deposits that truncate radar package 10. Berm (and beachface) progradation is resumed with the deposition of radar packages 5, 4, 3 and 2.

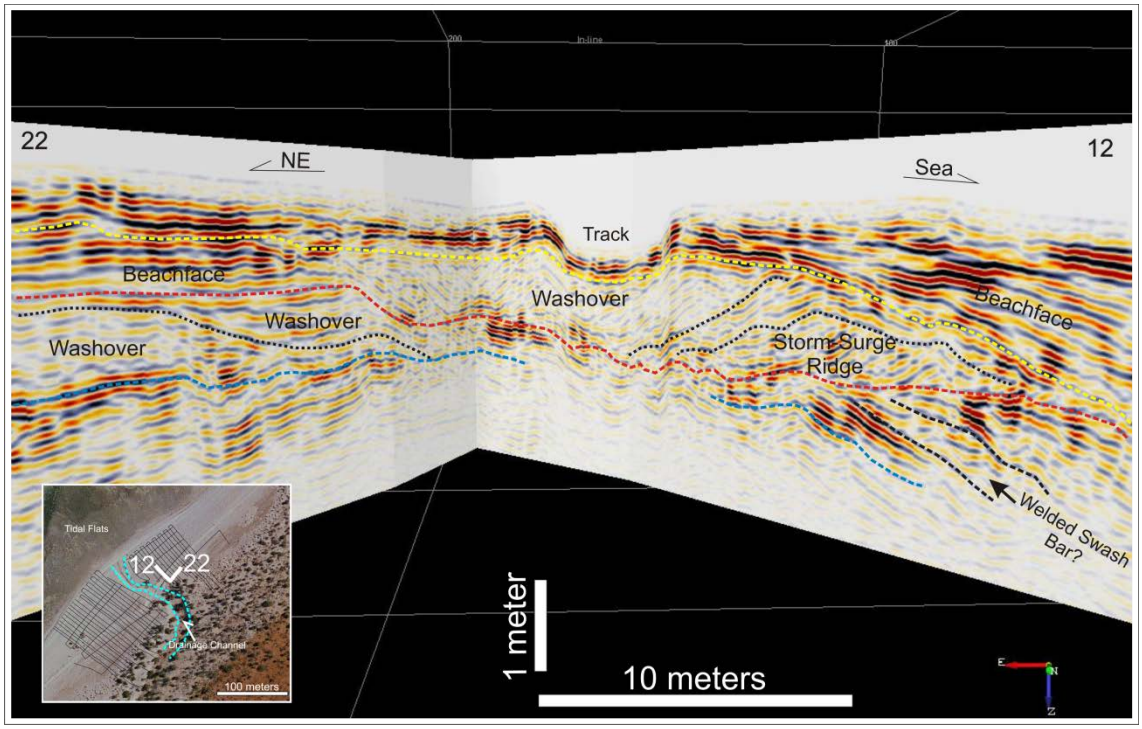

Figure 3.19 - Interpretation for selected GPR lines in grid NE of the drainage channel. Major erosive events followed by the deposition of storm-surge and washover deposits are interpreted in these lines. The washover deposits are traceable in the southern grid and in most of the northern grid.

3.4.4. Sedimentary Characteristics

The beach-ridge system in the studied site is made up of shell gravels composed of mollusks (almost entirely *Fragum erugatum* bivalve) and bioclastic sands constituted by foraminifers, micro-gastropods, serpulids, bryozoans and shell fragments. Secondarily, flat pebbles from the tidal flat breccia pavement (see Logan *et al.*, 1974; Jahnert and Collins, 2012), lithoclasts and ooids contribute with clasts to the system. Bed geometries observed in the field and GPR profiles are described as lenticular, wedge-shaped, mounded or tabular.

The main lithofacies present in the beach-ridge deposits (Figure 3.20) are composed of shell gravels with variable quantities of medium to very coarse bioclastic sand matrix. Sands, commonly shelly and composed of bioclasts (and more rarely ooids) are also important lithologies. Sedimentary structures observed in outcrop and trenches are plane-parallel lamination or stratification, foreset stratification, bed-concordant oriented shells and rare grading. When subaerially exposed for a sufficient amount of time, these sediments are subject to windblown silt and clay infiltration and soil forming processes. Moreover, bioclast micritization, peloid formation and micritic cementation are promoted by microbes present in either the marine environment or the saline phreatic zone. Table 3.2 summarizes the described lithofacies and their main characteristics.

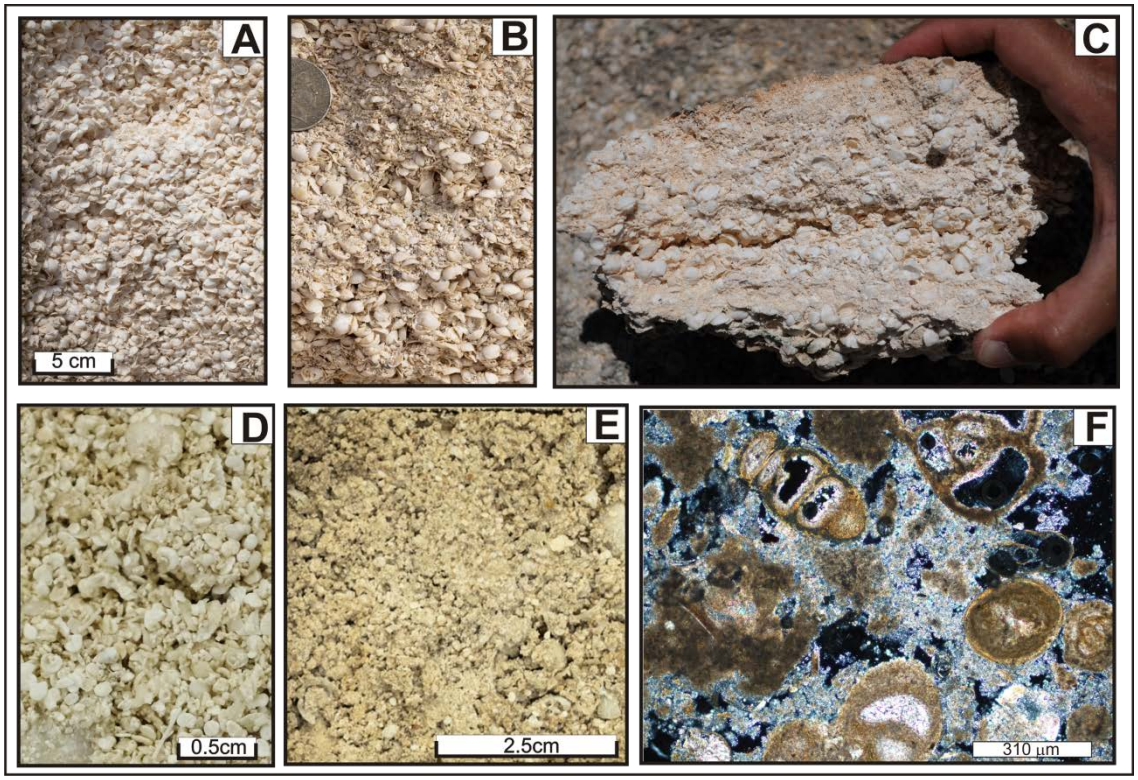

Figure 3.20 – Main lithofacies in the beach-ridge system at 'East Nilemah'. (A) Shell gravel. (B) Shell gravel with coarse/very coarse bioclastic sand matrix. (C) Indurated shell gravel with coarse/very coarse bioclastic sand matrix. (D) Shelly bioclastic sand. (E) Medium to coarse bioclastic, ooid and peloidal sand cemented by micrite. (F) Epoxy-impregnated thin-section of (E) displaying micritized bioclasts and superficial ooids, peloids and micrite cement.

Lithofacies	Texture	Components	Sedimentary Structures	Occurrence
Gsh	Gravel	Whole disarticulated shells, shell fragments, occasional flat pebbles, very rare articulated shells.	Structureless; horizontally oriented shells (bed-concordant);	Storm-Surge ridges; Beachface; Berm crest
Gshsm	Gravel with medium to very coarse sand matrix	Whole disarticulated shells, shell fragments, variable proportions of lithoclasts, bioclasts and ooids in the sandy fraction.	Structureless or plane-parallel lamination	Beachface; washover deposits and berm crest
VCSbi(sh)(oo)	Coarse to Very Coarse Sand	Bioclasts (shell fragments, forams, gastropods, occasional serpulids and rare bryozoans). Variable amount of whole disarticulated bivalve shells, lithoclasts and ooids.	Structureless	Beachface; washover deposits and berm crest
VCSbish(oo)ppl	Coarse to Very Coarse Sand	Bioclasts (shell fragments, forams, gastropods, occasional serpulids and rare bryozoans), whole disarticulated bivalve shells. Variable amount of lithoclasts and ooids.	Plane-parallel lamination and bedding concordant oriented shells	Beachface

Table 3.2 – Characteristics of the main lithofacies observed at the beach-ridge system in 'East Nilemah'. G: gravel; sh: shell; sm: sand matrix; VCS: very coarse sand; bi: bioclast; oo: ooids; ppl: plane-parallel lamination.

3.4.4.1. Sediment Cores and Trenches

3.4.4.1.1. Cores

Four cores were obtained in 'East Nilemah'. Three of them are located in EN-A and one is in EN-B. Figures 3.21 and 3.22 show their core logs and location in the GPR lines context.

Core 02-ENB-02 intersected 4 different radar packages, all of them in the beach depositional element. The topmost package is interpreted as berm top deposits resulting from overtopping and minor overwashing processes. The other three radar packages are interpreted as beachface deposits with a remarkable difference in slope angle between the second package and the other two on the bottom of the core (Figure 3.21).

Similarly, core 02-ENB-04 intersected 4 radar packages and the topmost represents berm top deposits. The packages below can be either interpreted as berm top or spit deposits as in radar profiles both may show horizontal radar facies in the depositional dip direction and textures alone do not provide unequivocal information for this interpretation (Figure 3.21).

Core 02-ENB-03 exhibits a dominance of shell gravels in the upper layers that overwash a package with landward dipping reflectors interpreted as a swash bar.

The lowermost beds in the cores located in EN-A display bioclastic and peloidal sands with micrite cement. These sands are interpreted as sand aprons on the lower beachface which undergoes early diagenesis when exposed to marine or saline phreatic waters for a sufficient amount of time (Figures 3.20(E) and 3.20(F)).

The core 02-ENB-01 was obtained in line EN-B and intersected 3 different depositional elements: Storm-surge deposits and soil, beach deposits and welded longshore bars (Figure 3.22). The base of the storm-surge and soil package is marked by an 11 cm shell gravel bed with little or no sand content. The beach deposits are divided into two packages by radar surface rs.B2. The upper package displays interlayered beds of shell gravel with very coarse sand matrix and beds of shelly coarse/very coarse bioclastic sand interpreted as the berm top. The package below rs.B2 has the same basic composition with thicker beds being interpreted as beachface deposits. At the bottom of the core, a bioclastic and peloidal sand layer with micrite cementation increasing with depth is also observed, as previously described in the cores of line EN-A.

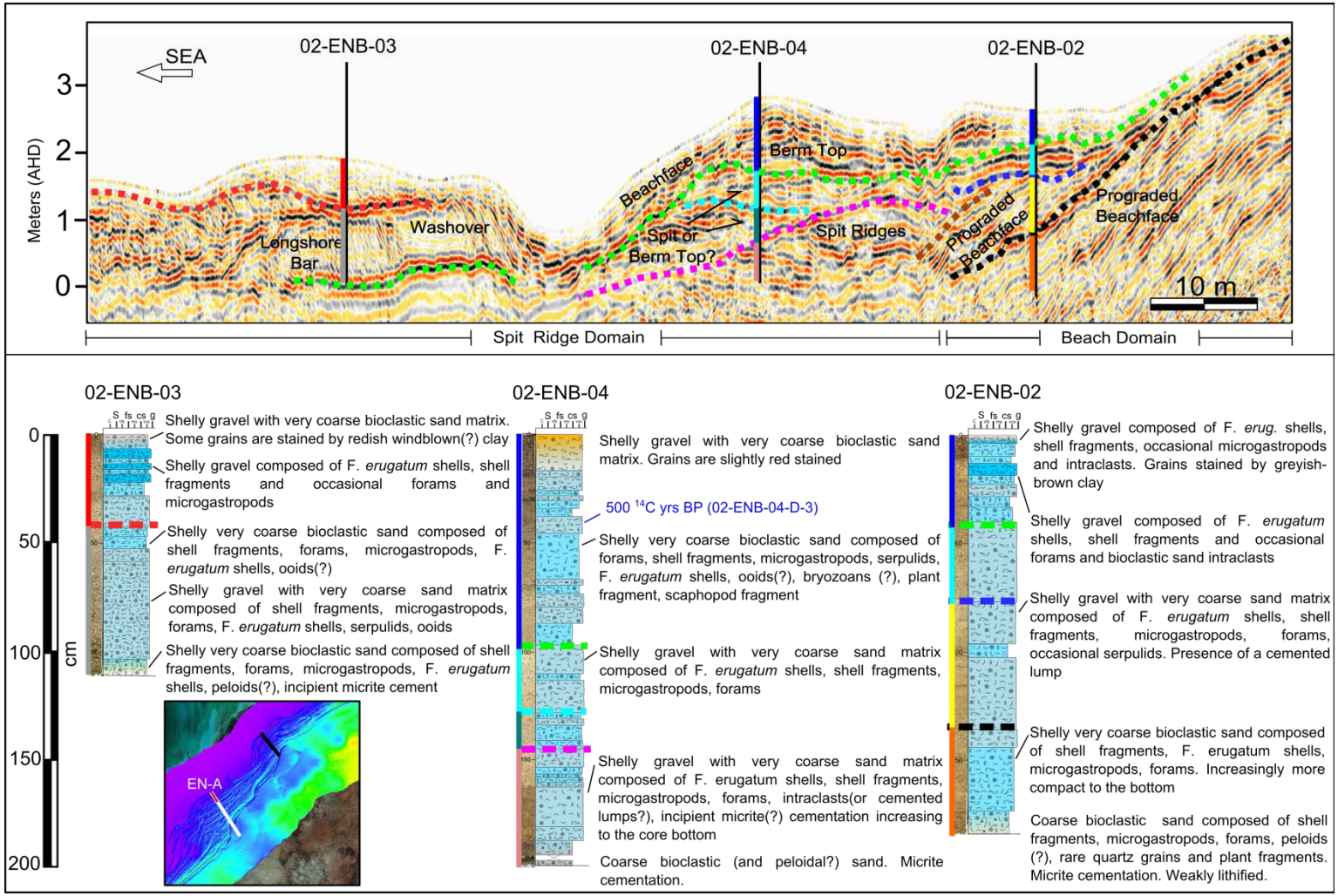

Figure 3.21 – Segment of GPR line EN-A where 3 cores were obtained in the transition of the beach domain to the spit ridge domain. An articulated *F. erugatum* shell was dated in core 02-ENB-04. Bottom of the cores exhibit coarse bioclastic (and peloidal?) sands with micrite cementation. See Fig. 3.23 which presents a legend for the sedimentary logs.

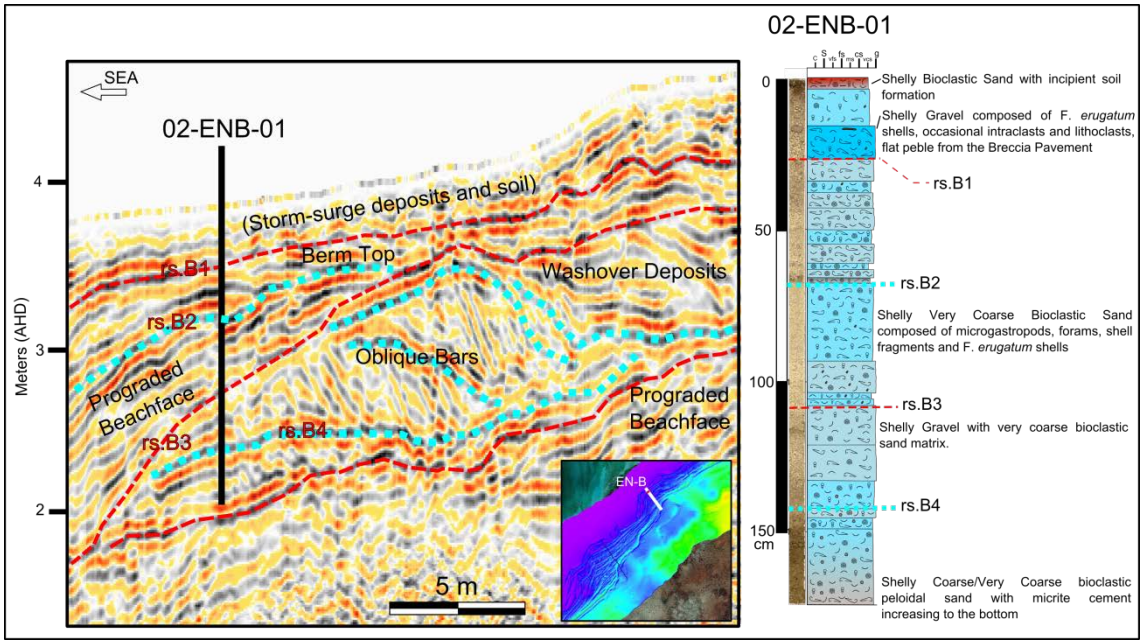

Figure 3.22 – Segment of GPR line EN-B where core 02-ENB-01 was obtained intersecting storm-surge and soil deposits, berm top, beachface and oblique bar sediments as interpreted in the radar profile. See Fig. 3.23 which presents a legend for the sedimentary log.

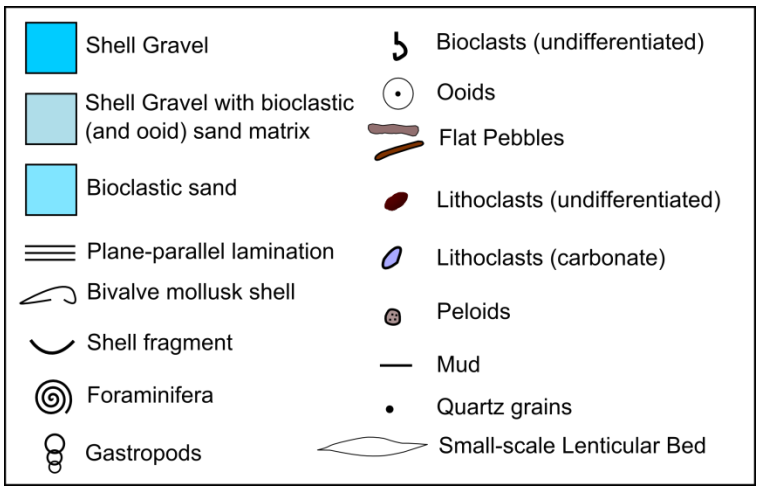

Figure 3.23 – Legend valid for all sedimentary logs.

3.4.4.1.2. 'East Nilemah' Trenches and Pits

Two trenches located along GPR line EN-A were excavated to assess facies and internal geometries of selected storm-surge ridges (Figure 3.5). The trenches reached 0.60 and 1.20 meters displaying sand-free shell gravels and centimetric irregular layers of shell gravels containing variable amounts of organic matter, plant roots and fine grained particles (clay and silt). These fine particles are interpreted as windblown implying ridge construction by multiple episodes of sedimentation and subaerial exposure as opposed to a single event deposit. Smaller

pits excavated for sediment sampling revealed this same alternation of sand-free shelly gravels and incipient soil characterized by fines-rich shell gravels with plant roots. Where weakly cemented portions of the sand-free shell gravels are found, it is observed that shells are oriented concordant to the bedding, commonly convex-up (Figures 3.5(C) and 3.5(E)) as also observed by Jahnert et al. (2012) in deposits they named 'convex-up ridges' and interpreted as being generated by storm surges. The bottom of both trenches intersected the beach depositional element denoted by the occurrence of horizontally or gently seaward-dipping indurated sandy coquina facies.

Additionally three abandoned water pits were used to obtain sedimentary information at "East Nilemah" site (Figure 3.1). Pit AWP-01 is 1.56 meters deep and was intersected by GPR line EN-E (Figure 3.24) where it is possible to recognize two main radar facies occurring in the location of the core: an upper, curved convex reflector configuration, separated by a major radar surface (*rs.E1*) from a lower inclined seaward-dipping radar facies. The upper curved convex radar facies, interpreted as storm-surge deposits, consists of two sand-free shell gravel beds separated by a discontinuous layer of shell gravel with matrix of silt to coarse sand. The lower inclined, seaward dipping planar radar facies is interpreted as the beach depositional element relating to interlayered centimetric bioclastic sand and shell gravel layers with or without bioclastic sand matrix.

The pit AWP-02 (Figure 3.25) was not intersected by any GPR line and shows apart from two beds of shell gravel with bioclastic sand matrix, overall sandy deposits, sometimes with non-oriented shell layers and plane-parallel lamination. Two layers of clast-supported shell gravels with silt and clay in the matrix are interpreted as exposure surfaces containing windblown included fines, implying that deposition in this area occurred during repeated episodes of inundation (storms). Qualitative XRD results for these gravels with infiltrated fines show a mineralogical composition of calcite, aragonite, quartz, ankerite, magnesian calcite, muscovite and halloysite.

Pit AWP-04 (Figure 3.25), not covered by GPR lines, displays shell gravels overlain by a bioclastic sandy package punctuated by the occurrence of centimetric shelly layers. In this pit, the occurrence of layers rich in fine particles is rare implying that subaerial exposure was not as common in this site during the time of deposition or the beds with infiltrated silt and clay have been eroded by succeeding storm events.

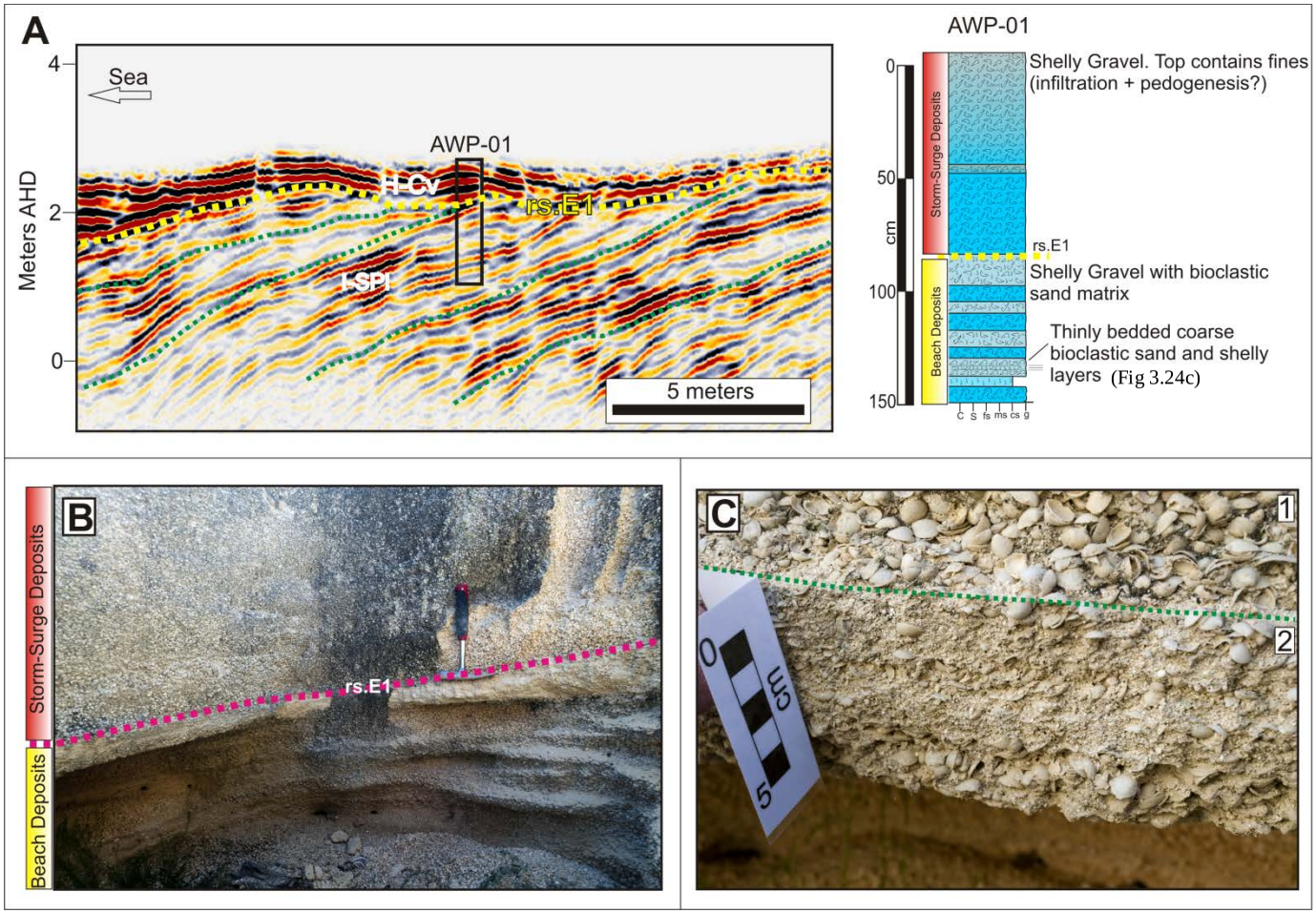

Figure 3.24 – Abandoned water pit AWP-01. (A) Segment of GPR line EN-E and composite sedimentary log made in AWP-01. Radar surface rs.E1 is indicated in both GPR and log and separates storm-surge deposits and beach deposits. See Fig. 3.23 which presents a legend for the sedimentary log. (B) Photograph of AWP-01 wall showing sand-free shell gravel on top of radar surface rs.E1 and interlayered shell gravels with and without bioclastic sand matrix below rs.E1. (C) 1- Shell gravel with coarse/very coarse bioclastic sand matrix. 2 - Shelly coarse/very coarse bioclastic sand with plane-parallel lamination and bed concordant oriented shells.

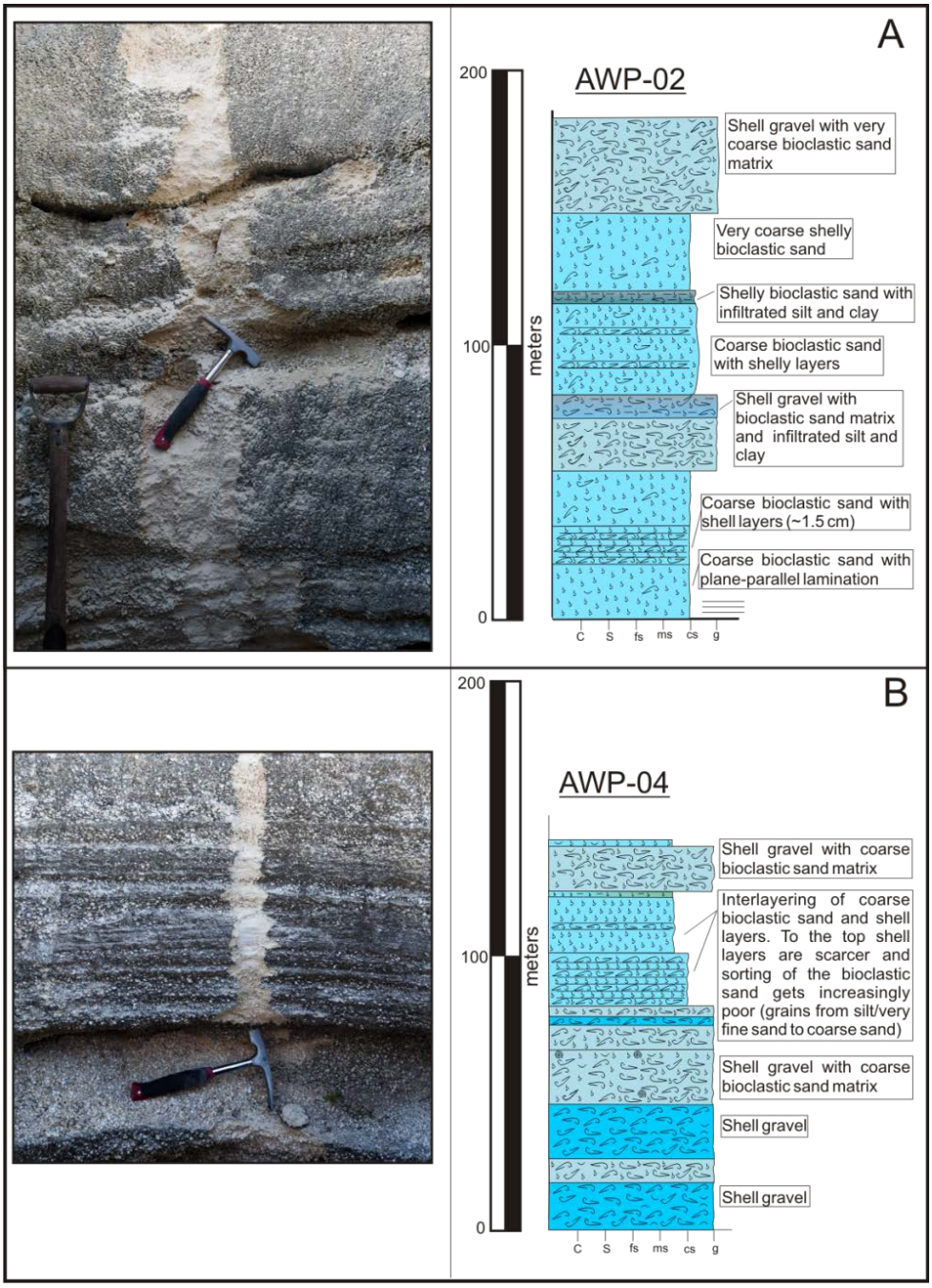

Figure 3.25 – Logs in 2 abandoned water pits not covered by GPR transects. (A) Left: photograph of AWP-02 wall. Right: AWP-02 composite sedimentary log showing a predominance of sandy layers in this location. Photos on the left are not scaled 1:1 with the pit logs. See Fig. 3.23 which presents a legend for the sedimentary logs. (B) Left: photograph of AWP-04 wall. Right: AWP-04 composite sedimentary log showing a predominance of shell gravels to the bottom of the pit and sandier facies to the top.

3.4.4.2. Ridge Outcrop at "East Nilemah" site

A drainage channel cuts through a beach ridge at the northernmost part of the study area and partially exposes facies and internal geometry (Figure 3.26). The bedding geometries observed are horizontal and seaward dipping being a result of berm construction by swash processes in the beachface and overtopping (and minor overwashing) on the berm crest. The facies are composed of bivalve mollusk shells (*F. erugatum* predominates) and bioclastic sands, which are present in each individual bed in variable proportions. Flat pebbles from the breccia pavement (Logan *et al.*, 1974; Jahnert and Collins, 2012) and lithoclasts are also common in these deposits. Truncation surfaces identified on the outcrop are interpreted on the GPR lines acquired in this site (Figure 3.26).

The exposure of the internal architecture of a ridge allowed the interpretation of different parts of a berm based on the bedding geometries observed. Facies were logged in distinct locations of the ridge and major truncation surfaces were correlated between logs (Figure 3.27). In the interpreted upper beachface, a predominance of shell gravels with bioclastic sand matrix and shell gravels with no matrix is observed. The facies in the lower beachface are composed of coarse shelly bioclastic sands exhibiting seaward-dipping layers, rich in shells oriented concordant to the bedding plane. The berm crest displays bioclastic sands and shell gravels with bioclastic sand matrix interlayered in centimetric beds.

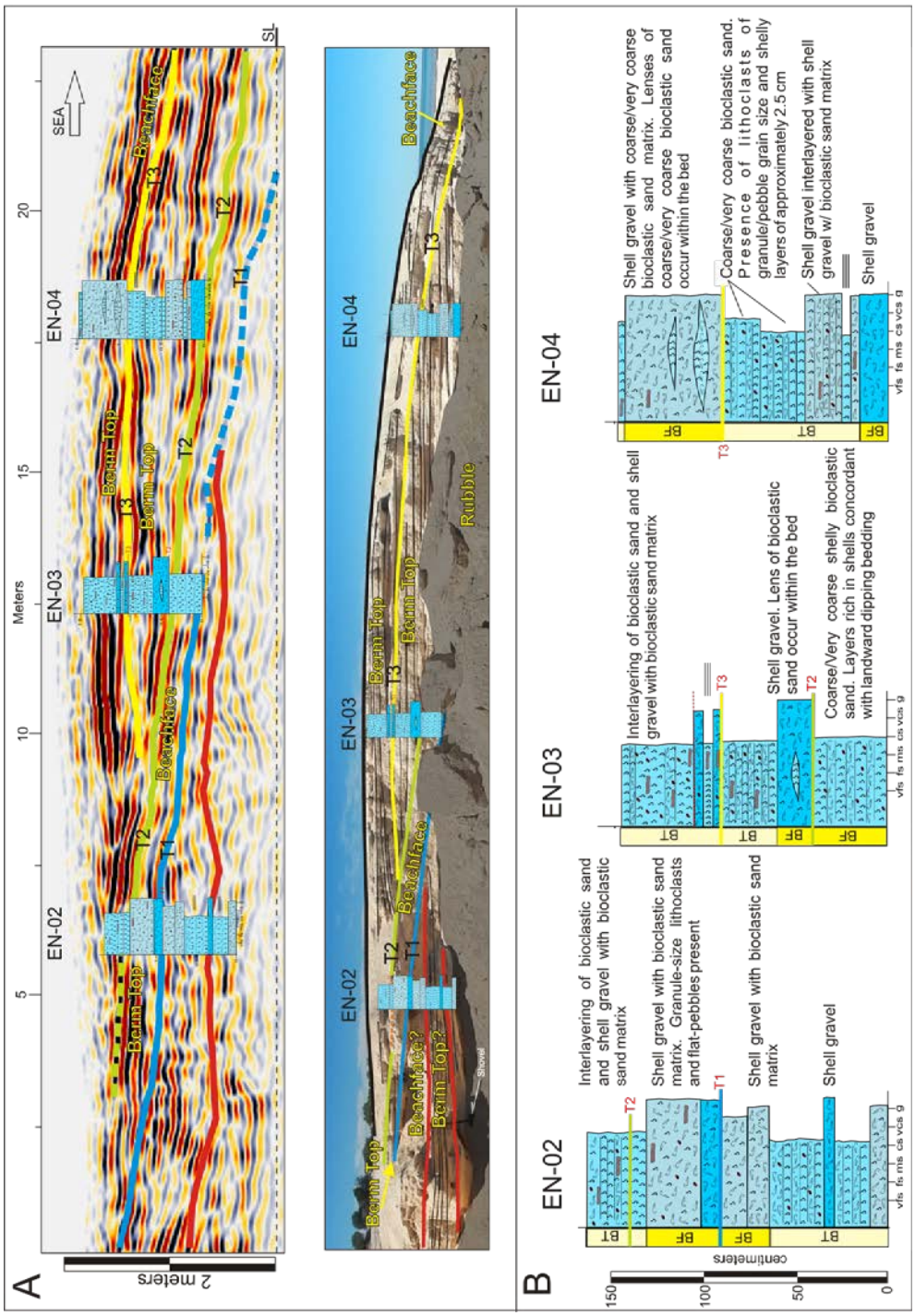

Figure 3.26 – Drainage outcrop adjacent to the GPR irregular grids. (A) Top: Interpreted GPR line parallel to outcrop (sedimentary logs are projected). T1, T2 and T3 are radar surfaces which correlate to truncation surfaces in the outcrop. Bottom: Photograph of the outcrop with truncation surfaces and sedimentary log locations indicated. (B) Sedimentary logs of the drainage outcrop. BT – berm top deposits; BF – beachface deposits; T1, T2, T3 – truncation surfaces. See Fig. 3.23 which presents a legend for the sedimentary logs.

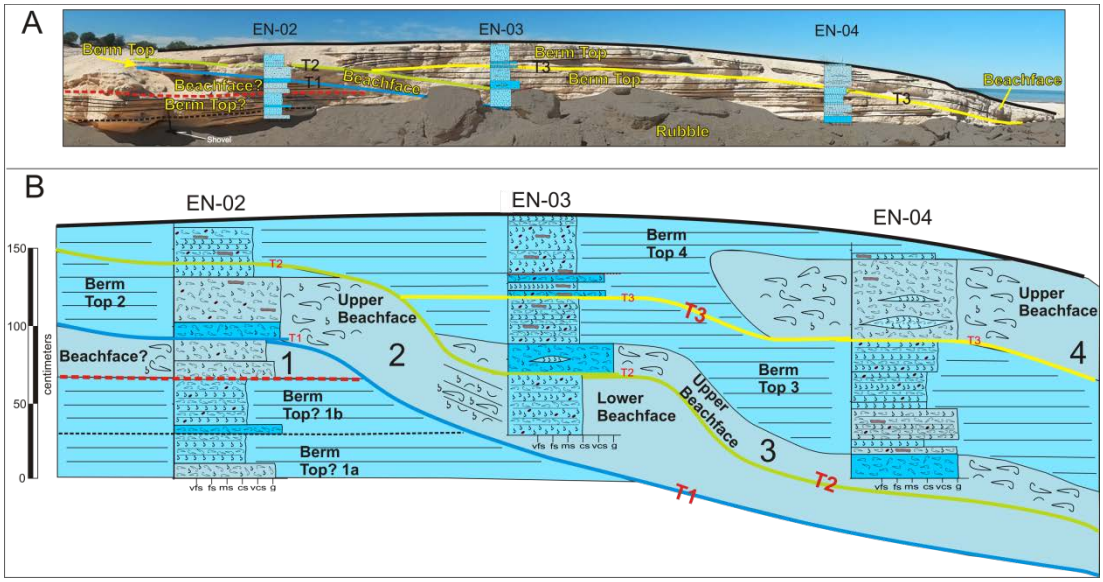

Figure 3.27 – Ridge internal geometry, facies and interpreted depositional sub-environments. (A) Photograph of the outcrop with truncation surfaces and sedimentary log locations indicated.T1, T2 and T3 are major truncation surfaces. (B) Sedimentary log correlation based on outcrop and GPR geometries, truncation surfaces and facies. See Fig. 3.23 which presents a legend for the sedimentary logs. At least 4 main episodes of erosion and deposition were responsible for the formation of this ridge.

3.4.5. Ridge and Depositional Domain Chronology

For the purpose of assessing the chronology of ridge formation and their evolution, 19 shell samples were radiocarbon dated in 'East Nilemah' (Table 3.3). Some of the samples were collected before GPR acquisition, most of which were in storm-surge ridges prone to contain reworked material. For that reason age reversals were observed in transects studied along the depositional dip of the beach-ridge system. Although other samples were carefully planned using the GPR profiles to avoid storm-surge deposits, some reworking was still evident in samples collected in the beach depositional element. Hence, dating results presented should be used as maximum ^{14}C ages, except for the sample where an articulated *Fragum erugatum* shell was obtained in core 02-ENB-04 (Figure 3.21). However, the time of residence of an articulated shell within the basin is unknown and is potentially a cause of error in the order of decades.

Of 19 radiocarbon dated samples, 11 were obtained in storm-surge deposits and 8 are from beach deposits. Figure 3.28 displays the location and depositional context of dated samples and the ages used to constrain the beach-ridge system evolution in 'East Nilemah', bearing in mind that prograded beach deposits get younger seaward and storm-surge deposits do not necessarily get younger seaward and are more likely to contain reworked material.

In the studied area, the initiation of the beach-ridge system construction, i.e. deposition of ridge set 1 and the washover domain, started about 4500-5000 ^{14}C years BP as evidenced by the 4780 ^{14}C years date obtained in the washover domain and the oldest age measured in the area is

5040 ^{14}C years BP. This initiation at approximately 4500-5000 ^{14}C years BP is in accordance with results obtained by Jahnert *et al.* (2012) for the beach ridges at Telegraph Station site, to the north of 'East Nilemah'.

No dates were obtained in ridge set 2, which is discontinuous and truncated by ridge set 3 in the GPR line EN-D vicinity. Furthermore, ridge set 2 thins until becoming completely absent north of EN-E line (Figure 3.28).

The only reliable age measured in ridge set 3 is 2620 ^{14}C years BP evidencing an erosional gap in EN-A and EN-D transects of at least 1100 years between the onset of the system and the first overwash events over ridge set 1 and the deposition of ridge set 3. Similarly, the next reliable sample is in ridge set 4 displays a date of 1640 ^{14}C years BP.

Ridge set 5 has the most reliable sample, an articulated *Fragum erugatum* shell, having a measured age of 500 ^{14}C years BP. In GPR lines EN-A, EN-C and EN-D the transition from ridge set 4 to ridge set 5 is marked by the occurrence of a high elevation ridge followed by a step which is the boundary between a domain where prograding beach depositional elements predominate and a domain of spit ridges predominance. This transition is not visible in GPR lines EN-B and EN-E although it is clear in the orthophoto that spits do occur in ridge set 5 between lines EN-B and EN-D.

Sample Id	Source of Carbon	^{14}C age (years BP)	error (years)	^{14}C age (years BP) calibrated 2 sigma
END-11	Bivalve Shell	2190	30	1850/1540
END-10	Bivalve Shell	2500	30	2260/1910
END-09	Bivalve Shell	3180	30	3050/2740
END-08	Bivalve Shell	3820	30	3830/3540
END-07	Bivalve Shell	2380	30	2070/1800
END-06	Bivalve Shell	1860	30	1510/1200
END-05	Bivalve Shell	2070	30	1700/1400
END-04	Bivalve Shell	2740	30	2510/2260
END-03	Bivalve Shell	2150	30	1800/1510
END-02	Bivalve Shell	3720	30	3690/3400
END-01	Bivalve Shell	4780	30	5120/4810
END-D-108	Bivalve Shell	2620	30	2330/2070
END-D-107	Bivalve Shell	2840	30	2690/2320
ENA-D-101	Bivalve Shell	5040	30	5450/5200
EN-DR-D-110	Bivalve Shell	1360	30	940/700
AWP1-G-01	Bivalve Shell	2530	30	2280/1950
AWP1-D-02	Bivalve Shell	3750	30	3730/3440
AWP1-D-01	Bivalve Shell	1640	30	1250/970
02ENB04-D-3	Articulated Bivalve Shell	500	30	230 to post 1950 AD

Table 3.3 – Radiocarbon chronology for *F. erugatum* shells of selected coquina deposits. A delta R of 70 ± 50 was used for marine reservoir correction. Data calibrated against Marine09 calibration curve (Reimer et al., 2009).

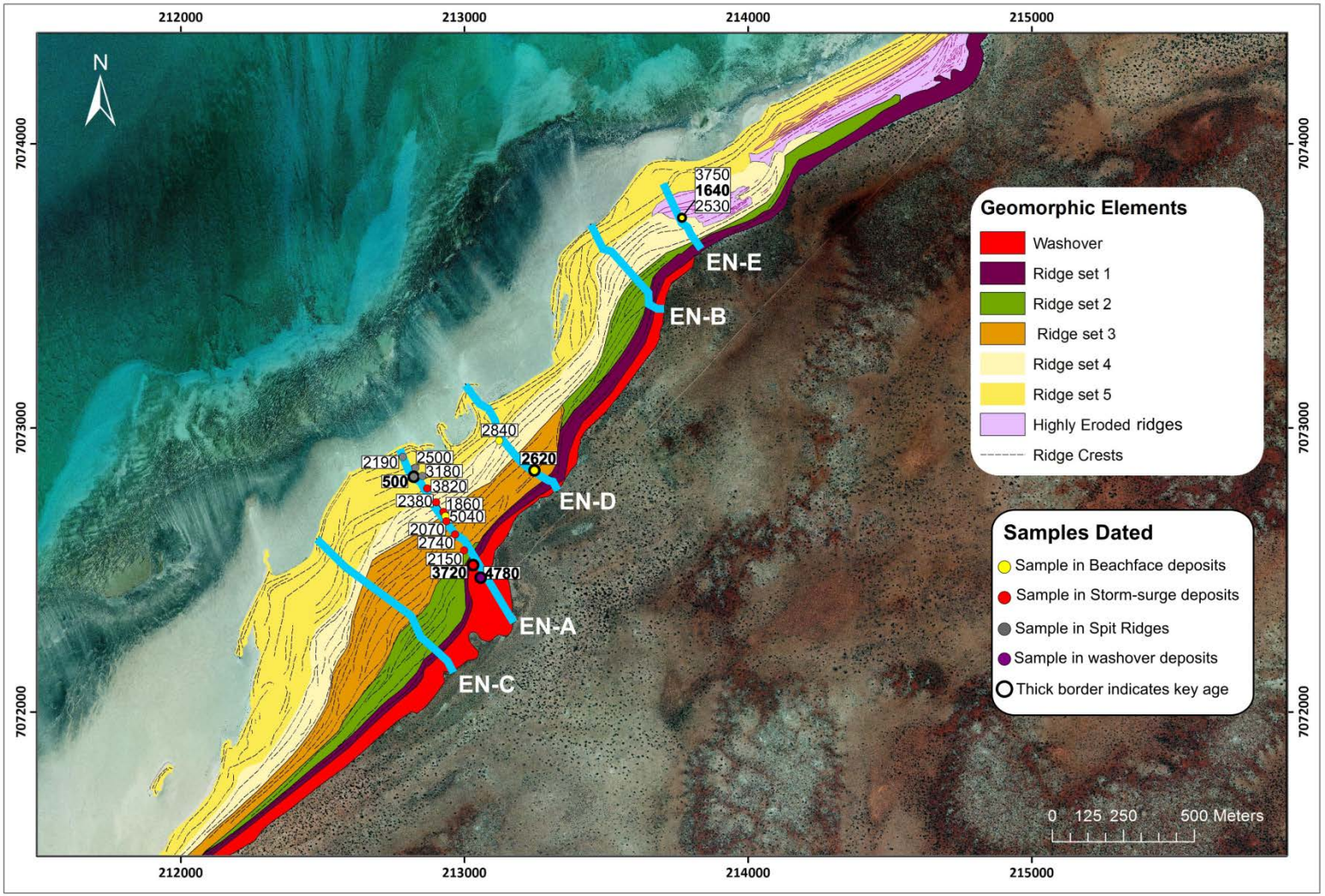

Figure 3.28 – Geomorphic map and aerial image of the coquina beach ridge system in 'East Nilemah' site with ^{14}C ages and GPR transect locations. Key ages for the interpretation of ridge chronology are indicated by thick-bordered circles.

Although depositional domains may endure and overlap in time, Figures 3.29(A) and 3.29(B) attempt to constrain their chronologies and expose their rough stratigraphic significance. The Washover Depositional Domain is the oldest and initiated about 5000 ^{14}C years BP. The Spit ridge depositional domain is the youngest and is less than 1640 ^{14}C years BP. The Beach Depositional Domain is probably the most persistent in time although it is not clear if deposition was taking place between 2620 and 3720 ^{14}C years BP due to lack of reliable samples for that interval. The Storm-surge Depositional Domain is diachronous and caps multiple amalgamated erosive surfaces over the Beach domain.

3.5. Discussion

Shark Bay region is vulnerable to sporadic tropical cyclones and storm surges. A number of indications mentioned by Jahnert et al. (2012) to evidence the major role storms played in ridge building at Telegraph Station site were also observed in 'East Nilemah'. In the study site these indications consist of washover fans, spit growth predominantly from north to south, ridges with elevations up to 8m, at least 5.5m above the Holocene maximum flooding at 6800 U/Th years reported by Collins et al. (2006) in Western Australia, and presence of flat pebbles from the breccia pavement located on the seaward flanks of younger ridges 3-4m above present day sea level. We propose a depositional model where washovers and storm-surge ridges are deposited in the peak phase of storms, mainly by overwash and inundation, and berms develop in the wanning phase predominantly by swash-backwash motions, overtopping and minor overwashing processes.

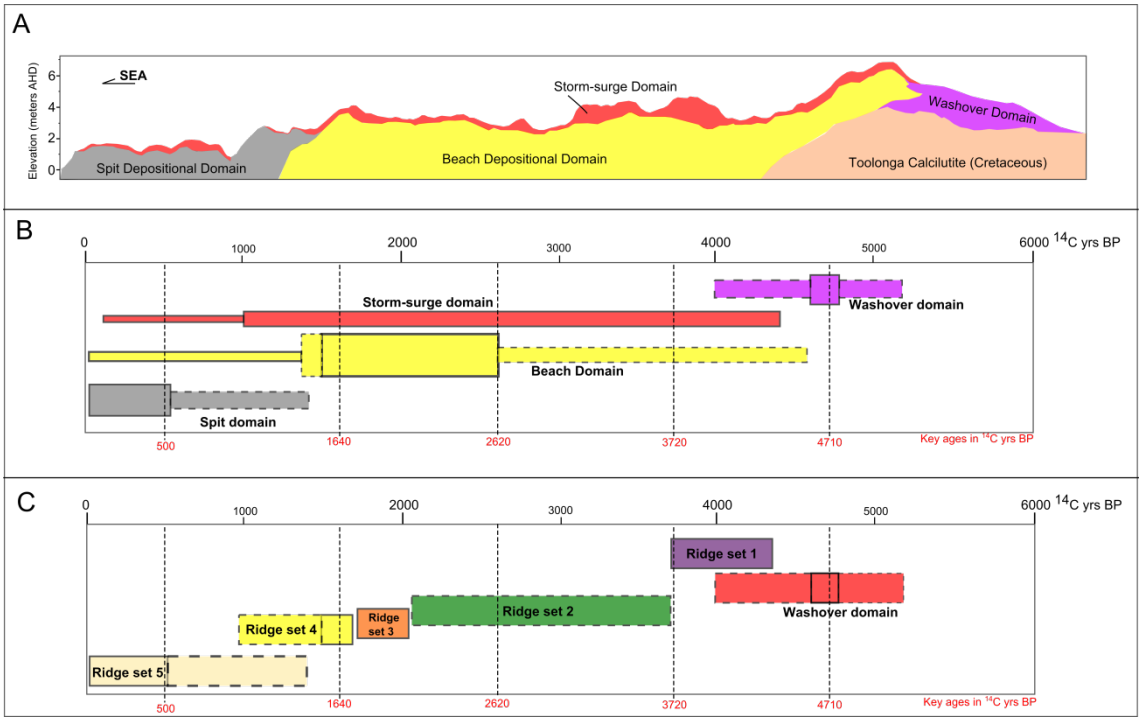

Figure 3.29 – Depositional domain and ridge set chronology. (A) Sketch of typical depositional domain arrangement in 'East Nilemah'. (B) Depositional domain chronology. Thickness of the bars indicates relative abundance and dashed line in the bar contour indicates inference of the occurrence of depositional domains. (C) Ridge set chronology. Dashed line in the bar contour indicates inference of the occurrence of ridge sets.

3.5.1. Depositional Model of 'East Nilemah' Coquina Ridges

The coquina beach-ridge system displays an internal structure in which the progradational style of the beach domain is prevalent. This depositional style is a result of the stacking of plane-parallel seaward dipping radar reflections produced by beachface progradation. Occasionally as is visible in some GPR transects (e.g. EN-B, Fig. 3.10) the beach depositional element also exhibits up-dip mounded or wedge-shaped ridges interpreted as berm crests. Several authors state that berm formation is directly linked to high water levels, storm waves and onshore sediment transport (e.g. Komar, 1998; Neal et al., 2002; Bendixen et al., 2013). In 'East Nilemah' the beach depositional element occurs as high as 6m AHD. Even considering a former higher than present sea level of +2m (Collins et al., 2006), only storm-surges could be responsible for the deposition of beach sediments at that elevation. The berm crest expected updip of the beachface prograded reflections is commonly eroded by succeeding larger storms that paradoxically may build a berm at higher elevations because of increased wave heights and run-up (Bascom, 1953). Komar (1998) states that the progradation of the beach may leave behind a set of inactive storm berms recording a past of extreme storm events. Although most of the berm crests in the area are eroded and draped by other storm-surge deposits (the storm-surge domain) the plain view of the beach-ridge system suggests that berm progradation exerts an important control on the beach-ridge external morphology. The GPR grid in the north of the

area provided clear images of how berm progradation is an important mechanism of the beach-ridge system growth. Furthermore, the outcrop of a berm internal geometries in a drainage channel (Figures 3.26 and 3.27), abandoned water pits and cores together with GPR profiles permitted the construction of a depositional model for the coquinas at 'East Nilemah'.

The berm (sensu Hine, 1979) is the building block of the beach depositional domain, and therefore of the beach-ridge system in the area. An idealized sketch of the depositional model for coquina ridge formation during a set of a few storm events is presented in Figure 3.30. Although grain size is not expected to be the preponderant factor influencing hydraulic behaviour in heterogeneous bioclastic deposits (Kench and McLean, 1997) an adaptation of the model proposed by Orford et al. (1991) for clast sorting in coarse clastic coastal barriers is useful to understand the sedimentary dynamics for ridge construction under storm high-energy conditions.

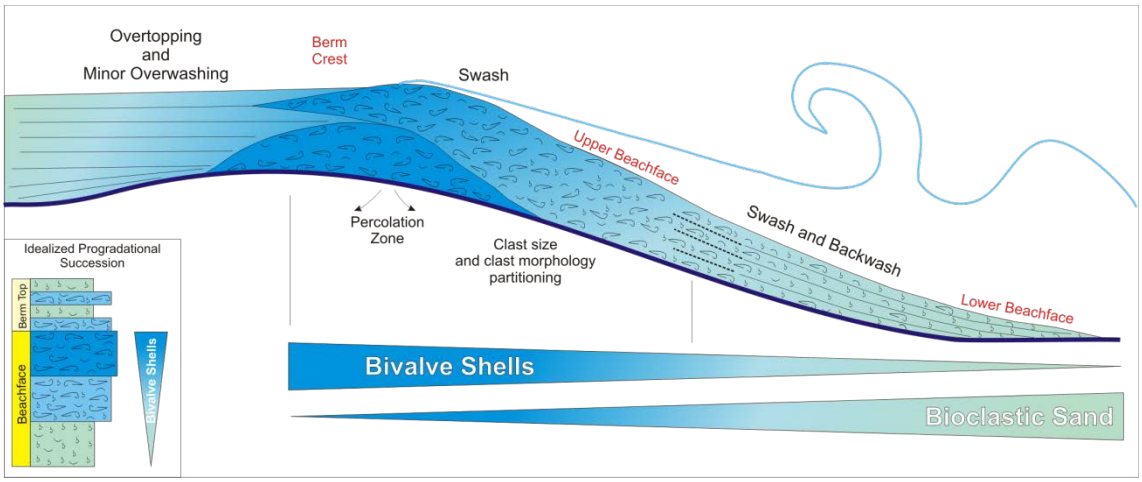

Figure 3.30 – Elementary depositional model for a coquina ridge during the waning phase of storm events.

During episodes of elevated water levels and moderate to high-energy conditions, bioclastic sediment is mobilized from the subtidal to the supratidal environment. At the upper beachface clast morphology and clast size partitioning will take place and its efficiency will depend on the characteristics of the storm (intensity, direction of approach and duration). This clast partitioning will lead to accumulation of *Fragum* shells in the upper beachface increasing beach permeability in this part of the beach. This high permeability zone favours percolation during uprush making the backwash motion negligible at the upper beachface. Backwash will regain importance at lower levels of the beachface and bioclastic deposits will exhibit plane-parallel lamination and oriented bivalve shells concordant with the bedding. These bioclastic deposits will be enriched in the sandy fraction as part of the *Fragum* shells have been transported further shoreward by clast partitioning. In even more energetic conditions the bioclastic sediments are

transported over the ridge crest and overtopping and minor overwashing will lead to berm ridge growth resulting in storm beach aggradation. The depositional model described above is expected to occur in the waning phase of major storms or during the passage of distant storms. On the other hand, the peak phase of major storms will be characterized by erosion and inundation overwash (Donnelly, 2006) leaving behind deposits that will comprise the storm-surge domain (Figures 3.5, 3.29 and 3.31).

3.5.2. Evolution of the Beach-ridge System in 'East Nilemah'

The onset of the Beach-ridge system in 'East Nilemah' took place with the washover domain deposition at about 5000 ^{14}C years BP. This was the beginning of a period when the sea level rose sufficiently under adequate storm periodicity and intensity, complemented by abundant sediment supply (i.e. high *F. erugatum* shell productivity) favored the development of the progradational beach depositional domain (Figure 3.31). It is not possible to determine the exact time interval for the development of ridge set 2 due to lack of reliable samples however it can be constrained within 3720 and 2620 ^{14}C years BP interval. After 2620 ^{14}C years BP, deposition occurred in the area of ridge sets 3, 4 and 5. The spit ridge domain is within the area of deposition of ridge set 5. A well-pronounced difference in elevation is observed between the spit depositional domain and the beach depositional domain. This elevation step was established between 500 and 1640 ^{14}C years BP (Figure 3.31). When lower sea levels are reached, it becomes difficult for storm-surges to overcome the coastal barriers. Thus, longshore currents are induced nearshore and a series of spit ridges locally develop (Figures 3.31 and 3.32B). Furthermore, environmental changes such as alteration of wind and wave climate, storminess and increase in sea-level fall rate are possible influences on the formation of this step and the deposition of the spit-ridge depositional domain. In this regard, Jahnert et al. (2012) also observed a change in layer organization and a shift in the focus of sediment deposition in Telegraph Station ridges they recognized to have occurred around 1000 years ago. Figure 3.32 illustrates this switch in the prevailing processes responsible for ridge construction, experienced in 'East Nilemah' during the latest Holocene.

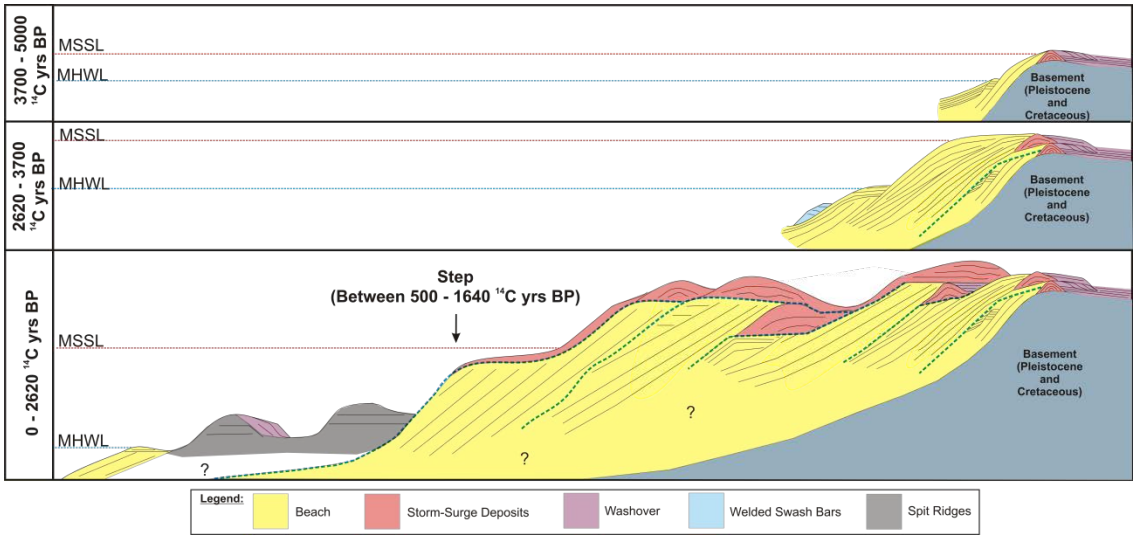

Figure 3.31 – Simplified evolutionary model for the depositional domains in 'East Nilemah' beach ridges. Depositional elements and major erosional surfaces have the same colour code used in GPR profiles. MSSL – Mean Storm-surge Level; MHWL – Mean High Water Level.

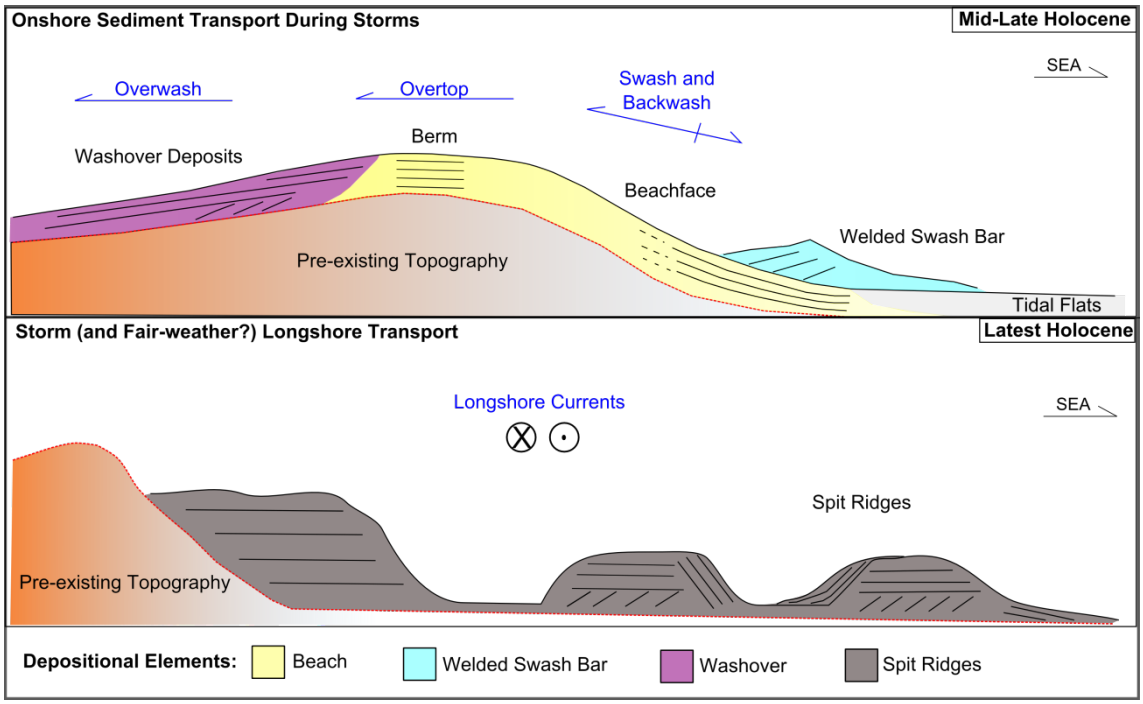

Figure 3.32 – Idealized sketch illustrating the prevailing processes switch experienced in 'East Nilemah' during the latest Holocene. Top: Onshore sediment transport during storms and overwash, overtop and swash processes prevailed in the Mid to late Holocene phase of ridge construction. Bottom: Longshore currents prevail in ridge construction processes and spit ridges develop during the latest Holocene.

3.6. Conclusion

This chapter documents a Holocene coquina beach-ridge system that developed during episodes of elevated water levels under overall falling sea level conditions. GPR and sedimentological data were used to define five depositional elements: beach, washover, welded longshore (or swash) bar, spit and storm-surge ridge. These depositional elements arrange in 2 different sets depending whether prevailing coastal process taking place are swash-backwash motions or longshore currents. Four depositional domains (washover, beach, spit and storm-surge) were defined in particular areas where given depositional elements tend to predominate. Together with depositional domains, major geomorphic elements and radiocarbon chronology were used to outline an evolutionary and stratigraphic framework of the system. The coquina beach-ridge system started with the deposition of the washover domain at about 5000 ^{14}C years BP followed by a period of adequate storminess and abundant sediment supply, between about 3700-1600 ^{14}C years BP, when the progradational beach depositional domain developed. Within 1600-500 ^{14}C years BP a pronounced distinction in ridge elevation was established between the spit depositional domain and the beach depositional domain. This elevation 'step' was formed by longshore currents induced nearshore when storm-surges were unable to overcome the coastal barrier because of increasingly lower sea levels. Other possible factors that contributed to the step formation were changes in wind and wave climate and storminess or increase in sea-level fall rate. Facies information coupled with GPR data allowed the construction of a depositional model for the coquina deposits where inundation and overwash induces the deposition of washovers and storm-surge ridges at the peak of major storms while berm construction takes place during the waning phase of storms (or the passage of distant storms) by swash, backwash, overtopping and minor overwashing processes.

Chapter **4**

Mixed Bioclastic-Siliciclastic Western Beach-Ridge System Sedimentary Architecture and Evolution in Hamelin Pool, Shark Bay

4.1. Introduction

Fragum erugatum coquina beaches and beach ridges surround the shores of 2 hypersaline basins within Shark Bay, namely Hamelin Pool and L'Haridon Bight. These coastal deposits form when a substantial amount of shells are transported to the shore by coastal processes. The high productivity of *Fragum* shells is typical of Shark Bay's hypersaline environment where this bivalve prospers by means of endosymbiosis with zooxanthellae (Berry and Playford, 1997).

Hamelin Pool has different geological foundations in its eastern and western shores. To the east and southeast Hamelin Pool waters reach Carbla Plateau which is underlain by the Cretaceous Toolonga Calcilutite (Figure 2.1). To the west, Hamelin Pool waters encounter Nanga Peninsula, whose country rock is composed of Plio-Pleistocene Peron Sandstone (Hagan and Logan, 1974). The site studied in this chapter is located in the western shore of Hamelin Pool (Figure 4.1) and the composition of beach sediments in the area is influenced by the high availability of quartz sand derived from neighboring Peron Sandstone and Denham Sand red dunes in Nanga Peninsula.

An additional distinctive aspect between eastern and western shores is the degree of exposure to storms. Tropical cyclones and storms progress in a south-west direction after originating in the Timor Sea. For that reason, coasts facing west or north-west like those occurring in the eastern shore (Chapter 3; Jahnert et al., 2012) are more vulnerable to storm impacts and tend to experience higher energy processes and higher elevation surges than east-facing coasts in the western shore.

The aim of this chapter is to document geometrical and sedimentological characteristics of a beach-ridge plain occurring in the western shore of Hamelin Pool using aerial orthophotos, GPR profiles, radiocarbon chronology and push cores to assess the depositional evolution and sedimentary architecture of these deposits.

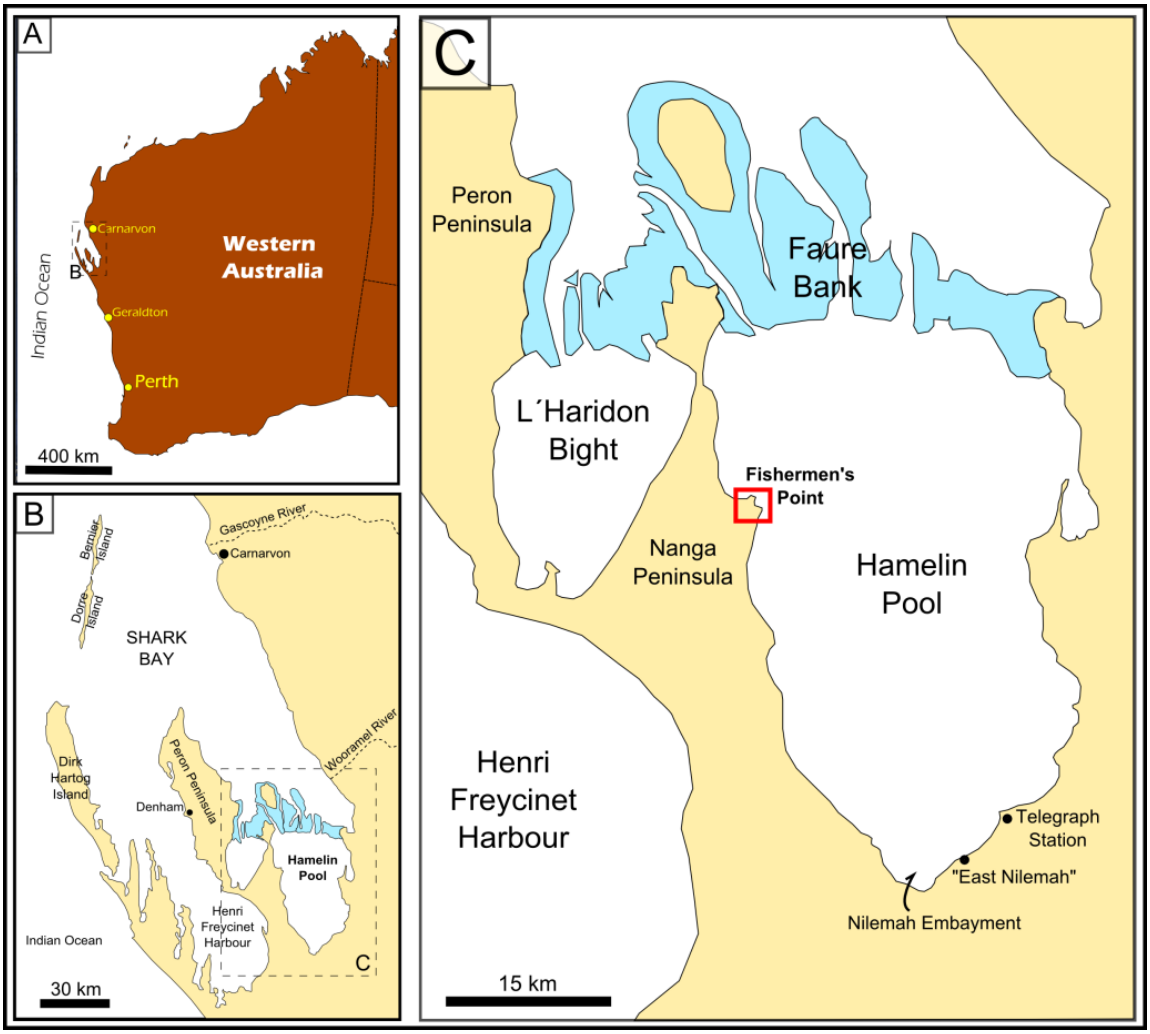

Figure 4.1 – Location map of Shark Bay showing the study area in the western shore of Hamelin Pool, locally known as Fishermen's Point.

4.2 Materials and Methods

Georeferenced maps were constructed using high resolution (50 cm/pixel) Shark Bay orthophotos from Department of Parks and Wildlife and from Landgate (Perth, Western Australia) on ArcGIS software.

Ground Penetrating Radar (GPR) equipment from Mala Professional Explorer coupled with a high precision real time kinematic (RTK) GPS system was employed to obtain subsurface images. GPR data was acquired using a 250 MHz antenna. The trace increment was 5 cm, and the time sampling interval 0.2 ns. The Thales ZMAX RTK GPS system is composed by a base station with radio transmitter continuously correcting positions measured by the mobile Rover unit to obtain centimeter accurate elevations. Coordinates were directly linked to the recorded GPR traces by the acquisition software Groundvision 2, while GPR measurements were triggered in the distance domain with a wheel. Radar penetration depth was limited by the saline water table.

Transects were produced using a high resolution DGPS system (SOKKIA antenna and Allegro System) to provide elevation within 25 cm precision and horizontal positioning accuracy of 50 cm.

Sediment sampling was by push cores and hand samples. The cores had a maximum depth of 1.87m, using 50mm PVC tubes. Sedimentary structures were generally not preserved in the push cores as coring was performed by percussion in mostly dry loose sediment. Only the last few centimeters of the core bottoms intersected the water table where sand or finer sediments tend to be more compact. Hand samples were collected at the surface or in pits with a maximum depth of 60 cm.

^{14}C ages were determined using analytical procedures of Beta Analytic Radiocarbon Dating Laboratory, Florida, USA. All samples were counted using AMS techniques on *Fragum erugatum* shells.

Thin-sections were produced by Minerex Services, Esperance, Australia and analyzed in a Nikon ECLIPSE LV100POL microscope (Nikon Corporation, Tokyo, Japan) and imaged with Nikon NIS Elements software at Curtin University, Australia.

4.3. Results

4.3.1. Geomorphic Elements of Fishermen's Point Beach-ridge Plain

Geomorphic elements are the surficial manifestation of the processes involved in beach-ridge system formation and the succeeding modifications that occurred during its development. The major geomorphic elements used in the interpretation of the system evolution at Fishermen's Point beach-ridge plain were spits, lagoons and isolated lagoons, beach ridges, ridge sets, tidal flats, eolian dunes and a flat eroded area where an indurated pavement occasionally outcrops (Figure 4.2). Moreover, washover deposits do occur, although they present smaller scales as compared to what is observed in the eastern shore of Hamelin Pool, which is more exposed to storms.

Two DGPS transects exemplify the overall ridge morphology in both north facing and east facing shores of the studied site (Figures 4.3 and 4.4). Both transects present trends of decreasing ridge elevation that can be related to the signal of Mid to Late Holocene falling sea-level in the area. In transect DGPSFP-B, the floors of isolated lagoons display increasingly lower elevation seaward which is related to the gradient of the tidal flat over which the beach-ridge system is prograding rather than an imprint of the sea-level fall.

Figure 4.2 – Major geomorphic elements at Fishermen's Point illustrated in a perspective image from Google Earth software version 7.1.2.2041 accessed in 30/01/2014.

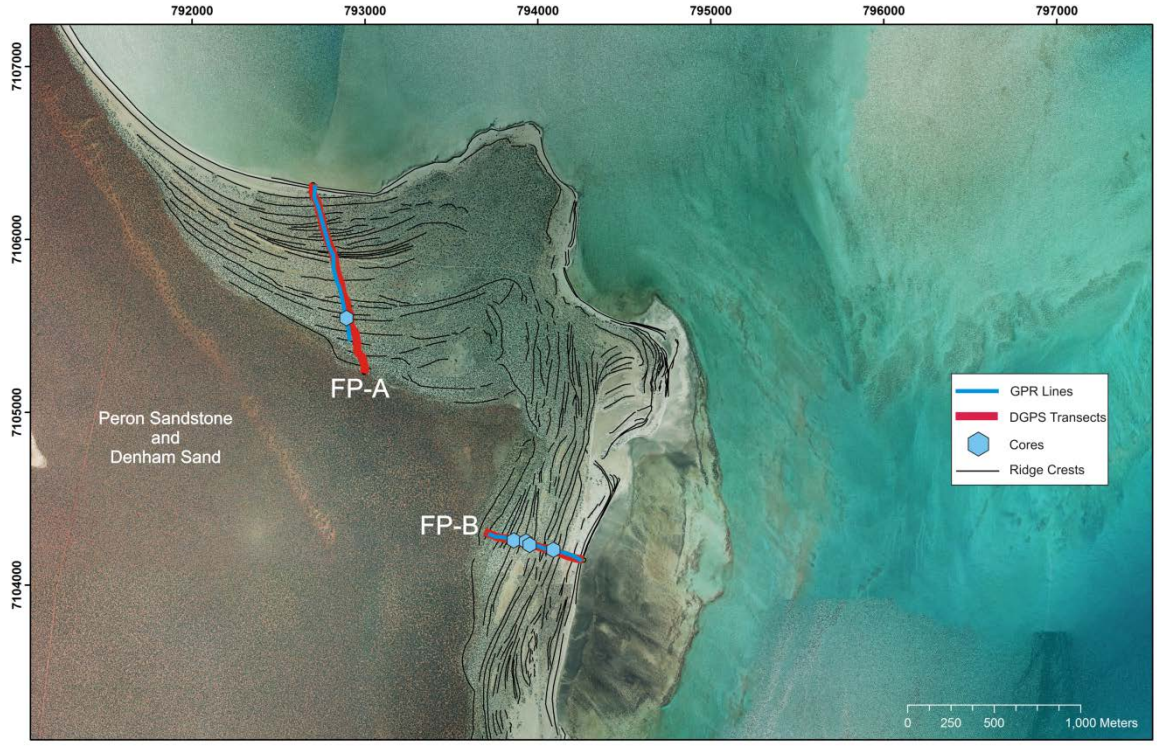

Figure 4.3 – Aerial image of the study area showing the mapped ridge crests and the acquired GPR lines, DGPS transects and cores.

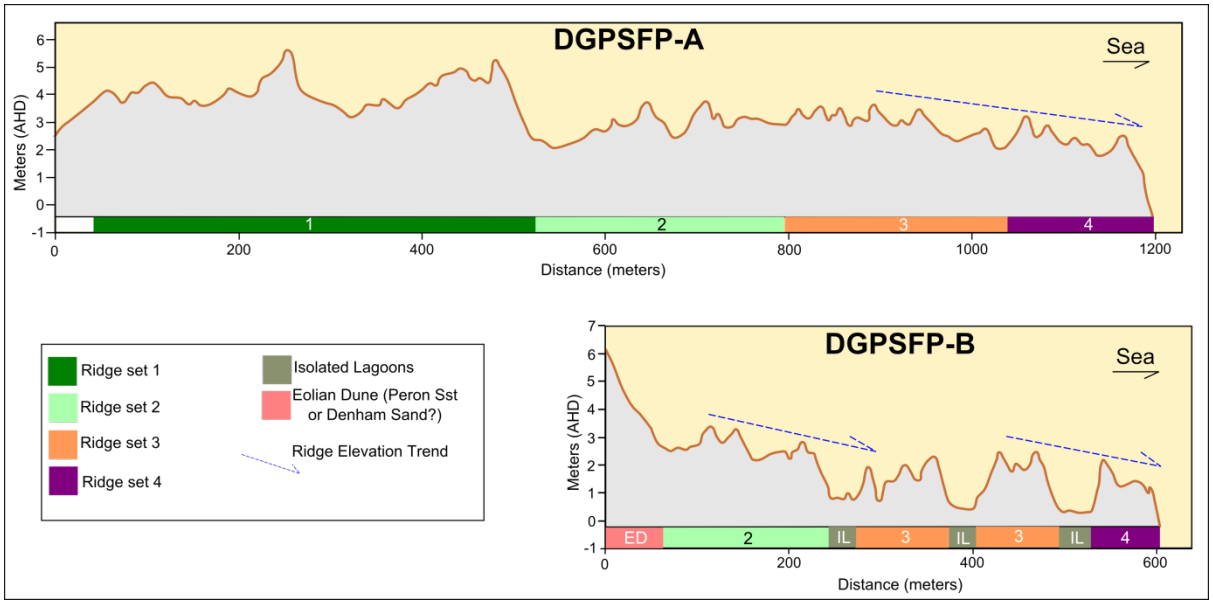

Figure 4.4 – DGPS transects across Fishermen's Point Beach-ridge Plain. See Fig. 4.3 for location.

4.3.2. GPR profile interpretation

In Fishermen's Point site 2 GPR lines were run parallel to the depositional dip direction. Line FP-A is located on a north facing shore and FP-B is on the east facing shore (Figure 4.3). These lines were acquired with a lower resolution 250 MHz antenna as compared with 'East Nilemah' site (Chapter 3) where a 500 MHz antenna was used.

4.3.2.1. GPR line FP-A

GPR line FP-A is split into two lines A-607 and A-11 and will be treated here as a single line totaling 996 meters (Figures 4.5 and 4.6). Although orthophotos and geomorphic maps of the beach-ridge system at Fishermen's Point suggest that alongshore transport is an important component in ridge growth, the overall pattern of FP-A transect shows the predominance of seaward inclined reflections as a result of beachface progradation rather than more complex internal geometries of spit ridges. Between 300 and 450m, horizontal to gently inclined seaward reflections, in a flat low-lying area, indicating an isolated lagoon bordered seaward by a spit ridge that exhibits convex-up, horizontal and seaward inclined reflections. This spit was responsible for the isolation of the lagoon from the bay. Landward inclined reflections on the flank of the spit ridge are interpreted as washover deposits. Blanketing all these deposits there is an overall reflection-free package that is interpreted to represent deposits similar to the storm-surge domain characterized in Chapter 3 although some eolian decoration is possible as sand is abundant in the site.

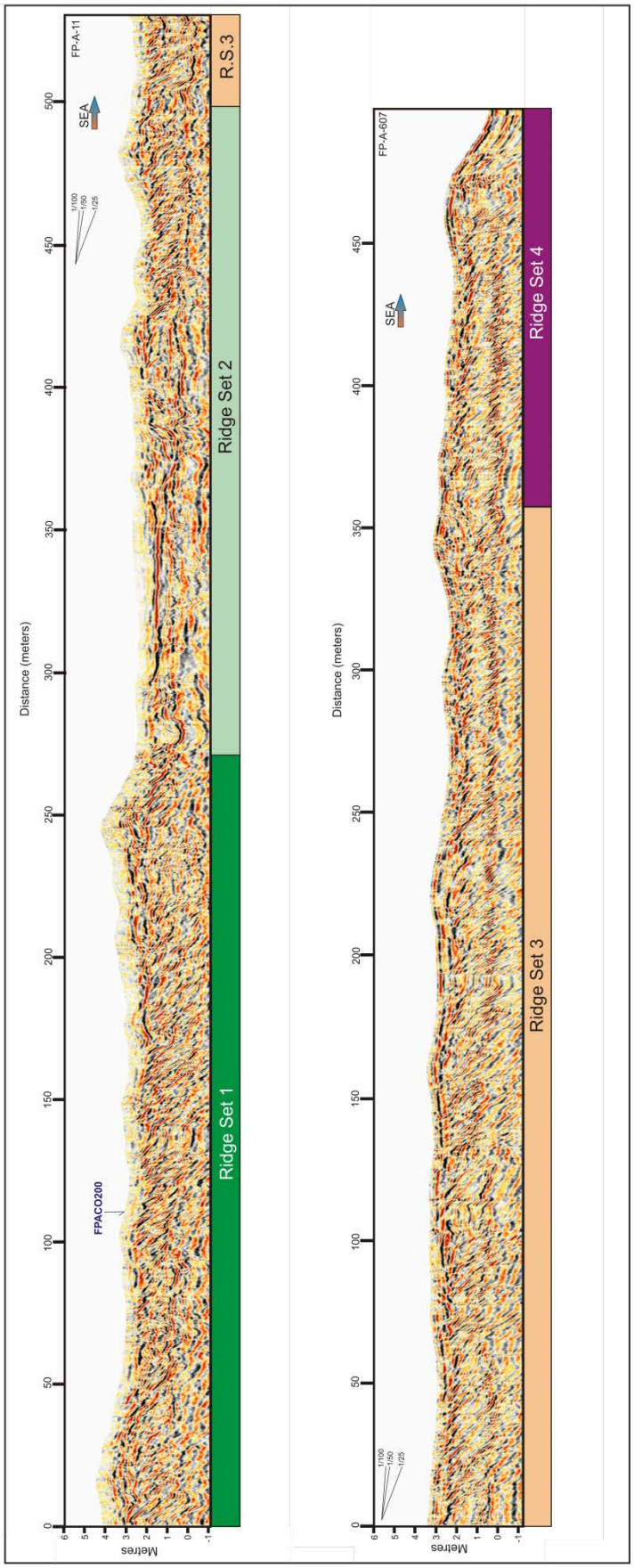

Figure 4.5 – FP-A uninterpreted GPR lines. Lines FP-A11 and FP-A-607 are in continuity.

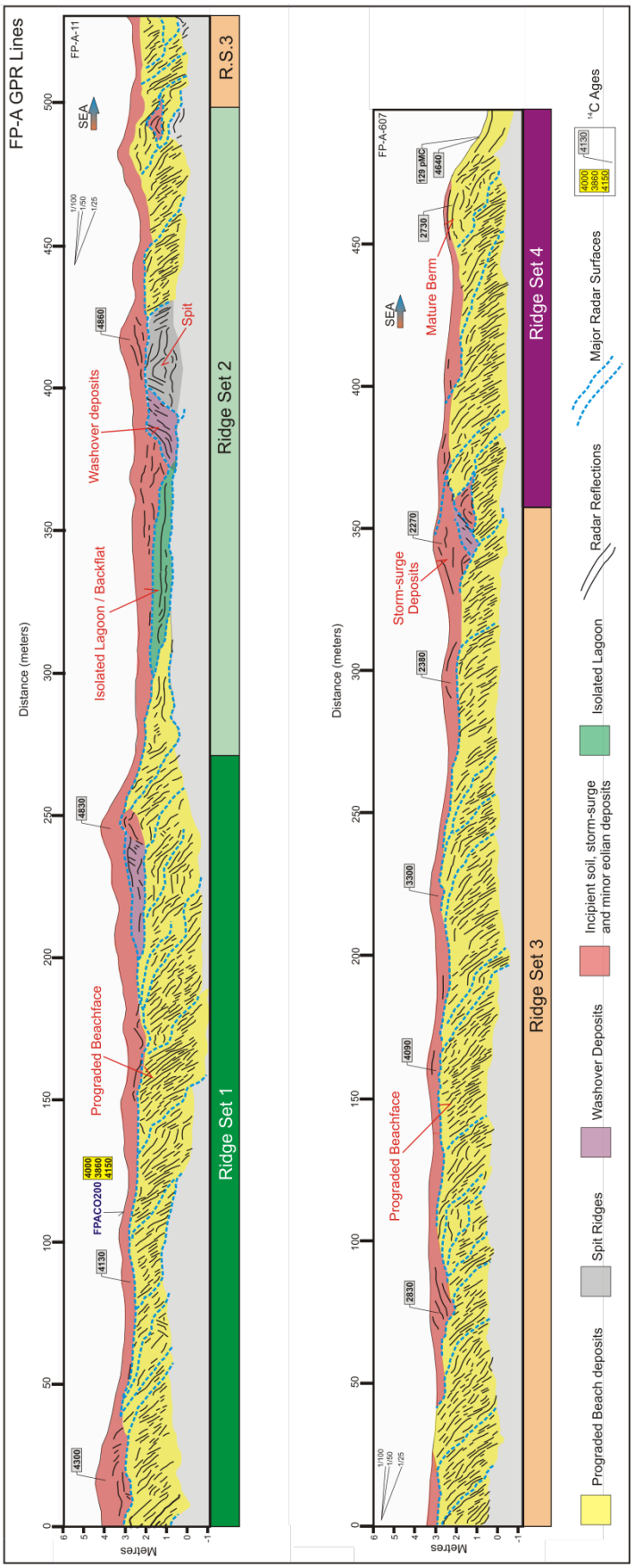

Figure 4.6 – FP-A interpreted GPR transect. Lines FP-A-11 and FP-A-607 are in continuity. Seaward inclined reflectors of prograding beachface deposits capped by a blanket of storm-surge deposits, eolian sediments and incipient soil are prevalent in this transect. Between 300 and 450m a spit ridge backed by an isolated lagoon occurs being covered by storm-surge and eolian deposits.

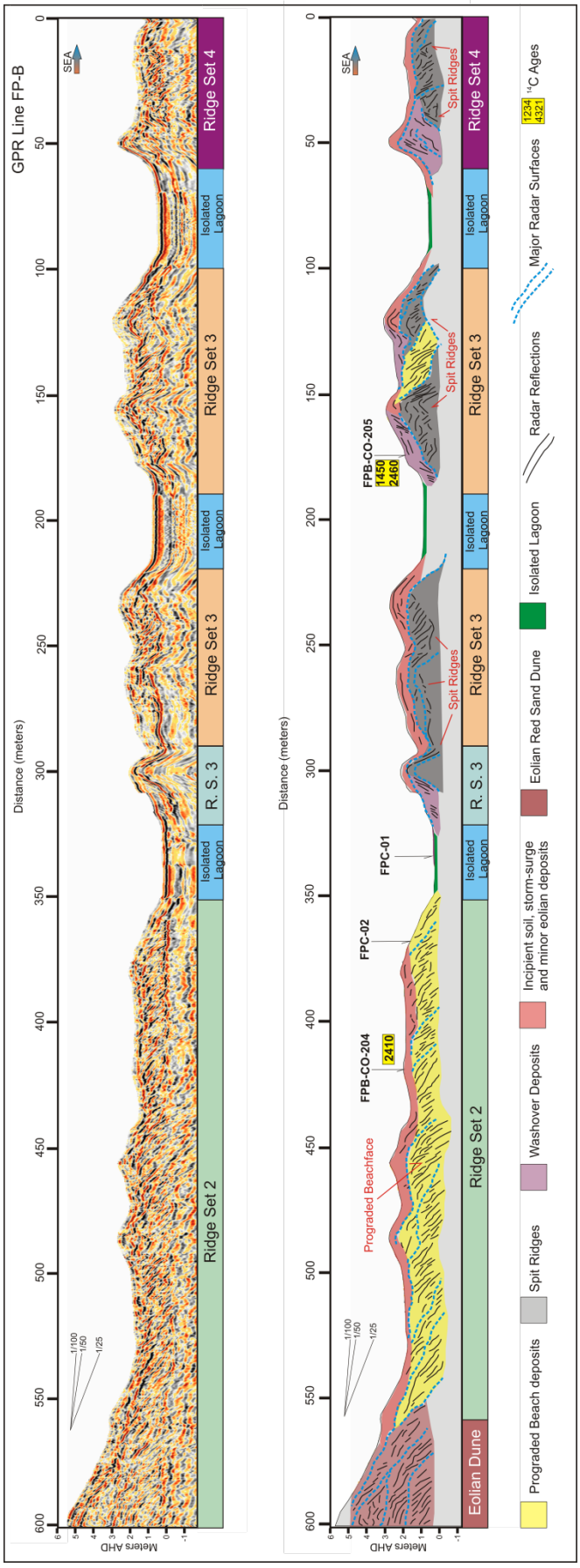

Figure 4.7 – Uninterpreted (top) and interpreted (bottom) GPR line FP-B. Seaward inclined reflectors of prograding beachface deposits are dominant in the landward-most portion of the transect, being later replaced by a succession of isolated lagoons and spit ridges.

4.3.2.2 GPR Line FP-B

GPR line FP-B encompasses 600m where two domains are discernible: one, between 550 and 350m, where seaward inclined reflectors of the prograded beachface predominate, and another, starting approximately at 350m, where alternating ridges and isolated lagoons dominate the scene. Occasionally, radar packages with landward dipping reflector configuration are observed adjacent to the landward flank of spit ridges, being interpreted as washover deposits. Although this east-facing shore at FP-B is more protected from storms reaching Shark Bay in northerly and westerly approaches, storm-surge deposits also blanket ridges in this location. However, ridge elevations are lower overall than in the eastern shore of Hamelin Pool and the north-facing shore of Fishermen's Point, not exceeding 3.5 meters. Within the storm-surge blanket, quartz grains are likely as they are abundant in Nanga Peninsula.

4.3.3. Sediment Cores

In Fishermen's Point, 5 cores were obtained along the GPR lines and lithologies observed were shell gravels and shelly bioclastic ooid and quartz sands. Shell gravels are composed of bivalve mollusks, mainly Fragum *erugatum*, with variable amounts of sandy matrix. Furthermore, shelly, bioclastic ooid and quartz sands occasionally exhibit micritized grains, peloids and micritic cementation (Figures 4.8 and 4.9).

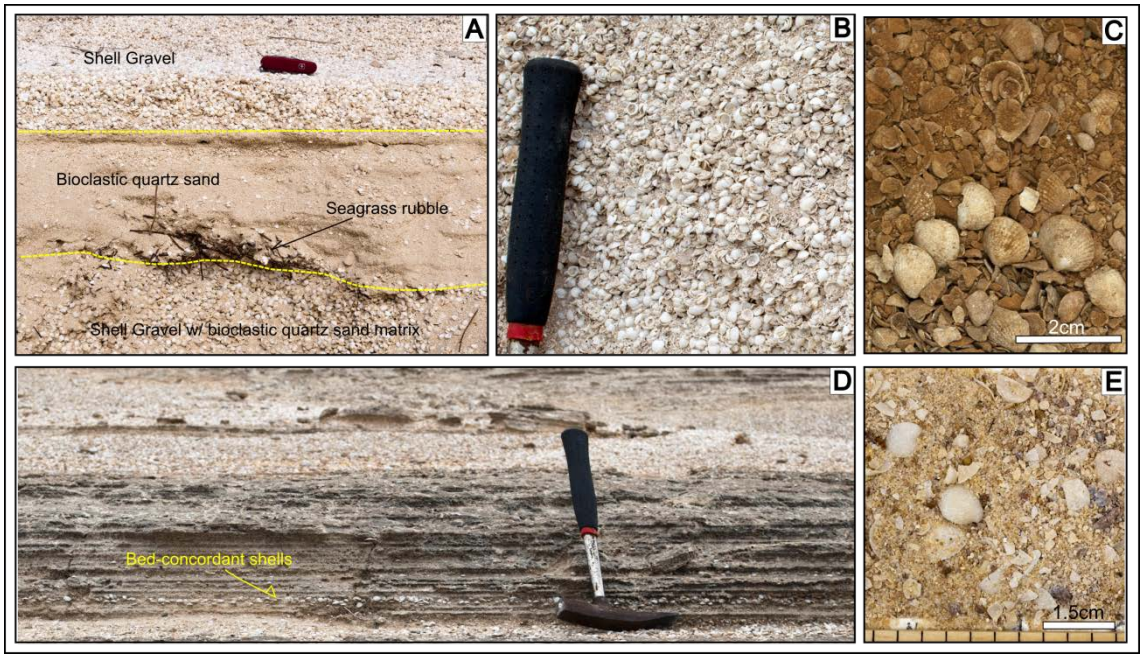

Figure 4.8 – Sedimentary deposits in Fishermen's Point Beach-ridge plain. (A) Lithologies in a beach terrace; (B) Shell gravel with sand matrix; (C) Shell gravel with infiltrated red clay and sand; (D) Quartz, ooid and bioclast sand with plane parallel lamination and a layer of oriented bed-concordant shells; (E) Shelly quartz sand with bioclasts and lithoclasts.

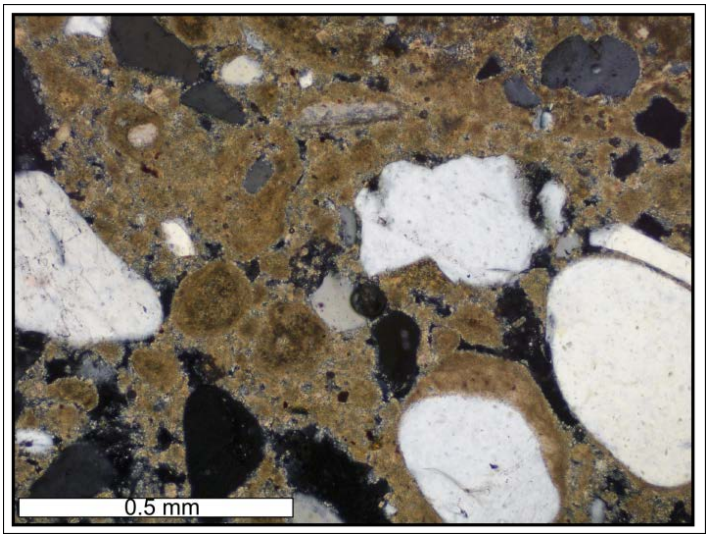

Figure 4.9 - Epoxy-impregnated thin-section of peloidal quartz sand with micrite cement from core FPC-02 at 1.245 meters below ground level.

In FP-A, the core FP-A-CO-200 intersected 3 radar packages representing prograded beachfaces capped by storm-surge deposits and incipient soil (Figure 4.10). The beachface deposits have high contents of quartz, derived from adjoining Nanga Peninsula whose country rock is the Plio-Pleistocene Peron Sandstone.

In GPR line FP-B, four additional cores provided textural and compositional information on the sediments at Fishermen's Point (Figure 4.11). Cores FPB-CO-204 and FPC-02 intersect prograded beachface deposits rich in quartz sediments as observed in FP-A. In FPC-02, the lowermost radar package corresponds to medium to coarse quartz sands where grain micritization and micritic cementation are common and are not only restricted to a few centimeters at the bottom of the core (Figures 4.11 and 4.09).

Core FPC-01 was obtained in an isolated lagoon and shows incipient soil and a shell gravel bed derived from a small scale washover overlying back flat deposits consisting of micrite-cemented quartz sands and a 2cm-thick sandy mud layer with plant root fragments. Below this muddy layer, micrite-cemented bioclastic quartz sands occur and are assumed to represent subtidal deposits over which the beach-ridge system is prograding (a former sublittoral platform (cf. Logan et al., 1970)).

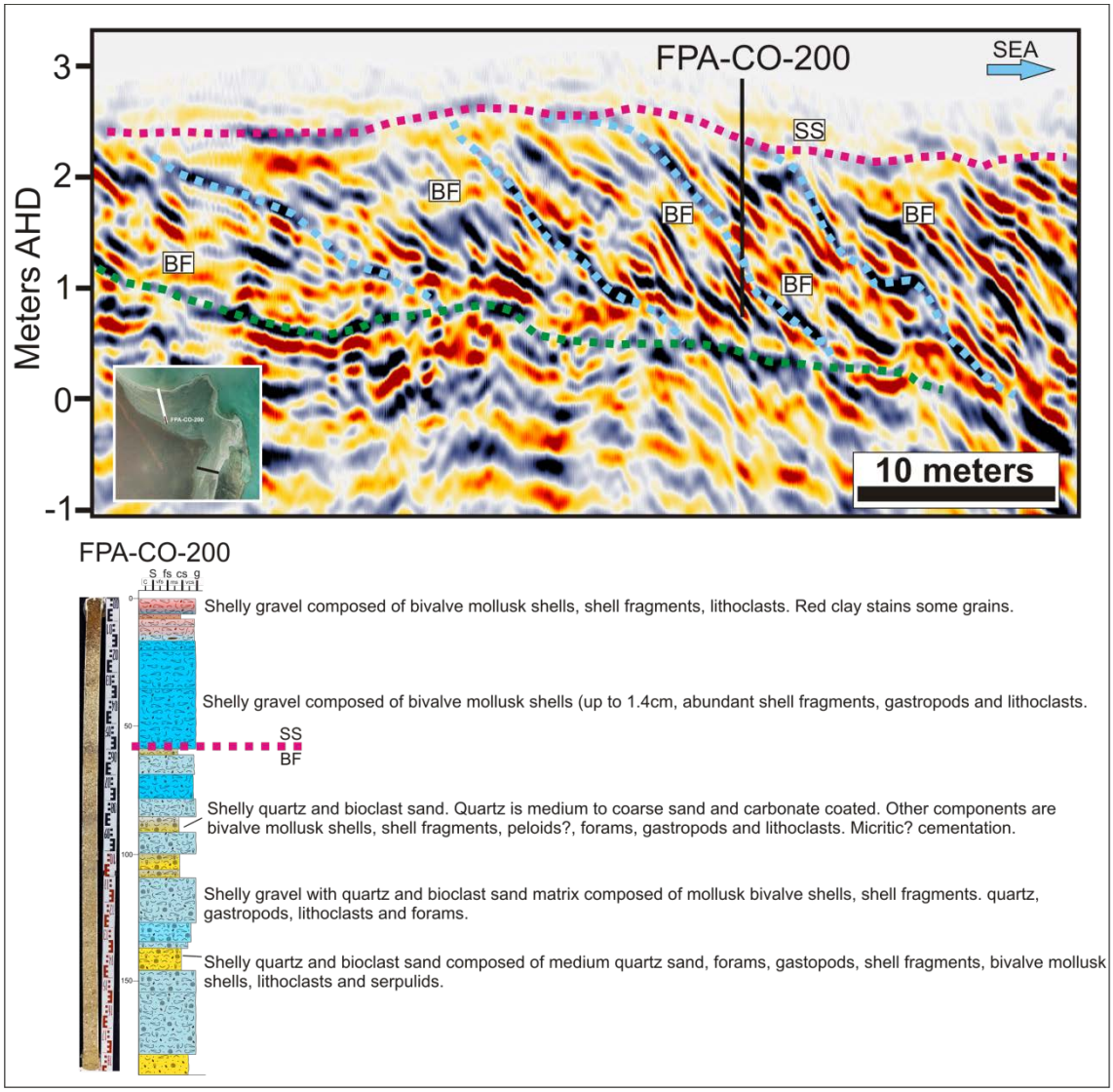

Figure 4.10 – Segment of GPR line FP-A where core FPA-CO-200 intersects storm-surge deposits and soil blanketing beachface shell gravels and quartz sands. SS: Storm-surge deposits and soil; BF: Beachface deposits.

Core FPB-CO-205 intersects the landward flank of a spit ridge and displays more shell gravels than the other cores in this transect. The upper 68 centimeters show a predominance of shell gravels associated with overwash events over the initial ridge deposits. To the bottom, sediments display higher quartz sand content and in GPR exhibit seaward and convex-up reflection configuration being interpreted as spit ridge deposits (Figure 4.11).

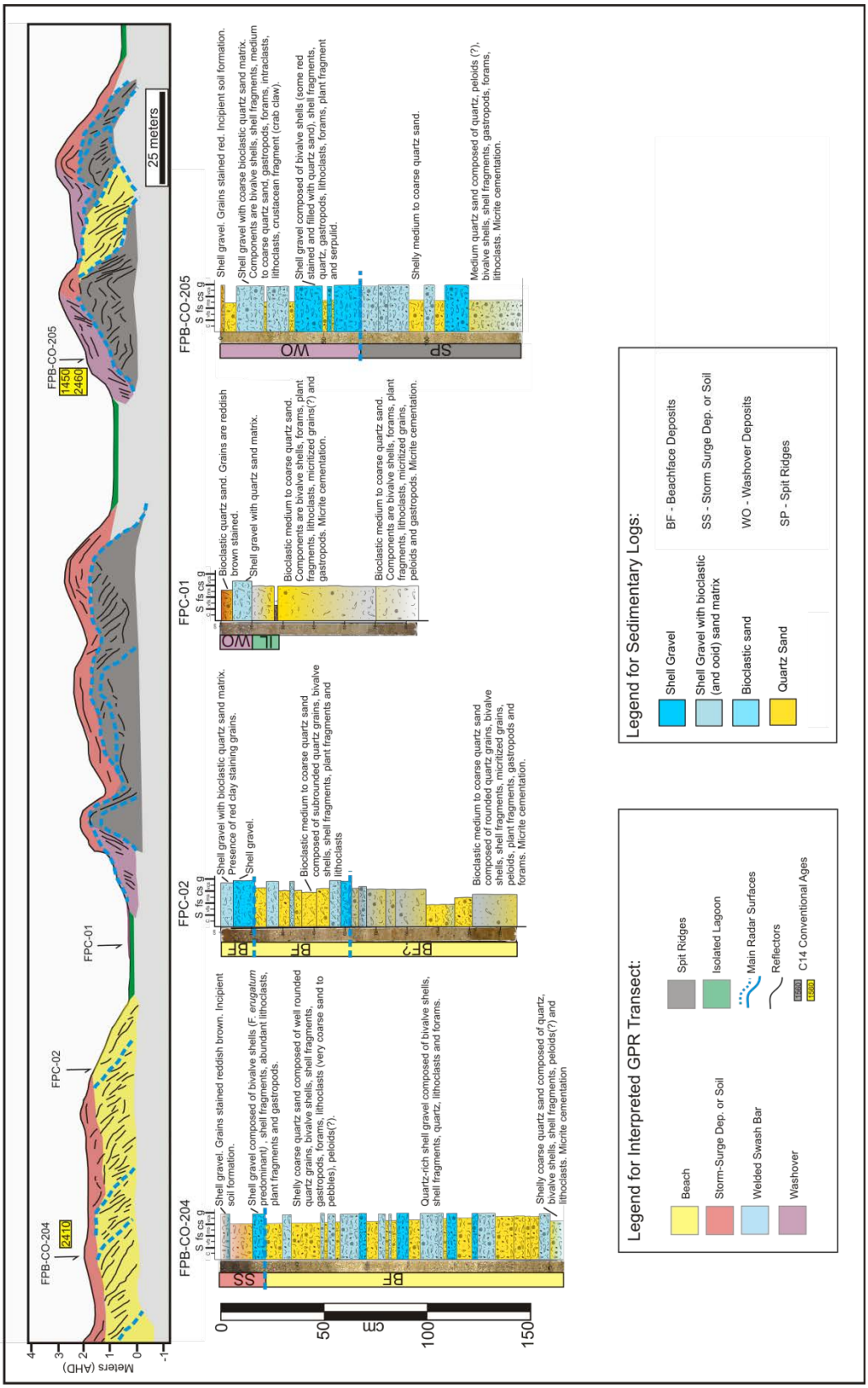

Figure 4.11 – Segment of GPR line FP-B where four push cores were obtained intercepting beach, spit ridges, washover, isolated lagoon and storm-surge deposits.

4.3.4. Indurated Pavement

Beach ridges in the north-facing shore of Fishermen's Point are interrupted by a low-elevation nearly flat area where an indurated pavement outcrops (Figures 4.12(A) and 4.13). This interruption evidences an erosive episode that impacted the beach ridges that were prograding over this indurated pavement.

The pavement is composed of cemented shelly quartz sands or sandy shell gravels, occasionally displaying polygonal structures similar to those observed in modern beach rocks (Figure 4.12(B)(D)). These shelly quartz sands exhibit micritic cement later fringed by well-developed aragonite needles (Figure 4.12(C)). These marine cements suggest this pavement is a beachrock preserved from a major erosive event (or period) that disrupted the beach-ridge system. DGPS data demonstrate that this beachrock area is about 1.5m in elevation which suggests it was formed at higher than present sea-level conditions. Although Kelletat (2006) question the use of beachrocks as sea-level indicators alone, other evidence of regressive conditions observed by some authors (e.g. Logan et al., 1974; Jahnert and Collins, 2011; Jahnert and Collins, 2013) reinforce the interpretation of the pavement as an indication of higher sea-levels during the onset of the beach-ridge system in accordance with an Holocene highstand of +2m at approximately 6800 U/Th years BP identified by Collins et al. (2006) in the Houtman Abrolhos Islands, Western Australia.

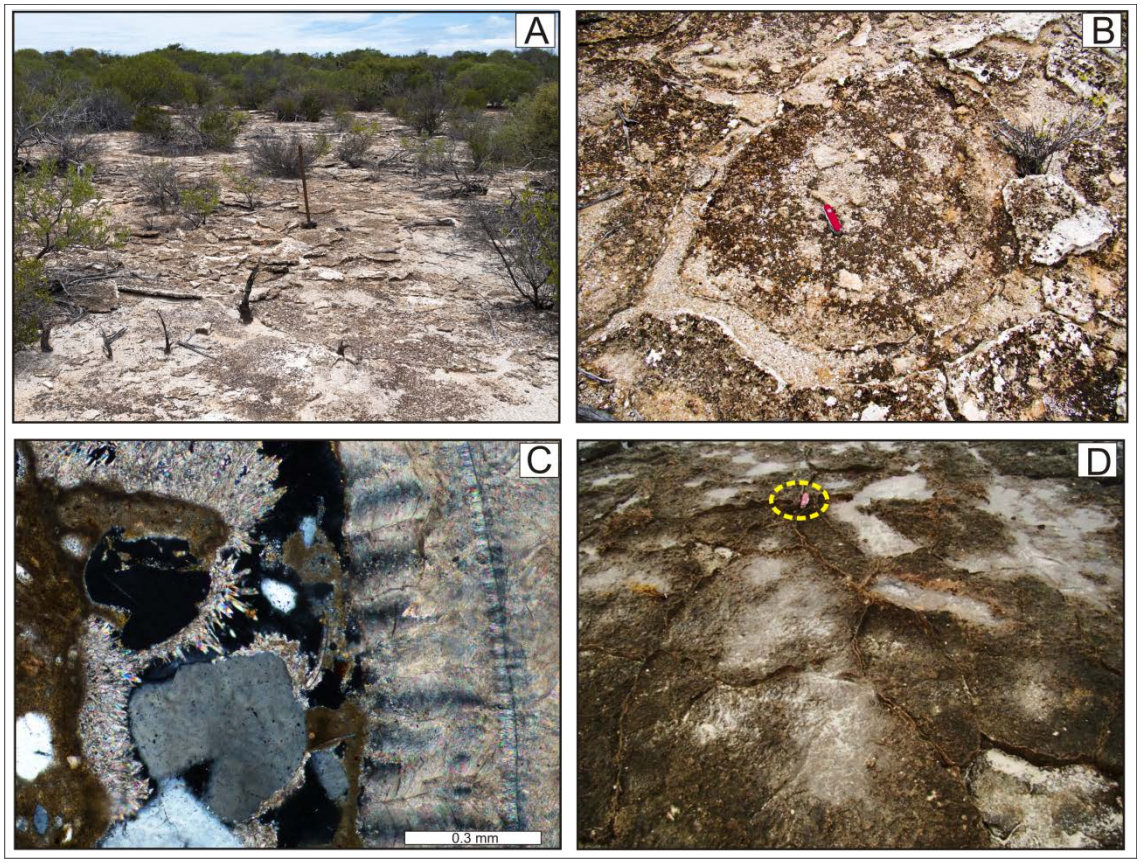

Figure 4.12 – (A) Flat eroded area where the indurated pavement outcrops; (B) Indurated pavement exhibiting polygonal structures (red pocket-knife for scale); (C) Epoxy-impregnated thin-section of indurated shelly bioclast and quartz sand cemented by dark brown micrite and acicular aragonite; (D) Modern beachrock in Fishermen's Point exhibiting polygonal structures (red pocket-knife for scale in the upper part of the photo (yellow circle); photo courtesy of João Guerreiro).

4.3.5. Ridge Chronology

In order to establish a chronological framework for ridge formation and evolution, 22 shell samples were dated using the radiocarbon AMS technique at the Fishermen's Point site. Most of the samples were collected in storm-surge deposits prone to contain reworked material. For this reason age reversals are common in the studied transects and radiocarbon dates from these samples can only be used as maximum ages. However, six articulated shell samples were obtained from the cores and provide reliable ^{14}C ages that were used as key ages to delineate ridge chronology (Figure 4.13).

The deposition of ridge set 1 took place between 4660-3860 ^{14}C years BP. An onset of the beach-ridge system around 4500-5000 ^{14}C years BP was also observed at 'East Nilemah' site (Chapter 3) and by Jahnert et al. (2012) at Telegraph Station, both in the eastern shore of Hamelin Pool.

An age of 5530 ^{14}C years BP was obtained in the indurated pavement, nevertheless the most reliable date for this unit is around 4690 ^{14}C years BP, very close to the oldest age considered in place for ridge set 1.

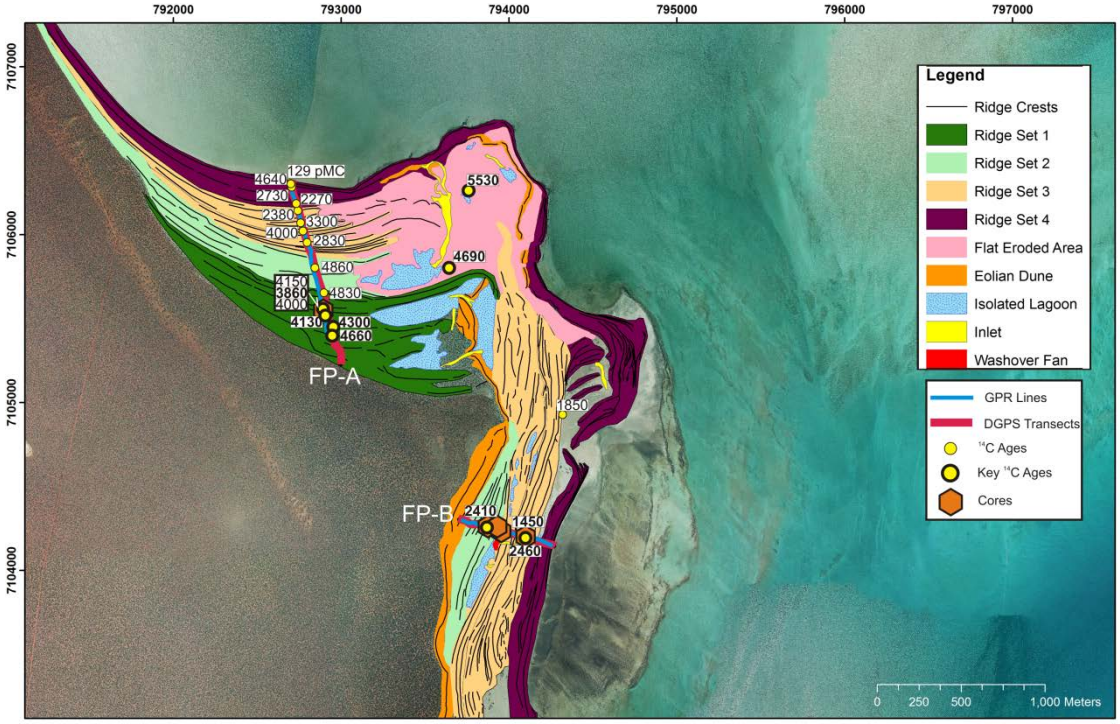

Figure 4.13 – Geomorphic map and aerial image of Fishermen's Point beach-ridge plain with ^{14}C dates, cores, GPR and DGPS transect locations. Key ages for the interpretation of ridge chronology are indicated by thick-bordered circles.

Ridge set 2 only possess one reliable dated sample corresponding to 2410 ^{14}C years BP, obtained from an articulated shell in a core acquired at transect FP-B, located in the eastfacing shore of the site.

The next reliable dated sample is 2460 ^{14}C years BP in ridge set 3. Although this result is an apparent reversal, the ages can be considered in place as the results are within the uncertainty boundaries shown in Table 4.1. Another possible explanation for this reversal is that shells had a significant residence time in the basin before being transported ashore and the younger date of 1450 ^{14}C years BP obtained in ridge set 3 for washover deposits is closer to the actual age of the ridge.

The erosional event that exposed the underlying indurated pavement has an age of 1450 ^{14}C years BP or younger, as it affects ridge set 3 but not ridge set 4. This event can be related to the changes that led to the development of the spit ridge domain described in Chapter 3 and the

change in layer organization and shift in focus of sediment deposition observed by Jahnert et al. (2012) in Telegraph Station ridges.

Ridge set 4 initiation could not be dated but is inferred to have taken place soon after 1450 ^{14}C years BP and is still under development as it encompasses active berms and beachfaces. This age range is in accordance with the inferred ages observed for the younger ridge set in 'East Nilemah' studied in Chapter 3.

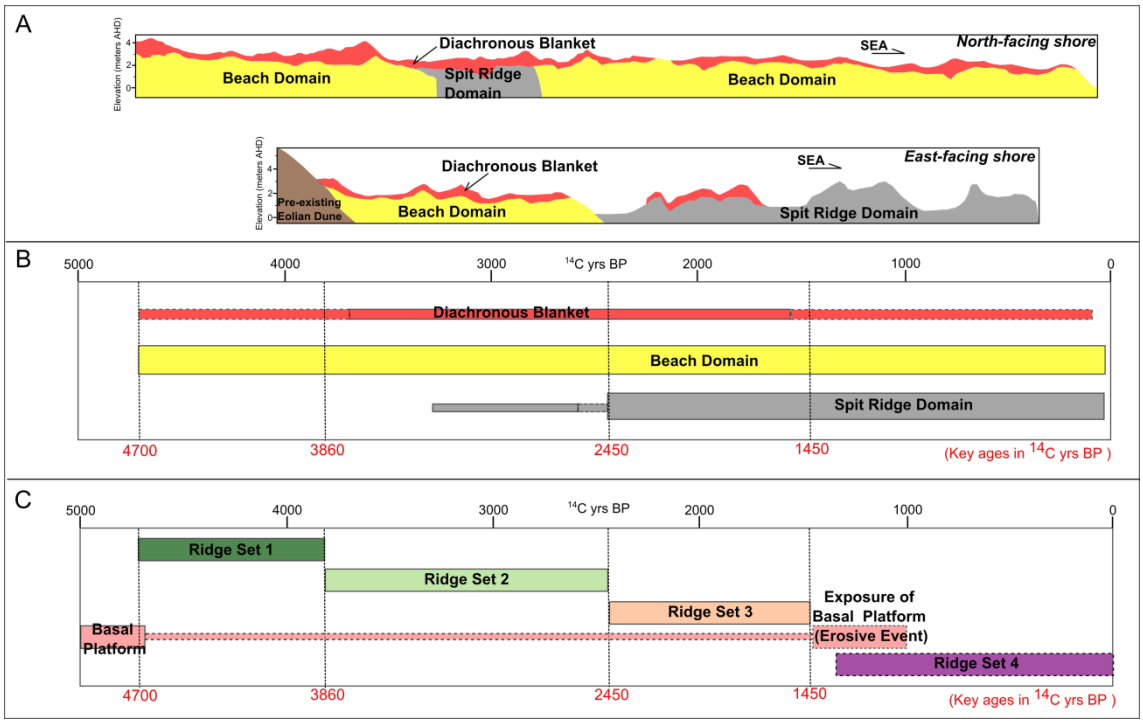

Figure 4.14- Depositional domain and ridge set chronology. (A) Sketches of the typical depositional styles in Fishermen's Point. (B) Depositional domain chronology. Thickness of the bars indicate relative abundance and dashed line in the bar contour indicate inference of the occurrence of depositional domains. (C) Ridge set chronology.

Figure 4.14(A-B) is an attempt to constrain the chronology of depositional domains revealing their rough stratigraphic significance. Figure 4.14(C) exposes the chronology of ridge set deposition and the erosive event which exposed the indurated pavement which is the basal platform over which the system is prograding.

Sample Id	Source of Carbon	^{14}C age (years BP)	error (years)	^{14}C age (years BP) calibrated 2 sigma
FPD-14	Bivalve Shell	129.9 pMC	0.3	
FPD-12	Bivalve Shell	4640	30	4880/4610
FPD-11	Bivalve Shell	2730	30	2490/2240
FPD-10	Bivalve Shell	2270	30	1920/1670

FPD-09	Bivalve Shell	2380	30	2070/1800
FPD-08	Bivalve Shell	3300	30	3210/2870
FPD-07	Bivalve Shell	4090	30	4210/3860
FPD-06	Bivalve Shell	2830	30	2680/2320
FPD-05	Bivalve Shell	4860	30	5260/4860
FPD-04	Bivalve Shell	4830	30	5270/4820
FPD-03	Bivalve Shell	4130	30	4250/3920
FPD-02	Bivalve Shell	4300	30	4490/4140
FPD-01	Bivalve Shell	4660	30	4930/4640
FPG-05B	Bivalve Shell	4690	30	4960/4700
FP-D-207	Bivalve Shell	5530	30	5940/5690
FP-D-205	Bivalve Shell	1850	30	1500/1170
FPBCO205-D2	Articulated Bivalve Shell	2460	30	2150/1870
FPBCO205-D1	Articulated Bivalve Shell	1450	30	1040/780
FPBCO204-D1	Articulated Bivalve Shell	2410	30	2140/1780
FPACO200-D3	Articulated Bivalve Shell	4150	30	4280/3950
FPACO200-D2	Articulated Bivalve Shell	3860	30	3880/3570
FPACO200-D1	Articulated Bivalve Shell	4000	30	4070/3760

Table 4.1 - Radiocarbon chronology for *F. erugatum* shells of selected coquina deposits. A delta R of 70 ± 50 was used for marine reservoir correction.

4.4. Discussion and Conclusion

The western shore of Hamelin Pool is less vulnerable to the impact of storms than the eastern shore. Evidences of the major role storms play in ridge building are abundant in 'East Nilemah' (Chapter 3) and Telegraph Station (Jahnert et al., 2012). This evidence is less pronounced at Fishermen's Point. Differing from the eastern shore, washover fans were not abundant during the onset of the system in this area. Furthermore, the washover fans observed are small scale and occur in lagoons, most of which were isolated as a consequence of the beach-ridge system progradation. Ridge height is also lower than reported in the eastern shore. At Fishermen's Point elevation of the beach-ridges do not exceed 5.6m. Nanga Peninsula is composed of Peron Sandstone and Denham Sand red dunes which provide abundant quartz grains to be reworked by nearshore processes. For that reason, the beach-ridge deposits in the area are mixed bioclastic-siliciclastic, exhibiting sediments composed of variable amounts of shells and bioclastic, quartz and ooid sands. In cores, sand abundance increases with depth and is

apparently more abundant in the east-facing shore, less exposed to storms, but more cores in the north-facing shore would be required to support that assumption.

The evolution of the beach-ridge system at Fishermen's Point is depicted in Figure 4.15. The onset of the system and deposition of ridge set 1 took place between 4700-3860 ^{14}C years BP. Ridge external morphology suggest that longshore currents played an important role in ridge formation although the internal architecture of the ridges in GPR line FP-A (Fig. 4.6) show predominantly prograded beachface depositional style, indicating that swash and backwash processes were prevalent in that transect.

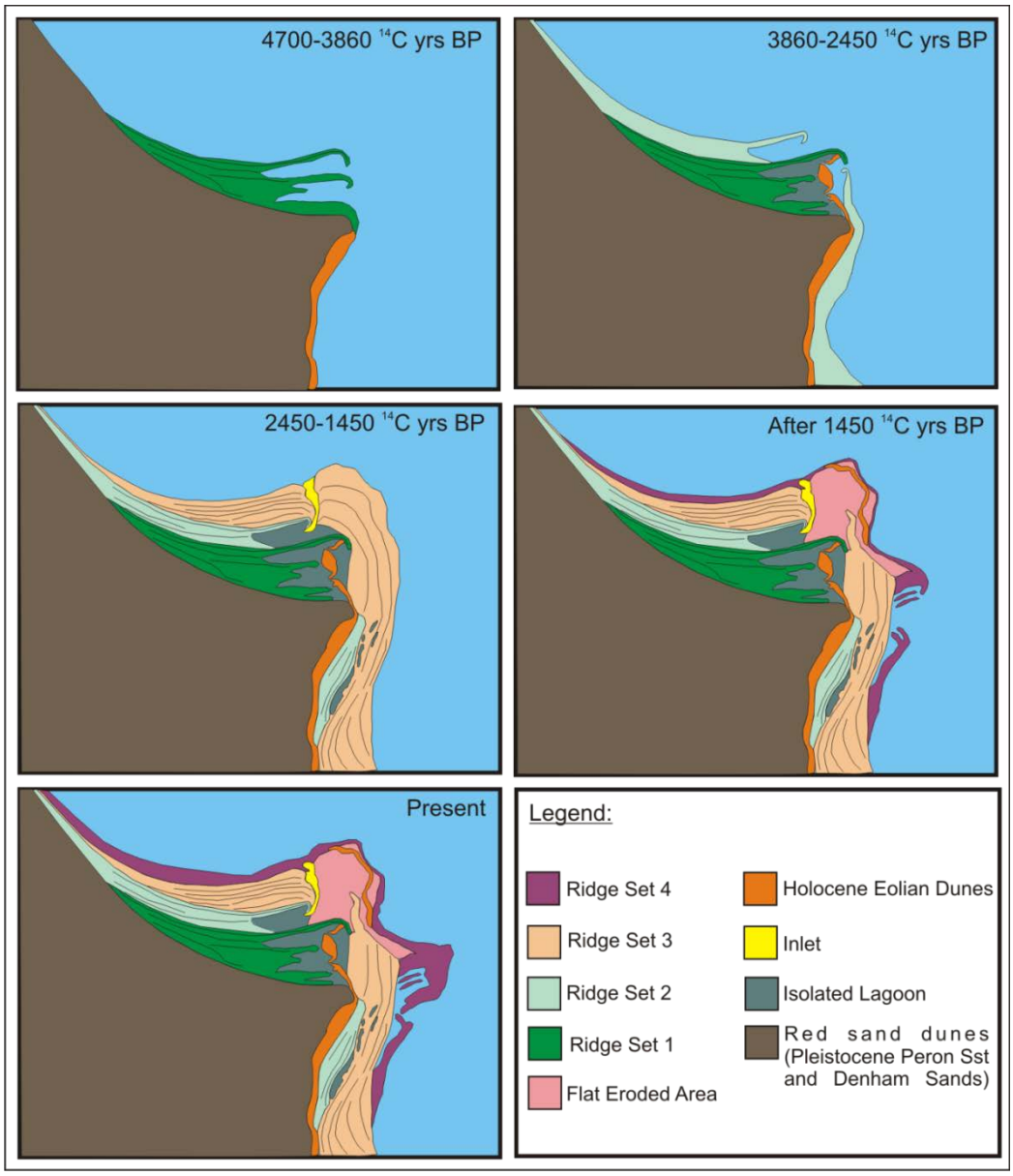

Figure 4.15 - Depositional and geomorphic evolution sketch of Fishermen's Point beach-ridge plain.

Ridge set 2 deposition occurred between about 3860-2450 ^{14}C years BP and GPR line FP-A (Fig. 4.6) shows it started with the replacement of the prograded beachface depositional style by an isolated lagoon bordered by spit and washover deposits. At the transition to ridge set 3 the seaward inclined reflections of prograded beachfaces dominate the scene again.

Between about 2450-1450 ^{14}C years BP, ridge set 3 deposition took place initially showing a period of rapid progradation as evidenced by the ages obtained in transect FP-B. This ridge set deposition isolated major lagoons existing in the north-facing shore.

After 1450 ^{14}C years BP a major erosive event or, most likely, a period of rearrangement and coastal erosion removed part of ridge set 3 and exposed an indurated pavement not older than 4690 ^{14}C years BP. This indurated pavement can reach up to 1.5m in elevation and present marine cements and structures similar to modern beachrocks that indicate a higher than present sea-level at that time.

Ridge set 4 is younger than the erosive event that exposed the indurated pavement and shows spits growing in both north to south and south to north directions. The spits growing north to south are more prominent and relate to longshore currents that develop during storms.

This chapter documents an Holocene mixed bioclastic-siliciclastic beach-ridge system occurring in the western shore of Hamelin Pool, Shark Bay. Differences in the depositional style, sediment composition and ridge elevation were observed between the north and east-facing shores of the area. The north-facing shore is more exposed to storms and presents a dominance of prograded beachface deposits and sediments are more abundant in shells whereas the east-facing shore presents a dominance of alternating isolated lagoons and spit ridges and sediments show more sand content. The north-facing shore also presents higher ridge elevations that can reach up to 5.6m as opposed to the east-facing shore where beach ridges are less than 3.5m in elevation.

Chapter **5**

Stable Oxygen and Carbon Isotopic Composition of *Fragum erugatum* Shells in Hamelin Pool and Its Potential for Palaeosalinity Reconstruction

5.1 Introduction

Mollusk shells have been successfully employed in palaeoenvironmental studies using stable carbon and oxygen isotopes as proxies (e.g. Lloyd, 1964; Mátyás et al., 1996; Hendry & Kalin, 1997). In Shark Bay, Price et al. (2012) demonstrated a high positive correlation (R^2>0.80) between water $\delta^{18}O$ and salinity. Moreover, Bastow et al. (2002) observed a linear relationship between $\delta^{18}O$ and $\delta^{13}C$ in fish otolith carbonate and water salinity in Shark Bay. Hamelin Pool had high metahaline / hypersaline conditions since at least 5000 years BP, as the age of the oldest coquina deposits indicate, however it is not known how salinity varied after the onset of hypersalinity during the Mid to Late Holocene.

The aim of this chapter is to investigate the potential for palaeosalinity reconstruction using carbon and oxygen isotopic composition of *Fragum erugatum* bivalve mollusk shells to delineate a salinity variation assessment for the Mid to Late Holocene at Hamelin Pool, Shark Bay.

5.2 Methods

Shells were collected in push cores and hand samples. The cores have a maximum depth of 1.99m, using 50mm PVC tubes.

Water samples were placed in glass bottles (100ml) for laboratory analysis. Bottles were rinsed three times and then filled below the water surface. Bottles were overfilled and then capped to minimize air bubbles in the sample. Water parameters were obtained with a WTW 3500-I hand held instrument equipped with a SensoLyt MPP-A(pH) and SensoLyt MPP-A-PT(ORP) probes.

^{14}C ages were determined using analytical procedures of Beta Analytic Radiocarbon Dating Laboratory, Florida, USA. All samples were counted using AMS techniques in *Fragum erugatum* shells.

Carbon and oxygen isotopes from shells and water were measured by West Australian Biogeochemistry Centre, The University of Western Australia (UWA). For carbonates the

maximum external error was 0.10‰ for carbon and 0.15‰ for oxygen isotopes. For water the maximum external error was 0.10‰ for oxygen isotopes measurements.

5.3. Results

Forty two samples of *Fragum erugatum* bivalve mollusk shells from Hamelin Pool were analyzed for $\delta^{18}O$ and $\delta^{13}C$ measurements. 4 samples clearly show influence of meteoric diagenesis. The other samples exhibit values of $\delta^{13}C$ ranging from 3.51 to 5.21 ‰ and $\delta^{18}O$ varying from 1.87 to 4.33 ‰ (Figure 5.1). From the 42 samples, 14 contained a single shell per sample making possible a reliable chronological assessment of shell stable isotopic composition.

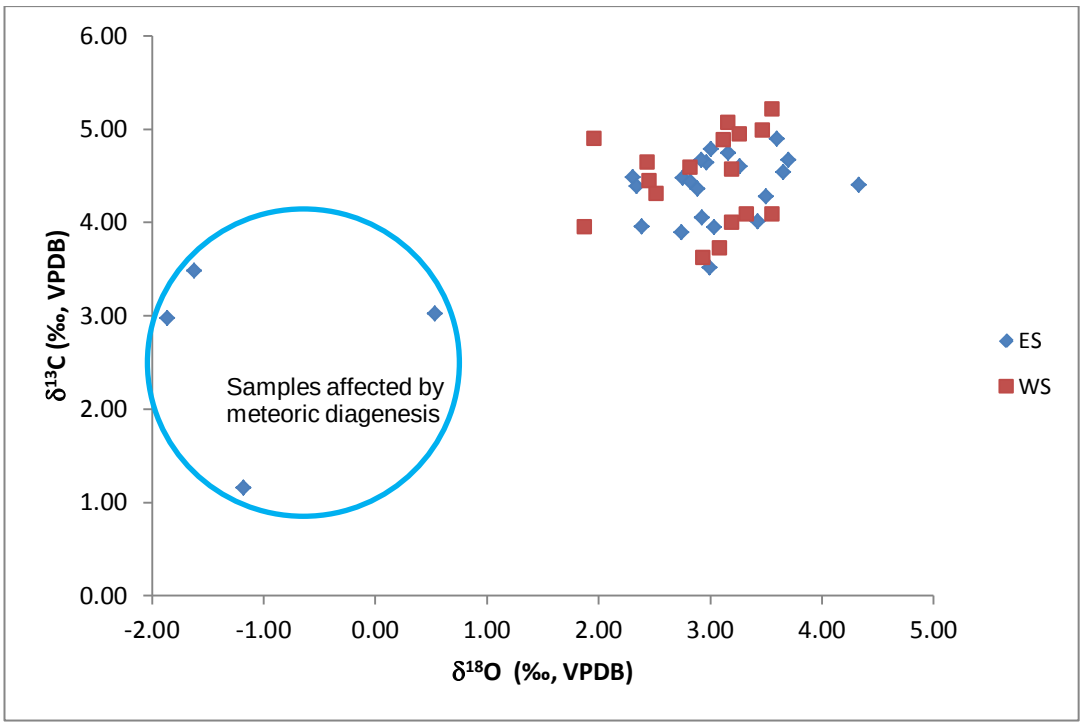

Figure 5.1 – $\delta^{18}O$ versus $\delta^{13}C$ plot *Fragum erugatum* shell samples. Four outliers show evidence of being affected by meteoric diagenesis. ES – Eastern Shore; WS – western Shore.

Sample	$\delta^{13}C$ [‰, VPDB]	$\delta^{18}O$ [‰, VPDB]
FP-ISO-01	3.72	3.08
FPD-14	3.62	2.93
KP-G-100(S)	4.01	3.42
02ENB04-D-3	3.89	2.75
CBPT-G-01	4.05	2.93
EN-DR-D-110	3.51	3.00
ENE-D-01	2.97	-1.86
ENA-D-102	3.02	0.53

AWP1-D-01	3.94	3.04
ENA-D-100	3.48	-1.62
FP-D-205	4.09	3.33
END-06	4.36	2.89
END-D-106	1.15	-1.18
END-05	4.74	3.16
END-03	4.64	2.97
END-11	4.40	4.33
FPD-10	4.90	1.96
END-07	4.67	2.92
FPD-09	4.65	2.43
END-10	4.89	3.60
AWP1-G-01	4.67	3.70
END-D-108	4.44	2.83
FPD-11	4.09	3.55
END-04	4.78	3.01
FPD-06	4.95	3.26
END-D-107	4.60	3.26
END-09	4.54	3.65
FPD-08	3.96	1.87
END-02	4.47	2.76
AWP1-D-02	4.38	2.34
END-08	4.27	3.50
FPD-07	4.99	3.47
FPD-03	4.59	2.82
FPD-02	4.57	3.19
FPD-12	4.01	3.19
FPD-01	4.89	3.11
FPG-05B	4.31	2.52
END-01	4.48	2.31
FPD-04	5.07	3.16
FPD-05	5.21	3.55
ENA-D-101	3.96	2.39
FP-D-207	4.45	2.45

Table 5.1 - $\delta^{18}O$ and $\delta^{13}C$ values for *Fragum erugatum* samples of Hamelin Pool, Shark Bay.

5.3.1. Oxygen Isotopic Composition and Radiocarbon Chronology

Samples showing evidence of meteoric diagenesis were not used in the assessment of variations in the isotopic composition through time. Figure 5.2 shows $\delta^{18}O$ measured values and corresponding radiocarbon ages. The values for the older samples (>3000 ^{14}C years BP) show values $2.3 < \delta^{18}O < 2.55$ ‰. After 3000 ^{14}C years BP the shells are overall enriched in ^{18}O and can exhibit values as high as 3.70 ‰ for $\delta^{18}O$. An overall trend of decline in $\delta^{18}O$ is clear until 370 ^{14}C years BP after when values peak above 3.0‰ again.

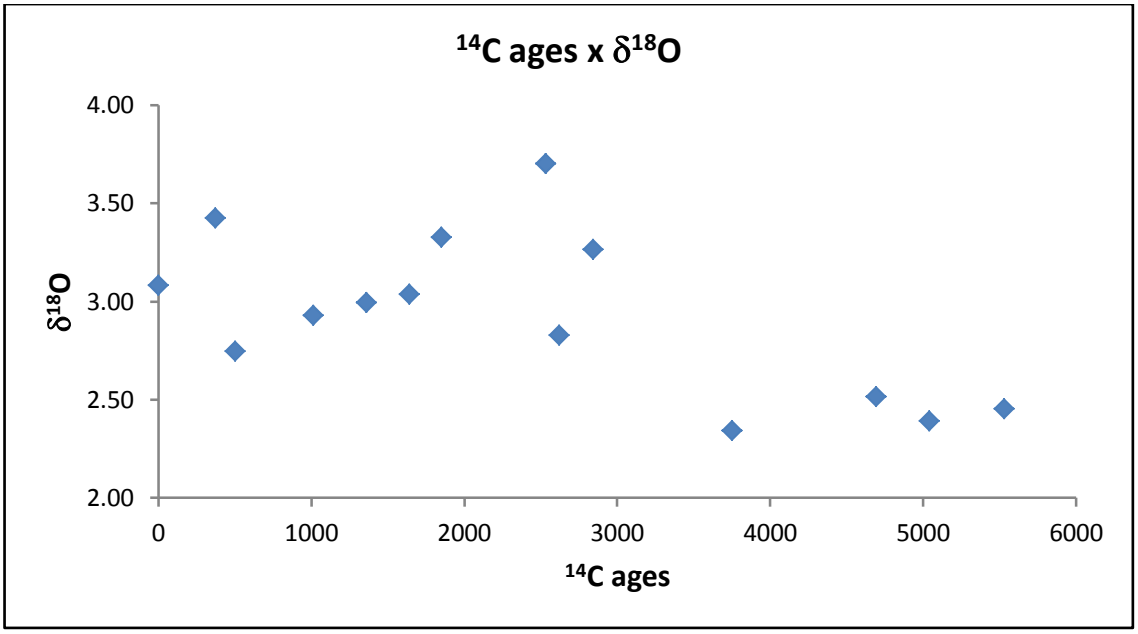

Figure 5.2 – $\delta^{18}O$ and radiocarbon ages for *Fragum erugatum* shells from Hamelin Pool.

Sample	^{14}C Age (yrs BP)	$\delta^{13}C$ [‰, VPDB]	$\delta^{18}O$ [‰, VPDB]
FP-D-207	5530	4.45	2.45
ENA-D-101	5040	3.96	2.39
FPG-05B	4690	4.31	2.52
AWP1-D-02	3750	4.38	2.34
END-D-107	2840	4.60	3.26
END-D-108	2620	4.44	2.83
AWP1-G-01	2530	4.67	3.70
FP-D-205	1850	4.09	3.33
AWP1-D-01	1640	3.94	3.04
EN-DR-D-110	1360	3.51	3.00
CBPT-G-01	1010	4.05	2.93
02ENB04-D-3	500	3.89	2.75
KP-G-100(S)	370	4.01	3.42
FP-ISO-01	Modern	3.72	3.08

Table 5.2 - δ–values for *Fragum erugatum* samples and their radiocarbon ages.

5.3.2. Carbon Isotopic Composition and Radiocarbon Chronology

A chronological assessment of shell stable carbon isotopic composition was performed in the same 14 samples used for $\delta^{18}O$ (Figure 5.3). Between 2530 and 5530 ^{14}C years BP stable carbon isotopic composition is overall at the same level between 4.3 and 4.7 ‰ (except for one outlier at 3.9‰). The marked change between 3750 and 2840 detected in $\delta^{18}O$ is not observed in $\delta^{13}C$. On the other hand the change observed in $\delta^{18}O$ at 1850 ^{14}C years BP is also noticeable in $\delta^{13}C$ where values range from 3.88 to 4.09‰ (except for one outlier at 3.5 ‰).

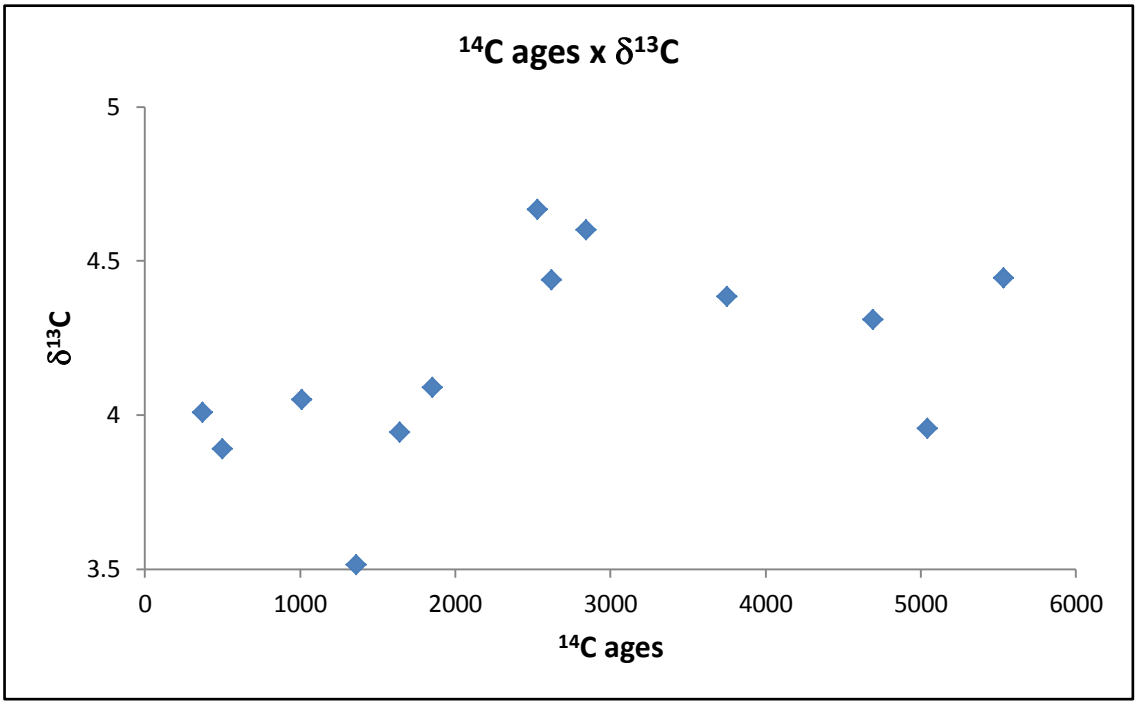

Figure 5.3 – $\delta^{13}C$ and radiocarbon ages for *Fragum erugatum* shells from Hamelin Pool.

5.3.3. Paleosalinity reconstruction using $\delta^{18}O$

Several authors demonstrated a positive correlation of $\delta^{18}O$ of basin waters and salinity (e.g. Ingram et al., 1996; Dettman et al., 2004; MacLachlan et al., 2007; Price et al., 2012). In Shark Bay Price et al. (2012) demonstrated a strong positive correlation of surface water salinities with oxygen and hydrogen isotopic compositions.

In order to investigate the correlation of water $\delta^{18}O$ with salinities, 5 surface water samples were collected within Shark Bay and salinity, pH and temperature were determined to each location in the field (Table 5.3; Figure 5.4). Salinities obtained range between 65 (Hamelin Pool's bay head) and 45 (Freycinet Reach near Nanga Resort). Plotting salinity vs. water $\delta^{18}O$ (VSMOW) shows a linear relationship with a slope of 0.115 and an intercept of -2.97‰ (R^2 = 0.98) (Figure 5.5). This relationship is similar to that obtained by Price et al. (2012) who demonstrated that most Shark Bay water samples when plotted in a $\delta^{18}O$ (VSMOW) vs. salinity plot could be described by a linear regression line with a slope of 0.12 and an intercept of -4.12‰ (R^2 = 0.83 with a much bigger dataset).

To reconstruct paleosalinities based on $\delta^{18}O$(VPDB) from shell carbonate it is necessary to predict the oxygen isotopic composition of the water where *Fragum erugatum* bivalves lived. These mollusks have originally aragonitic shells and the formula from Grossman and Ku (1986)

was used to determine $\delta^{18}O$ of the water as follows: $T(^oC) = 20.6 – 4.34(\delta^{18}O_a - \delta^{18}O_w)$, where T is the water temperature, $\delta^{18}O_a$ refers to oxygen isotopic composition of aragonite in VPDB, $\delta^{18}O_w$ refers to oxygen isotopic composition of water in VSMOW.

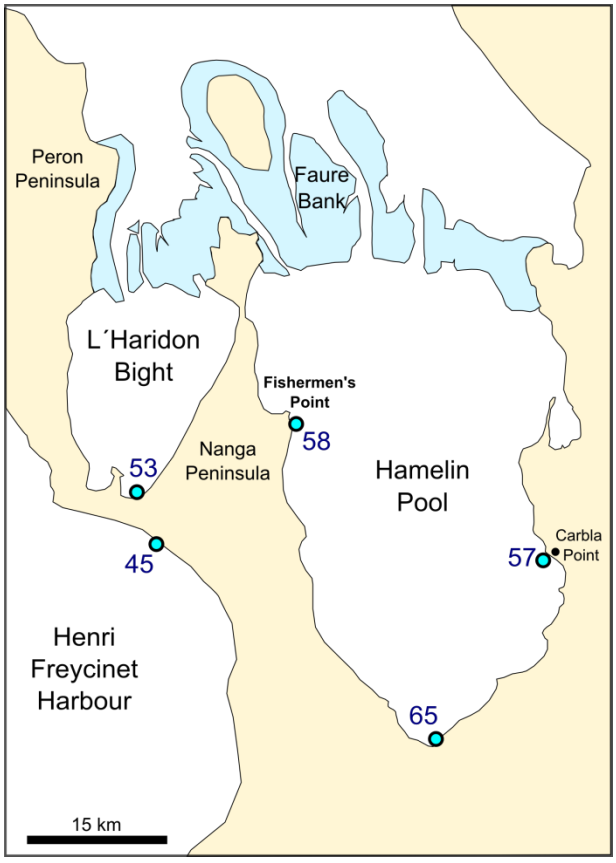

Figure 5.4 – Location for 5 water samples collected in Shark Bay and the salinities measured in each site.

Location Name	Date	Temperature (°C)	Salinity	pH	$\delta^{18}O$(‰) VSMOW
Nilemah Embayment	27/07/2013	19.9	65	8.214	4.41
Carbla point	29/07/2013	18.5	57	8.161	3.77
Shell Beach (L'Haridon Bight)	30/07/2013	16.6	53	8.18	3.09
Nanga Resort (Freycinet Reach)	30/07/2013	20.3	45	8.108	2.21
Fisherman's Point	01/08/2013	16.4	58	8.153	3.74

Table 5.3 – Water parameters and $\delta^{18}O$ values for water samples collected in Shark Bay.

The predicted $\delta^{18}O$ of the water is shown in Table 5.4 and assumes an average water temperature of 23°C which is within the range reported by Logan and Cebulski (1970) of winter minimums between 15-18°C and summer maxima of 26-30°C. The paleosalinities were

calculated using the linear relationship salinity = ($\delta^{18}O_w$ + 2.97) / 0.115 derived from our $\delta^{18}O_w$ vs. salinity plot (Figure 5.5). Sample FP-ISO-01 was collected at a high-water line marked by articulated *Fragum* shells in Fishermen's Point. It is assumed that these shells are modern and their time of residence in the basin after organism death is negligible. Their isotopic values were used as a point of calibration to verify the validity of $\delta^{18}O_w$ and paleosalinities calculation and show a good match as the calculated salinity of 57 is very close to the measured salinity (58) in Fishermen's Point, assuming the bivalve was living at a relatively short distance from the deposition site and the average salinities did not vary greatly since the organisms death.

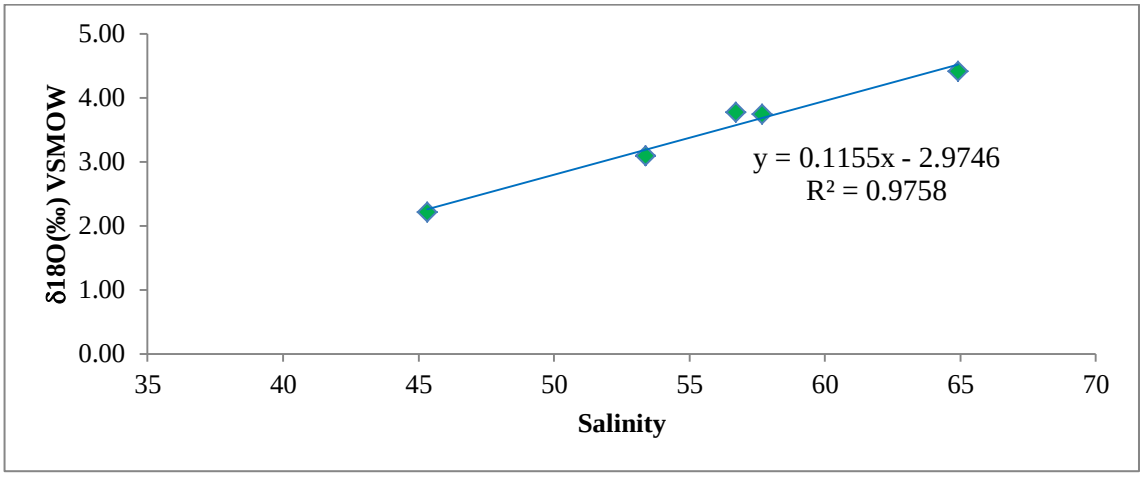

Figure 5.5 – $\delta^{18}O$ ratios versus salinity of surface water samples collected in Shark Bay (Hamelin Pool (3), L'Haridon Bight (1), Freycinet Harbour(1)).

Sample	^{14}C Age (yrs BP)	$\delta^{18}O_a$ (‰, VPDB)	$\delta^{18}O_w$ (‰, VSMOW)	Salinity
FP-D-207	5530	2.45	3.01	52
ENA-D-101	5040	2.39	2.94	51
FPG-05B	4690	2.52	3.07	53
AWP1-D-02	3750	2.34	2.90	51
END-D-107	2840	3.26	3.82	59
END-D-108	2620	2.83	3.38	55
AWP1-G-01	2530	3.70	4.25	63
FP-D-205	1850	3.33	3.88	60
AWP1-D-01	1640	3.04	3.59	57
EN-DR-D-110	1360	3.00	3.55	57
CBPT-G-01	1010	2.93	3.48	56
02ENB04-D-3	500	2.75	3.30	55
KP-G-100(S)	370	3.42	3.98	60
FP-ISO-01	N/A	3.08	3.63	57

Table 5.4 – Results of radiocarbon dating, stable oxygen isotopic ratios of *Fragum* shells, calculated oxygen isotopic ratio of water assuming an average water temperature of 23°C and reconstructed paleosalinities. $\delta^{18}O_a$ refers to *Fragum* shell samples, $\delta^{18}O_w$ refers to calculated isotopic ratio of water.

5.3 Discussion and Conclusions

It is important to note that for the reconstruction of paleosalinities using the steps above, some assumptions were made in order to predict the oxygen isotopic composition of Hamelin Pool waters in the past 6000 years and then extrapolate their salinities. These assumptions are the following: (1) although it is not known how or if the temperature varied, average water temperature is assumed constant during the Late Holocene and similar to present day average of about 23^{o}C; (2) *Fragum erugatum* shells precipitate in equilibrium with ambient water; (3) shells are aragonitic and have little recrystallization; (4) shells are from within Hamelin Pool and are not reworked from outside this sub-basin.

The salinities calculated for the last 5530 years are shown in Figure 5.6. It is possible to indentify 3 main clusters indicating important changes in overall salinities. A first cluster >3000 ^{14}C years BP where high metahaline conditions were prevalent and calculated salinities range between 51 and 53; a second cluster between 2000-3000 ^{14}C years BP where salinities finally reach fully hypersaline conditions (55-63); and a third cluster where hypersaline conditions are more stabilized ranging between 55-60 with a declining trend suggested between 1850 and 500 ^{14}C years BP. In that scenario the 2360 ^{14}C years BP age for the first microbial deposits in Hamelin Pool obtained by Jahnert and Collins (2013) is correlative to a period of peak salinity favourable to microbial benthic communities to thrive under reduced predation and competition. Izuno (2012) made an attempt to reconstruct palaeosalinities based on height/length ratios of *Fragum erugatum* shells and suggested that overall salinities tend to increase with time and increased more rapidly after 2000 ^{14}C years BP. Isotopic data do not support that conclusions, although a marked change is detected after 2000 ^{14}C years BP.

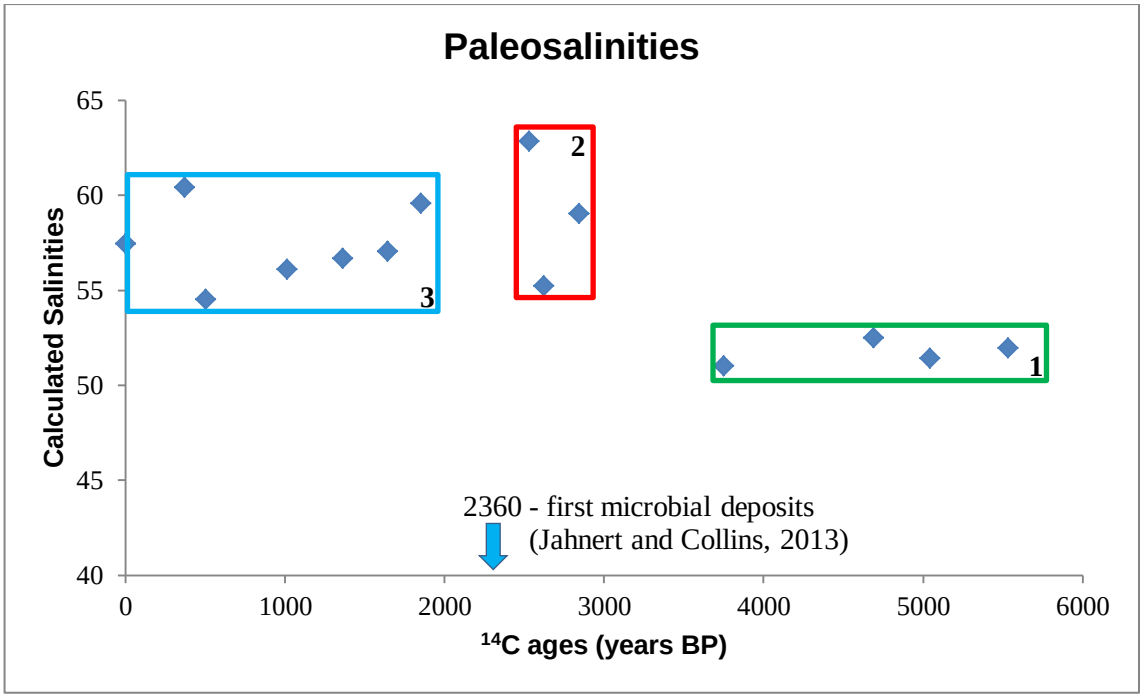

Figure 5.6 – Reconstructed salinities for Hamelin Pool in the last 5530 ^{14}C years. 3 clusters of similar salinities were individualized.

A word of caution needs to be made in reference to the variance between δ^{18}O and δ^{13}C values. Figure 5.7 plots both δ–values vs. time showing a rough covariance between oxygen and carbon isotopes except for the marked break at about 3000 ^{14}C years BP in δ^{18}O which is not well pronounced in δ^{13}C. A possible interpretation for that is the water temperature was actually higher before 3000 ^{14}C years BP as it is expected that both carbon and oxygen isotopes will respond to salinity changes but only oxygen is sensitive to temperature. If this is true, the paleosalinity reconstruction for ages >3000 ^{14}C years BP is not accurate. Another possible explanation is a vital effect affecting carbon and oxygen stable isotopes differently.

This Chapter investigated the potential for the use of stable carbon and oxygen isotopes for paleosalinity reconstruction in the Mid to Late Holocene coquina record in Hamelin Pool. When plotted against ^{14}C ages, δ^{18}O values present three marked clusters that are inferred to be a result of salinity changes. It is concluded that stable isotopes of carbon and oxygen in *Fragum erugatum* mollusk shells have a reasonably good potential for paleoenvironmental assessment during the Late Holocene in Shark Bay, especially for palaeosalinity reconstructions. A less limited data set and a wider spatial distribution of samples would be required to obtain reliable interpretations and fulfill the potential of this method. However, the tentative conclusions are that Hamelin Pool experienced peak salinities between 2000 and 3000 ^{14}C years BP and

salinities remained in the hypersaline field ever since which favored the flourishing of microbial benthic communities and the development of Shark Bay extensive microbial deposits.

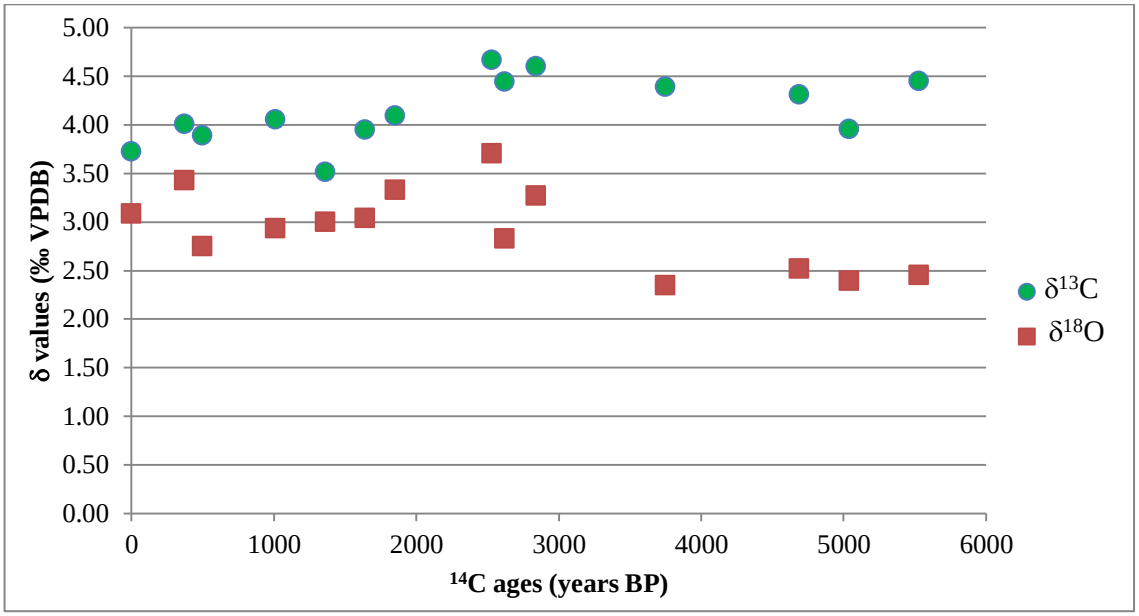

Figure 5.7 - $\delta^{18}O$ and $\delta^{13}C$ ratios for *Fragum erugatum* shells as a function of radiocarbon age.

Chapter 6

Discussion and Conclusions

The objective of this study was to contribute to the understanding of coquina deposits by documenting architectural and sedimentological characteristics of the Shark Bay coquina beach-ridge system. GPR, radiocarbon chronology, stable carbon and oxygen isotopes, outcrop, trench and core data were used to propose a depositional model and outline an evolutionary framework for coquinas and associated facies deposited in two sites: one in the eastern shore of Hamelin Pool, and another, in the western shore of this hypersaline basin.

Shark Bay region is vulnerable to sporadic tropical cyclones and storm surges. However, the degree of exposure to these hazards within Hamelin Pool varies in relation to geographical and geomorphological particularities of different sites. For example, Hamelin Pool eastern shore is more exposed to storms, usually approaching the bay from north and northwest quadrants. Furthermore, north- and west-facing shores tend to be more impacted by storms than south- and east-facing ones.

This difference in vulnerability to storms is revealed by a number of indications in the studied sites. 'East Nilemah', located in the eastern shore, has higher ridges, well developed washover fans and abundant flat pebbles originating in the tidal flats, deposited in the flanks of the seaward-most ridges. In contrast, coquina ridge elevations are lower at Fishermen's Point, not exceeding 5.6 meters as opposed to 8 meters at 'East Nilemah'. Moreover, DGPS transects at Fishermen's Point suggest declining trends of ridge elevation (Figure 4.4) indicating that the signal of falling sea levels during the Mid to Late Holocene is more evident in the western shore beach ridges than in those located in the eastern shore which is more vulnerable to storm impacts.

An important difference between 'East Nilemah' and Fishermen's Point sites refers to sediment composition. As Hamelin Pool possesses different geological foundations in eastern and western shores, the sandy fraction of sediment reflects that characteristic. The eastern shore is bordered by the Carbla Plateau which is underlain by the Cretaceous Toolonga Calcilutite. In contrast, the western shore of Hamelin Pool is at Nanga Peninsula whose country rock is composed of the Plio-Pleistocene Peron Sandstone, rich in quartz. Consequently, the sandy fraction of sediments in the western shore exhibits a high content of quartz, not observed in 'East Nilemah'. The beach-ridge plain at Fishermen's Point can be considered a mixed bioclastic-siliciclastic system as the reworking of quartz sands from the adjoining Nanga

Peninsula by storms and other marine processes yields siliciclastics to the system despite the absence of any significant fluvial input.

Similarities were also observed between beach-ridge deposits in eastern and western shores, especially in their sedimentary architecture. In general, the seaward inclined reflections of prograding beachface deposits are the prevalent architectural element at both sites. In many of the GPR lines, these inclined reflectors are replaced in the seaward direction by the geometrically more complex spit ridges. Furthermore, a diachronous blanket of storm-surge deposits, incipient soil and eolian deposits also occurs in both sites studied.

The differences observed in sedimentary architecture and coastal morphology in the studied sites result from variable degrees of vulnerability to storms. Additionally, reworking processes such as tidal currents, longshore currents and waves may also be energetic enough under fair-weather conditions to transport sediment and leave their imprint in coastal morphology (Figure 6.1A and Table 6.1).

'East Nilemah' is highly exposed to storms because of the northeasterly aspect of its shore and has coastal features that suggest processes operating in variable directions (Figure 6.1B). Apart from the NW direction of overwash, the spits indicating SW and NE direction of transport were generated by longshore currents which may operate either during storms or under fair-weather conditions. Furthermore, ebb tidal currents are expected to be dominant in the eastern shore of Hamelin Pool (Figure 6.1A), facilitated by wind set-up (Logan and Cebulski, 1970). An additional characteristic of 'East Nilemah' is the occurrence of welded swash bars, as interpreted in the GPR lines, which were not observed in the transects at the western shore of Hamelin Pool.

Fishermen's Point, located in the western coast of Hamelin Pool, has shores facing north and east. Its north-facing shore displays spit-ridge growth to the east suggesting longshore currents operating from west to east (Figure 6.1C). These currents are either induced by storms approaching from north/northwest or result from the deflection of flood tidal currents. In the east-facing shore the sediment transport is overall from north to south also resulting either from flood tidal currents that are dominant in the western shore of Hamelin Pool or from longshore currents induced by north/northwest approaching storms. Moreover, isolated lagoons are additional elements that were not observed in 'East Nilemah' and occur associated with spit ridges in Fishermen's Point. These isolated lagoons are particularly detectable in GPR transect FP-B (Fig. 4.7) which is located in the east-facing shore, more protected from storm impacts. The indication of south to north spit growth in the east-facing shore, although small, results from the wind drift.

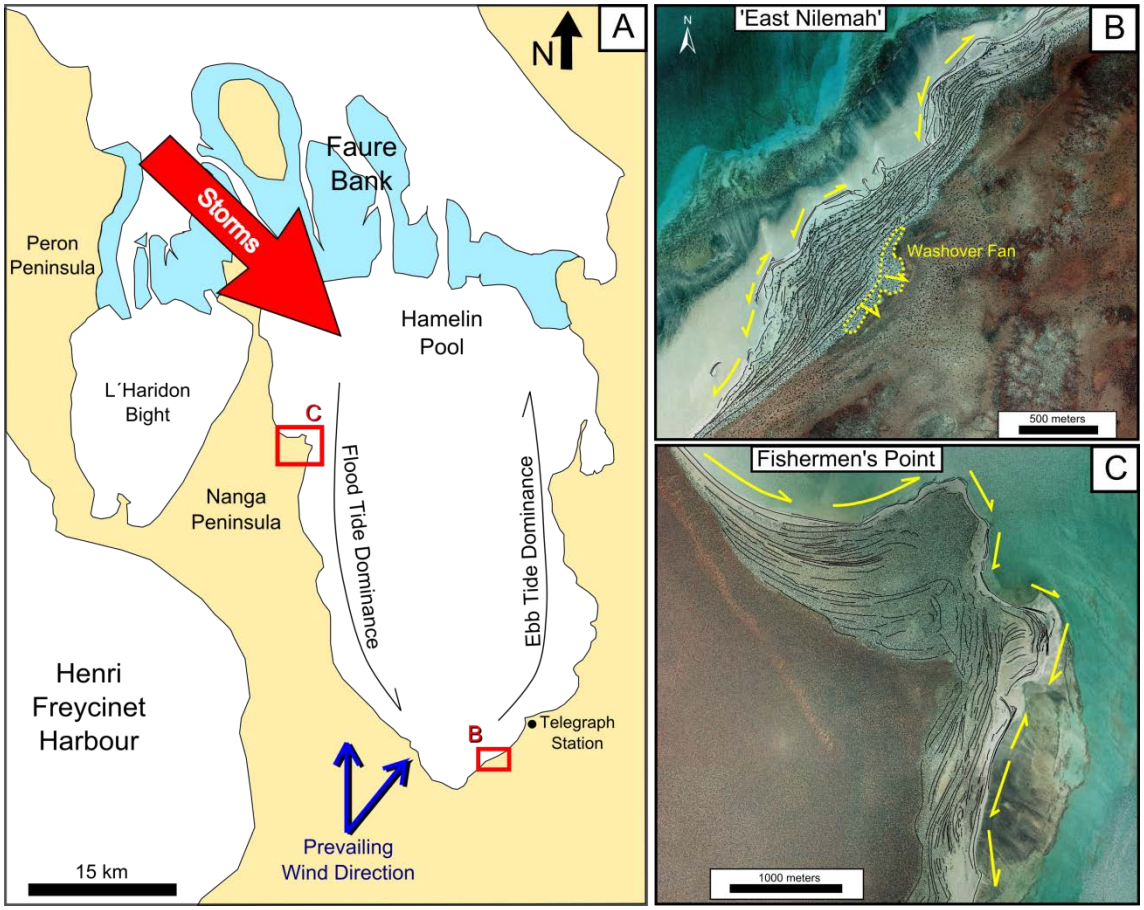

Figure 6.1 – (A) Map with the directions of main energetic coastal processes at Hamelin Pool. Prevailing winds are southerly and south-westerly which favors flood tide dominance in east-facing coasts and ebb tide dominance in west-facing shores. Storms and tropical cyclones usually approach Hamelin Pool from the northwest. (B) Interpreted directions of energetic processes responsible for coastal morphology in 'East Nilemah'. (C) Interpreted directions of energetic processes responsible for coastal morphology in Fishermen's Point.

Depositional domains do not display well-defined chronological boundaries except for the washover domain in 'East Nilemah' which relates to the onset of the system in the eastern shore, and the spit domain which tends to be well developed after 1450 ^{14}C years BP in both sites studied (Figure 6.2B). However, the spit domain develops earlier (or is better preserved) in Fishermen's Point eastern coast, which is more protected from storm attack, starting to develop at about 2450 ^{14}C years BP. On the other hand, ridge sets on both sites show a relatively good chronological correlation (Figure 6.2C) indicating that the beach-ridge system growth is controlled by periods of high sediment availability and adequate storminess which in conjunction with operating marine processes will favor the system's progradation.

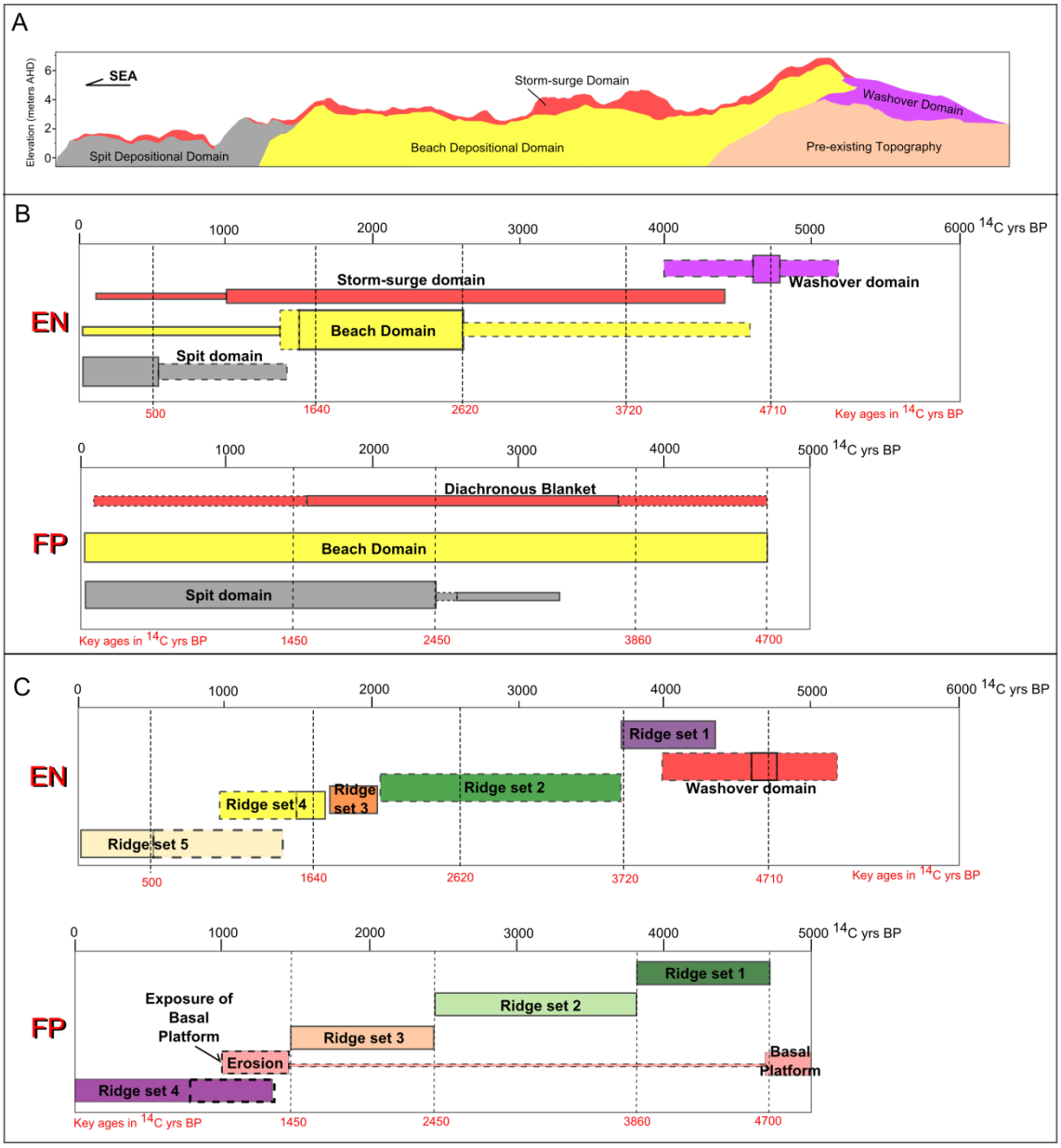

Figure 6.2 – Depositional domain and ridge set chronology. (A) Sketch of typical depositional domain arrangement. (B) Depositional domain chronology in 'East Nilemah' (top) and Fishermen's Point (bottom). Thickness of the bars indicates relative abundance and dashed line in the bar contour indicate inference of the occurrence of depositional domains. (C) Ridge set chronology in 'East Nilemah' (top) and Fishermen's Point (bottom). Dashed lines in the bar contour indicate inference of the occurrence of ridge sets.

In summary the beach-ridge system development can be divided in three main stages responsible for the deposition of the washover, beach and spit depositional domains which are modified by sporadic events responsible for the deposition of a diachronous blanket (Table 6.2). The first stage is represented by an early washover domain characterized by higher than present sea level, possibly higher storm intensities and higher storm-surge water levels. In the second stage, the beach depositional domain develops by beachface progradation under falling sea-level conditions, although the beachface is active only during elevated water levels in either the waning phase or the passage of distant storms, when swash and backwash processes predominate. The third stage, when the deposition of the spit domain takes place, is characterized by even lower sea-level and lower storm intensities which now are unable to overcome beach-ridges thus inducing longshore currents that predominate during spit ridge growth. Indications of changes in coastal dynamics correlative to this third stage were also described by Jahnert et al. (2012), who observed remobilization of shells followed by a marked decrease in layer dip angles that occurred since 2000 years ago in an unit geometrically similar to the beach depositional element, as spit ridge development was limited in their study area. A diachronous blanket that caps the domains originated in these three stages is composed of mixed-origin deposits: (1) storm-surge ridges deposited by multiple episodes of inundation overwash and sub-aerial exposure when windblown clay and silt infiltrate the upper parts of exposed coquina deposits; (2) eolian deposits that occur during sub-aerial exposure of beach ridges and result from eolian sedimentation and reworking; and (3) incipient soil which develops between major inundations caused by storm events.

Features	"East Nilemah"	Fishermen's Point	
		North-facing shore	East-facing shore
Degree of exposure to storms	Extremelly High	High	Moderate
Depositional Elements	Beach > Storm-surge > Spit > Washover	Beach > Storm-Surge >> Spit >> Washover	Beach ≥ Spit > Storm-surge >> Washover
Dominant Ridge Building Process	Storms >>> Longshore and Ebb Tidal Currents	Storms > Flood Tidal and Longshore Currents	Storms ≥ Flood Tidal Currents >> Longshore Currents
Maximum Beach Ridge Height	8m (EN-E)	5.6m (FP-A)	3.4m (FP-B)
Composition	Bioclastic	Bioclastic > Quartz	Bioclastic ≥ Quartz

Table 6.1 – Comparison of characteristics observed in the eastern and western shores of Hamelin Pool (‘East Nilemah’ vs Fishermen’s Point).The eastern shore is more vulnerable to storms and displays ridges with higher maximum elevations. Beach and storm-surge depositional elements are prevalent in ‘East Nilemah’ and the north-facing shore of Fishermen’s Point, while in the east-facing shore of Fishermen’s Point the spit and beach depositional domains have equivalent prevalence.

Chronology (^{14}C yrs)	Domain / Element	Dominant Processes	Characteristics
(1) 3700 - 5000	Washover Domain	Overwash	- Higher than present sea level; - Higher storm intensities
(2) 1640 - 3700	Beach Depositional Domain	Swash-Backwash	- Falling Sea level; - Elevated water level episodes caused by storms; -Onshore sediment transport during storms; - Erosive and constructional events (Berm construction and storm erosion); - Beachface progradation
(3) 1640 - 0	Spit Ridge Domain	Longshore Currents	- Lower sea level; - Lower intensity storms unable to overcome beach-ridges inducing longshore currents; - Decreased storminess
Diachronous	Diachronous Blanket / Storm-surge Domain	- Inundation Overwash; - Eolian Reworking; - Incipient Soil Development	- Storm-surge ridges deposited by multiple episodes of inundation overwash and sub-aerial exposure; - During subaerial phase eolian reworking may occur and eolian infiltration of fines do occur; - Incipient development of soil between storm events

Table 6.2 – Summary of the three main stages responsible for the development of beach-ridges and the diachronous events that originate deposits that cap the system. The first stage is the washover depositional domain that took place during a period of higher than present sea level and higher storm intensities. The second stage responsible for the beach depositional domain reflects beachface progradation during periods of elevated water levels caused by storms. The third stage, when the spit depositional domain developed, reflects a period of lower sea level and decreased storminess. The diachronous blanket (storm-surge depositional domain) was deposited by multiple episodes of inundation overwash and sub-aerial exposure when eolian reworking and infiltration of fines occur.

The use of stable oxygen and carbon isotopes in *Fragum erugatum* bivalve mollusk shells has a good potential to be used in paleosalinity reconstruction within Hamelin Pool as our data indicates. The onset of the *Fragum* coquina beach-ridge system itself may indicate that high metahaline or hypersaline conditions are present since at least 5000 ^{14}C years BP; however, it is not known how salinity varied within this high salinity field. Paleosalinities were calculated using δ^{18}O values and radiocarbon chronologies (Figure 5.6). Until about 3000 ^{14}C years BP high metahaline conditions were prevalent in Hamelin Pool with salinities ranging between 51 and 53. Between 2000-3000 ^{14}C years BP, salinities finally reach fully hypersaline conditions (55-63) followed by a period where hypersaline conditions are more stabilized ranging between 55-60 with a declining trend suggested between 1850 and 500 ^{14}C years BP. The period of peak salinity can be correlated to the 2360 ^{14}C years BP age for the first microbial deposits in Hamelin Pool reported by Jahnert and Collins (2013). This period of elevated salinity was favourable for microbial benthic communities to thrive under reduced predation and competition. Although stable isotopes of carbon and oxygen showed a good potential for paleoenvironmental assessment during the Mid to Late Holocene in Shark Bay, a less limited data set and a wider spatial distribution of samples are required to obtain reliable interpretations and fulfill the possibilities of this method.

This study documented a Holocene coquina beach-ridge system that developed during episodes of elevated water levels (storm surges) under overall falling sea level conditions. GPR profiles and sedimentological data support the construction of a depositional model for the coquina deposits, in which overwash promotes the deposition of washovers and storm-surge ridges at the peak of major storms while berm construction and beachface accretion takes place during the waning phase of storms (or the passage of distant storms) by high waves and related swash, backwash, overtopping and minor overwashing processes. Radiocarbon chronology indicates that the onset of the system took place at about 5000 ^{14}C years ago. After about 2000 ^{14}C years BP marked environmental changes have occurred within Hamelin Pool as indicated by a number of observations such as change in the depositional style of beach-ridge deposits (spit ridges start to predominate and ridges have overall lower elevations); the occurrence of an important erosive period after 1450 ^{14}C years BP in Fishermen's Point; and the suggestion by isotopic data of a well-defined cluster after 2000 ^{14}C years BP, interpreted as a period of stabilization of salinities in the hypersaline field. Finally, the contrasts observed between the beach ridges in the western and eastern shores (Table 6.1) result from the different degree of exposure to storms that usually approach Hamelin Pool from the northwest and north (Figures

2.7and 6.1A) resulting in distinct external and internal beach-ridge morphologies. Marine processes such as longshore drift and tidal currents have a secondary role in the architecture and depositional style of the beach-ridge system during fair-weather periods.

Chapter **7**

References

Aharon, P. (1994). Geology and Biology of Modern and Ancient Submarine Hydrocarbon Seeps and Vents - an Introduction. *Geo-Marine Letters, 14*(2-3), 69-73. http://dx.doi.org/10.1007/Bf01203716

Aigner, T. (1985). *Storm depositional systems: dynamic stratigraphy in modern and ancient shallow-marine sequences*. Berlin; Heidelberg; New York; Tokyo: Springer-Verlag.

Bascom, W. N. (1953). Characteristics of natural beaches. *Coastal Engineering Proceedings, 1*(4), 10.

Bastow, T., Jackson, G., & Edmonds, J. (2002). Elevated salinity and isotopic composition of fish otolith carbonate: stock delineation of pink snapper, Pagrus auratus, in Shark Bay, Western Australia. *Marine biology, 141*(5), 801-806.

Bendixen, M., Clemmensen, L. B., & Kroon, A. (2013). Sandy berm and beach-ridge formation in relation to extreme sea-levels: A Danish example in a micro-tidal environment. *Marine Geology, 344*, 53-64. http://dx.doi.org/10.1016/j.margeo.2013.07.006

Berry, P. F., & Playford, P. E. (1997). Biology of modern *Fragum erugatum* (Mollusca Bivalvia, Cardiidae) in relation to deposition of the Hamelin Coquina, Shark Bay, Western Australia. *Marine and Freshwater Research, 48*(5), 415-420.

Bowler, J. M. (1976). Aridity in Australia: Age, origins and expression in aeolian landforms and sediments. *Earth-science reviews, 12*(2–3), 279-310. doi: 10.1016/0012-8252(76)90008-8

Boyajian, G. E., & Thayer, C. W. (1995). Clam Calamity - a Recent Supratidal Storm-Deposit as an Analog for Fossil Shell Beds. *Palaios, 10*(5), 484-489.

Bureau of Meteorology. (n.d.-a). Average annual & monthly maximum, minimum & mean temperature. Retrieved July 13, 2012, from http://www.bom.gov.au/jsp/ncc/climate_averages/temperature/index.jsp

Bureau of Meteorology. (n.d.-b). Average annual, monthly and seasonal evaporation. Retrieved July 13, 2012, from http://www.bom.gov.au/jsp/ncc/climate_averages/evaporation/index.jsp

Bureau of Meteorology. (n.d.-c). Tropical Cyclones Affecting Carnarvon. Retrieved July 13, 2012, from http://www.bom.gov.au/cyclone/history/wa/carnarvon.shtml

Bureau of Meteorology. (n.d.-d). Wind Roses for Selected Locations in Australia. Retrieved July 13, 2012, from http://www.bom.gov.au/climate/averages/wind/selection_map.shtml

Burling, M. C., Pattiaratchi, C. B., & Ivey, G. N. (2003). The tidal regime of Shark Bay, Western Australia. *Estuarine Coastal and Shelf Science, 57*(5-6), 725-735. http://dx.doi.org/10.1016/S0272-7714(02)00343-8

Butcher, B. P., Van de Graaff, W. J. E., Hocking, R. M., & Geological Survey of Western Australia. (1984). *Shark Bay - Edel, Western Australia: sheets SG/49-8 and SG/49-12 international index*. Perth, W.A.: Geological Survey of Western Australia.

Carvalho, M. D., Praça, U. M., Silva-Telles, A. C., Jahnert, R. J., & Dias, J. L. (2000). Bioclastic Carbonate Lacustrine Facies Models in the Campos Basin (Lower Cretaceous), Brazil. In E. H. Gierlowski-Kordesch & K. R. Kelts (Eds.), *Lake basins through space and time* (Vol. 46): AAPG.

Collins, L. B., Zhao, J. X., & Freeman, H. (2006). A high-precision record of mid-late Holocene sea-level events from emergent coral pavements in the Houtman Abrolhos Islands, southwest Australia. *Quaternary International, 145*, 78-85. http://dx.doi.org/10.1016/j.quaint.2005.07.006

Conti, S., & Fontana, D. (1999). Miocene chemoherms of the northern Apennines, Italy. *Geology, 27*(10), 927-930. http://dx.doi.org/10.1130/0091-7613(1999)027<0927:Mcotna>2.3.Co;2

Davies, J. (1957). The importance of cut and fill in the development of sand beach ridges. *Australian Journal of Science, 20*, 105-111.

Denman, P. D., Hocking, R. M., Moore, P. S., Williams, I. R., & van de Graaff, W. J. E. (1985). *Wooramel, Western Ausralia: Sheet SG/50-5 international index.* (Vol. 1). Perth, Western Australia.

Dettman, D. L., Flessa, K. W., Roopnarine, P. D., Schöne, B. R., & Goodwin, D. H. (2004). The use of oxygen isotope variation in shells of estuarine mollusks as a quantitative record of seasonal and annual Colorado River discharge. *Geochimica Et Cosmochimica Acta, 68*(6), 1253-1263.

Donnelly, C., Kraus, N., & Larson, M. (2006). State of knowledge on measurement and modeling of coastal overwash. *Journal of Coastal Research, 22*(4), 965-991. http://dx.doi.org/10.2112/04-0431.1

Fürsich, F., & Oschmann, W. (1993). Shell beds as tools in basin analysis: the Jurassic of Kachchh, western India. *Journal of the Geological Society, 150*(1), 169-185.

Fürsich, F. T., & Pandey, D. K. (1999). Genesis and environmental significance of Upper Cretaceous shell concentrations from the Cauvery Basin, southern India. *Palaeogeography Palaeoclimatology Palaeoecology, 145*(1-3), 119-139. http://dx.doi.org/10.1016/S0031-0182(98)00099-6

Grossman, E. L., & Ku, T.-L. (1986). Oxygen and carbon isotope fractionation in biogenic aragonite: temperature effects. *Chemical Geology: Isotope Geoscience section, 59*, 59-74.

Hagan, G. M., & Logan, B. W. (1974). Development of Carbonate Banks and Hypersaline Basins, Shark Bay, Western Australia. In B. W. Logan, J. F. Read, G. M. Hagan, P. Hoffman, R. G. Brown, P. J. Woods & C. D. Gebelein (Eds.), *Evolution and diagenesis of Quaternary carbonate sequences, Shark Bay, Western Australia* (Vol. 22, pp. 358 p.). Tulsa, Okla.: American Association of Petroleum Geologists.

Hendry, J. P., & Kalin, R. M. (1997). Are oxygen and carbon isotopes of mollusc shells reliable palaeosalinity indicators in marginal marine environments? A case study from the Middle Jurassic of England. *Journal of the Geological Society, 154*(2), 321-333.

Hesp, P. A. (2006). Sand Beach Ridges: Definitions and Re-Definition. *Journal of Coastal Research*(ArticleType: research-article / Issue Title: Special Issue No. 39. Proceedings of the 8th International Coastal Symposium (ICS 2004), Vol. I / Full publication date: Winter 2006 / Copyright © 2006 Coastal Education & Research Foundation, Inc.), 72-75.

Hickman, C. S. (2003). Mollusc-microbe mutualisms extend the potential for life in hypersaline systems. *Astrobiology, 3*(3), 631-644. http://dx.doi.org/10.1089/153110703322610717

Hine, A. C. (1979). Mechanisms of Berm Development and Resulting Beach Growth Along a Barrier Spit Complex. *Sedimentology, 26*(3), 333-351. http://dx.doi.org/10.1111/j.1365-3091.1979.tb00913.x

Hocking, R. M., Moors, H. T., & Van de Graaff, W. J. E. (1987). *Geology of the Carnarvon Basin, Western Australia*. Perth: State Print. Division.

Houser, C., & Greenwood, B. (2007). Onshore migration of a swash bar during a storm. *Journal of Coastal Research, 23*(1), 1-14. http://dx.doi.org/10.2112/03-0135.1

Houser, C., Greenwood, B., & Aagaard, T. (2006). Divergent response of an intertidal swash bar. *Earth Surface Processes and Landforms, 31*(14), 1775-1791. http://dx.doi.org/10.1002/Esp.1365

Iasky, R. P., D'Ercole, C., Ghori, K. A. R., Mory, A. J., & Lockwood, A. M. (2003). *Structure and petroleum prospectivity of the Gascoyne Platform, Western Australia*. East Perth: Geological Survey of Western Australia.

Iasky, R. P., & Mory, A. J. (1999). *Geology and petroleum potential of the Gascoyne Platform, southern Carnarvon Basin, Western Australia* (Vol. 69). Perth: Geological Survey of Western Australia.

Izuno, G. (2012). Holocene-recent paleosalinity reconstruction of Hamelin Pool, Western Australia, using bivalve morphology (*Fragum erugatum*); significance for stromatolite formation conditions. *Journal of Geography (Chigaku Zasshi), 121*(6), 998-1009 1009, and p. xiii (text in Japanese).

Jahnert, R. J., & Collins, L. B. (2011). Significance of subtidal microbial deposits in Shark Bay, Australia. *Marine Geology, 286*(1-4), 106-111. http://dx.doi.org/10.1016/j.margeo.2011.05.006

Jahnert, R. J., & Collins, L. B. (2012). Characteristics, distribution and morphogenesis of subtidal microbial systems in Shark Bay, Australia. *Marine Geology, 303*, 115-136. http://dx.doi.org/10.1016/j.margeo.2012.02.009

Jahnert, R., de Paula, O., Collins, L., Strobach, E., & Pevzner, R. (2012). Evolution of a coquina barrier in Shark Bay, Australia by GPR imaging: Architecture of a Holocene reservoir analog. *Sedimentary Geology, 281*, 59-74.

Jahnert, R. J., & Collins, L. B. (2013). Controls on microbial activity and tidal flat evolution in Shark Bay, Western Australia. *Sedimentology, 60*(4), 1071-1099. http://dx.doi.org/10.1111/Sed.12023

Keen, T. R., & Stone, G. W. (2000). Anomalous response of beaches to hurricane waves in a low-energy environment, northeast Gulf of Mexico, USA. *Journal of Coastal Research, 16*(4), 1100-1110.

Kelletat, D. (2006). Beachrock as sea-level indicator? Remarks from a geomorphological point of view. *Journal of Coastal Research, 22*(6), 1558-1564. http://dx.doi.org/10.2112/04-0328.1

Kench, P. S., & McLean, R. F. (1997). A comparison of settling and sieve techniques for the analysis of bioclastic sediments. *Sedimentary Geology, 109*(1), 111-119.

Kidwell, S. M. (1989). Stratigraphic condensation of marine transgressive records: origin of major shell deposits in the Miocene of Maryland. *Journal of Geology;(USA), 97*(1).

Kidwell, S. M. (1991). The stratigraphy of shell concentrations. In P. A. Allison & D. E. G. Briggs (Eds.), *Taphonomy: releasing the data locked in the fossil record* (pp. 211-290). New York: Plenum Press.

Kidwell, S. M., & Bosence, D. W. (1991). Taphonomy and time-averaging of marine shelly faunas. *Taphonomy: releasing the data locked in the fossil record. Plenum, New York*, 115-209.

Kidwell, S. M., Fürsich, F. T., & Aigner, T. (1986). Conceptual framework for the analysis and classification of fossil concentrations. *Palaios*, 228-238.

Komar, P. D. (1998). *Beach Processes and Sedimentation*: Prentice Hall PTR.

Kraus, N. C. (2005). Beach profile *Encyclopedia of coastal science* (pp. 169-172): Springer.

Li, X., & Droser, M. L. (1997). Nature and distribution of Cambrian shell concentrations; evidence from the Basin and Range Province of the Western United States (California, Nevada, and Utah). *Palaios, 12*(2), 111-126.

Lindhorst, S., Betzler, C., & Hass, H. C. (2008). The sedimentary architecture of a Holocene barrier spit (Sylt, German Bight): Swash-bar accretion and storm erosion. *Sedimentary Geology, 206*(1-4), 1-16. http://dx.doi.org/10.1016/j.sedgeo.2008.02.008

Liu, Z., Zhuang, Z., Han, D., & Qi, X. (2005). The sedimentary characteristics and formation mechanism of shell ridges along the southwest coast of Bohai Bay. *Journal of Ocean University of China, 4*(2), 124-130.

Lloyd, R. M. (1964). Variations in the oxygen and carbon isotope ratios of Florida Bay mollusks and their environmental significance. *The Journal of Geology*, 84-111.

Logan, B. W., & Cebulski, D. E. (1970). Sedimentary environments of Shark Bay, Western Australia. In B. W. Logan, G. R. Davies, J. F. Read & D. E. Cebulski (Eds.), *Carbonate sedimentation and environments, Shark Bay, Western Australia* (Vol. 13, pp. 1-37). Tulsa, Okla.: American Association of Petroleum Geologists.

Logan, B. W., Davies, G. R., Read, J. F., & Cebulski, D. E. (1970). *Carbonate sedimentation and environments, Shark Bay, Western Australia* (Vol. 13). Tulsa, Okla.: American Association of Petroleum Geologists.

Logan, B. W., Read, J. F., & Davies, G. R. (1970). History of carbonate sedimentation, Quaternary Epoch, Shark Bay, Western Australia. In B. W. Logan, G. R. Davies, J. F. Read & D. E. Cebulski (Eds.), *Carbonate sedimentation and environments, Shark Bay, Western Australia* (Vol. 13). Tulsa, Okla.: American Association of Petroleum Geologists.

Logan, B. W., Read, J. F., Hagan, G. M., Hoffman, P., Brown, R. G., Woods, P. J., & Gebelein, C. D. (1974). *Evolution and diagenesis of Quaternary carbonate sequences, Shark Bay, Western Australia* (Vol. 22). Tulsa, Okla: American Association of Petroleum Geologists.

Lynn Ingram, B., Ingle, J. C., & Conrad, M. E. (1996). Stable isotope record of late Holocene salinity and river discharge in San Francisco Bay, California. *Earth and Planetary Science Letters, 141*(1), 237-247.

MacLachlan, S. E., Cottier, F. R., Austin, W. E., & Howe, J. A. (2007). The salinity: $\delta^{18}O$ water relationship in Kongsfjorden, western Spitsbergen. *Polar Research, 26*(2), 160-167.

Martin, H. A. (2006). Cenozoic climatic change and the development of the arid vegetation in Australia. *Journal of Arid Environments, 66*(3), 533-563. http://dx.doi.org/10.1016/j.jaridenv.2006.01.009

Massari, F., D'Alessandro, A., & Davaud, E. (2009). A coquinoid tsunamite from the Pliocene of Salento (SE Italy). *Sedimentary Geology, 221*(1-4), 7-18.

Matyas, J., Burns, S. J., Mueller, P., & Magyar, I. (1996). What can stable isotopes say about salinity? An example from the Late Miocene Pannonian Lake. *Palaios*, 31-39. http://dx.doi.org/10.2307/3515114

McKee, E. D. (1959). Storm sediments on a Pacific atoll. *Journal of Sedimentary Research, 29*(3), 354-364. http://dx.doi.org/10.1306/74d7092a-2b21-11d7-8648000102c1865d

Meldahl, K. H. (1993). Geographic gradients in the formation of shell concentrations: Plio-pleistocene marine deposits, Gulf of California. *Palaeogeography Palaeoclimatology Palaeoecology, 101*(1-2), 1-25. http://dx.doi.org/10.1016/0031-0182(93)90149-D

Morales, J. A., Borrego, J., Miguel, E. G. S., Lopez-Gonzalez, N., & Carro, B. (2008). Sedimentary record of recent tsunamis in the Huelva Estuary (southwestern Spain). *Quaternary Science Reviews, 27*(7-8), 734-746.

Morton, B. (2000). The biology and functional morphology of *Fragum erugatum* (Bivalvia: Cardiidae) from Shark Bay, Western Australia: the significance of its relationship with entrained zooxanthellae. *Journal of Zoology, 251*, 39-52. http://dx.doi.org/10.1111/j.1469-7998.2000.tb00591.x

Mory, A. J., Iasky, R. P., & Ghori, K. A. R. (2003). *A summary of the geological evolution and petroleum potential of the Southern Carnarvon Basin Western Australia*. Perth: Western Australia Geological Survey.

Neal, A. (2004). Ground-penetrating radar and its use in sedimentology: principles, problems and progress. *Earth-science reviews, 66*(3-4), 261-330. http://dx.doi.org/10.1016/j.earscirev.2004.01.004

Neal, A., Pontee, N. I., Pye, K., & Richards, J. (2002). Internal structure of mixed-sand-and-gravel beach deposits revealed using ground-penetrating radar. *Sedimentology, 49*(4), 789-804. http://dx.doi.org/10.1046/j.1365-3091.2002.00468.x

Nott, J. (2006). Tropical cyclones and the evolution of the sedimentary coast of northern Australia. *Journal of Coastal Research, 22*(1), 49-62. http://dx.doi.org/10.2112/05a-0005.1

Nott, J. (2011). A 6000 year tropical cyclone record from Western Australia. *Quaternary Science Reviews, 30*(5-6), 713-722. http://dx.doi.org/10.1016/j.quascirev.2010.12.004

Orford, J. D., Carter, R. W., & Jennings, S. C. (1991). Coarse clastic barrier environments: evolution and implications for Quaternary sea level interpretation. *Quaternary International, 9*, 87-104.

Otvos, E. G. (2000). Beach ridges — definitions and significance. *Geomorphology, 32*(1–2), 83-108. http://dx.doi.org/10.1016/s0169-555x(99)00075-6

Playford, P. E., Cockbain, A. E., Berry, P. F., Roberts, A. P., Haines, P. W., & Brooke, B., (2013). *The Geology of Shark Bay* (Bulletin 146, 281p.). East Perth, W.A. Geological Survey of Western Australia.

Price, R. M., Skrzypek, G., Grierson, P. F., Swart, P. K., & Fourqurean, J. W. (2012). The use of stable isotopes of oxygen and hydrogen to identify water sources in two hypersaline estuaries with different hydrologic regimes. *Marine and Freshwater Research, 63*(11), 952-966.

Psuty, N. P. (1967). *The Geomorphology of Beach Ridges in Tabasco, Mexico*: Louisiana State University Press.

Quilty, P. G. (1977). Cenozoic Sedimentation Cycles in Western Australia. *Geology, 5*(6), 336-340.

Reimer, P. J., Baillie, M., Bard, E., Bayliss, A., Beck, J. W., Blackwell, P. G., & Weyhenmeyer, C. (2009). IntCal09 and Marine09 radiocarbon age calibration curves, 0-50,000 years cal BP. *Radiocarbon, 51*(4), 1111-1150.

Reolid, M., Garcia-Garcia, F., Tomasovych, A., & Soria, J. M. (2012). Thick brachiopod shell concentrations from prodelta and siliciclastic ramp in a Tortonian Atlantic-Mediterranean strait (Miocene, Guadix Basin, southern Spain). *Facies, 58*(4), 549-571.

Scheffers, A., Engel, M., Scheffers, S., Squire, P., & Kelletat, D. (2012). Beach ridge systems–archives for Holocene coastal events? *Progress in Physical Geography, 36*(1), 5-37.

Scheffers, S. R., Scheffers, A., Kelletat, D., & Bryant, E. A. (2008). The Holocene paleo-tsunami history of West Australia. *Earth and Planetary Science Letters, 270*(1-2), 137-146. http://dx.doi.org/10.1016/j.epsl.2008.03.027

Schellmann, G., & Radtke, U. (2010). Timing and magnitude of Holocene sea-level changes along the middle and south Patagonian Atlantic coast derived from beach ridge systems, littoral terraces and valley-mouth terraces. *Earth-science reviews, 103*(1–2), 1-30. http://dx.doi.org/10.1016/j.earscirev.2010.06.003

Schwartz, M. (2006). *Encyclopedia of coastal science*: Springer.

Tamura, T. (2012). Beach ridges and prograded beach deposits as palaeoenvironment records. *Earth-science reviews, 114*(3–4), 279-297. doi: http://dx.doi.org/10.1016/j.earscirev.2012.06.004

Tanner, W., & Stapor, F. (1971). Tabasco beach-ridge plain: an eroding coast. Trans. Gulf Coast Assoc. Geol. Soc., 21, pp. 231–232

Tanner, W. F. (1995). Origin of beach ridges and swales. *Marine Geology, 129*(1-2), 149-161. http://dx.doi.org/10.1016/0025-3227(95)00109-3

Taviani, M. (1994). The Calcari-a-Lucina Macrofauna Reconsidered - Deep-Sea Faunal Eases from Miocene-Age Cold Vents in the Romagna Apennine, Italy. *Geo-Marine Letters, 14*(2-3), 185-191. http://dx.doi.org/10.1007/Bf01203730

Taylor, M., & Stone, G. W. (1996). Beach-Ridges: A Review. *Journal of Coastal Research, 12*(3), 612-621.

Uda, T. (2006). Spits. In M. Schwartz (Ed.), *Encyclopedia of coastal science*: Springer.

Van de Graaff, W. J. E., Hocking, R. M., & Butcher, B. P. (1983). *Yaringa, Western Australia : sheet SG 50-9 international index*. Perth, W.A.: Geological Survey of Western Australia.

Varela, A. N., Richiano, S., & Poiré, D. G. (2011). Tsunami vs storm origin for shell bed deposits in a lagoon environment: an example from the Upper Cretaceous of Southern Patagonia, Argentina. *Latin American journal of sedimentology and basin analysis, 18*, 63-85.

Winter, W., Jahnert, R., & França, A. (2007). Bacia de campos. *Boletim de Geociências da PETROBRAS, 15*(2), 511-529.